

# **Luminescent properties of $\text{Y}_2\text{SiO}_5\text{:Ce}$ thin films**

*by*

**Elizabeth (Liza) Coetsee**  
**(M.Sc)**

*A thesis submitted in fulfilment of the requirements for the degree*

**PHILOSOPHIAE DOCTOR**

*in the*

**Faculty of Natural and Agricultural Sciences**  
**Department of Physics**

*at the*

**University of the Free State**  
**Republic of South Africa**

**Promoter: Prof. H.C. Swart**  
**Co-promoter: Prof. J.J. Terblans**

May 2010

*This thesis is dedicated to my father and mother, Gert and Marie  
Coetsee*

## **Acknowledgements:**

*“Our Father Who are in Heaven, help us to remember that we can do nothing without Your Almighty Guidance, Salvation and Noble Love.”* Appreciation and gratitude to the following persons:

- Prof. H. C. Swart for his professional and “paternal” leadership as my supervisor.
- Prof. J. J. Terblans for his most valuable insight, respect and recognition.
- Adriaan Hugo for a “novel” awakening to the meaning of life.
- Innes Basson, ‘bright spark’ from the Electronic department UFS, for his friendship.
- Paul Ripley from Phosphor Technology Ltd for supplying the  $Y_2SiO_5:Ce$  phosphor powder.
- My friends, personnel and junior colleague (Jacque Maritz) at the University of the Free State.
- Johan Steyn and Herman Rossouw from the NLC Pretoria for their friendship and generous, immediate and willing assistance.
- Prof. P. W. J. van Wyk of the electron microscopy unit at UFS.
- Prof. W. van der Westhuizen from Geology, UFS for XRD measurements.
- Prof. J. R. Botha from NMMU for the use of their laser facilities for PL measurements.
- UFS, NMISA and NRF for financial assistance.
- Dr. Andrew Forbes, Thomas du Plooy and Henk van Wyk for the use of the laser facilities at the NLC CSIR Pretoria.
- My martial arts parents and students for absolute devotion, support and faith.
- Elmarie Greyling and Stafford Mew for loyal companionship.
- My loving and honourable father and mother, twin brothers Andries and Gert, sisters Marleen, Emmie and father’s sister Ina van Wyk.
- David and Joan Collett for their significant interest and fortification for my parents.
- Grand Master Eddie Jacobsen for his respect and perseverance of a top martial arts role model.

- Masters Melanie, Jan, Godfrey and Cindy and the rest of my martial arts friends for their encouragements and interest in physics.
- Dirk Wijnbeeck for 27 years of religious education.
- Michael Pentz for the following phrase: “One day you’ll be doctor Liza Coetsee”

## Abstract

The luminescent properties of yttrium silicate doped with cerium ( $\text{Y}_2\text{SiO}_5:\text{Ce}$ ) phosphor thin films were investigated. A detailed investigation (cathodoluminescence (CL), photoluminescence (PL) and Gaussian peak fits) was first done on the luminescent mechanism of  $\text{Y}_2\text{SiO}_5:\text{Ce}$  phosphor powders in order to understand and find a plausible mechanism that could assist in future research to be done.

Luminescence in  $\text{Y}_2\text{SiO}_5:\text{Ce}$  occurs due to characteristic transitions in the  $\text{Ce}^{3+}$  ion itself. Splitting of the 4f energy level into the  $^2\text{F}_{5/2}$  and  $^2\text{F}_{7/2}$  energy levels is due to the 4f<sup>1</sup> electron in  $\text{Ce}^{3+}$  having the ability to exhibit a +1/2 and -1/2 spin. This creates the expectation of a luminescent spectrum with two main peaks in the blue region (between 400 and 500 nm).

$\text{Y}_2\text{SiO}_5:\text{Ce}$  has two different monoclinic crystal structures. A low temperature (synthesized at temperatures less than 1190 °C)  $X_1$  - phase (much weaker luminescent intensity, with space group  $P2_1/c$ ) and a high temperature (synthesized at temperatures above 1190 °C with a melting temperature at 1980 °C)  $X_2$  - phase (space group  $B2/c$ ). In each of these two phases there are two possible  $\text{Y}^{3+}$  sites in the  $\text{Y}_2\text{SiO}_5$  matrix. The most plausible explanation for the broad band luminescent spectra obtained from excitation and emission results in this research study is that the two different sites of the  $\text{Ce}^{3+}$  ion (Ce can substitute Y) (A1 and A2) in the host matrix are responsible for two sets of visible peaks. The difference in orientation of the neighbour ions in the crystal structure will be responsible for the broadening of the band emission.

Three sets of  $\text{Y}_2\text{SiO}_5:\text{Ce}$  thin films were grown with pulsed laser deposition (PLD) by using a 248 nm KrF and a XeCl ( $\lambda = 308$  nm) excimer laser. The thin films were grown on Si (100) substrates with different process parameters in order to investigate the surface morphology and luminescent properties. Process parameters that were changed during the growth process using a KrF laser were the  $\text{O}_2$  ambient pressure (vacuum, 10 mTorr and 1 Torr), the fluence ( $3 \pm 0.3$  and  $1.6 \pm 0.1$  J.cm<sup>-2</sup>), the substrate temperature (400 and

600 °C) and the gas species (N<sub>2</sub>, O<sub>2</sub> and Ar at 455 mTorr). The laser pulse frequency and the amount of pulses were kept constant at 8 Hz at 4000 pulses.

The increase in the pressure to 1 Torr O<sub>2</sub> shows a definite increase in particle size and roughness. The increased fluence led to bigger particle and grain sizes. The surface structure of the thin film ablated at 400 °C substrate temperature is less compact (lesser agglomeration of particles than the 600 °C). The increase in substrate temperature definitely resulted in a rougher surface layer.

Ablation done in N<sub>2</sub> gas resulted in small particles of mostly 20 nm in diameter. Ablation in O<sub>2</sub> gas produced bigger particles of 20, 30 and 40 nm as well as an agglomeration of these particles into bigger size clusters of about 80 to a 100 nm. Ablation in Ar gas showed particle sizes of mostly 30 nm. The particles are more spherically defined and evenly distributed on the surface in comparison with the agglomerated particles grown in O<sub>2</sub> gas. Thin film morphology and other characteristic properties strongly depend on the gas pressure during PLD. An increase to 1 Torr O<sub>2</sub> gas thus resulted in bigger particle sizes and the higher fluence also led to bigger particles with a decrease in particle density. The higher substrate temperature resulted in a rougher surface layer and ablation in Ar gas at 455 mTorr compared to N<sub>2</sub> and O<sub>2</sub> gas resulted in bigger and less agglomerated particles being formed.

CL scanning images were obtained to investigate the effect of a tin oxide (SnO<sub>2</sub>) coated layer on the light output. The CL scan results of the uncoated and tin oxide coated thin films showed a definite increase in luminescent intensity with the uncoated thin film which indicates the photon absorption effect of the extra tin oxide coated layer. The tin oxide acts as a coated layer to prevent electron stimulated reactions with the phosphor surface and thus inhibits degradation.

CL measurements that were done showed that the increased O<sub>2</sub> ambient (1 Torr) resulted in a higher CL intensity compared to the thin films ablated in vacuum. This is in agreement with the PL results where the nano – particles' shape ensure better light

output due to fewer photons being totally reflected internally. The ablation in high fluence also showed a higher CL and PL intensity with the vacuum and 1 Torr thin films compared to the low fluence. The higher substrate temperature (600 °C) results in better intensities due to the rougher surface formed. The thin film ablated in 455 mTorr Ar gas showed a higher CL intensity than the other two thin films. This is due to the spherically shaped and the less agglomerated particles on the surface of the substrate.

A 144 hr CL degradation study was done on the thin film ablated in Ar gas (coulomb dose of  $1.4 \times 10^4 \text{ C.cm}^{-2}$ ) at an  $\text{O}_2$  pressure of  $1 \times 10^{-6}$  Torr, 2 keV electron energy and 10  $\mu\text{A}$  electron beam current. There was a definite decrease in the CL intensity measured at 440 nm while a second broad band peak emerged at 650 nm, which increased with an increase in the degradation time; leading to a broad spectrum ranging from 400 to 850 nm. The blue colour again changed (the same as with the powders) to a whitish colour. The degradation results were again ascribed to the formation of  $\text{SiO}_2$  with a defect level at 1.9 eV (650 nm).

The XPS analysis showed that a  $\text{SiO}_2$  layer formed on the surface under electron bombardment. The thin films are therefore also degrading but are more chemically stable than the phosphor powders. The light output intensity however; is lower.

## **Keywords**

$\text{Y}_2\text{SiO}_5:\text{Ce}$ : An inorganic phosphor, intentionally doped with the rare earth, cerium, for blue light emission.

PLD: Pulsed laser deposition (PLD) is a fast and effective thin film growth method.

Process parameters: During the PLD process there is certain parameters, like background pressure, that could influence the growth process and surface morphology of the thin film.

Nano - thin films: Thin films grown as nano – particle layers.

AFM: Atomic force microscopy.

Cathodoluminescence: A phenomenon whereby the emission of light occurs due to electron beam irradiation.

Photoluminescence: A phenomenon whereby the emission of light occurs due to photonic excitation.

Degradation: Reduction of the efficiency of a phosphor material through prolonged electron bombardment.

XPS: X-ray photoelectron spectroscopy.

FED: Field emission display.

## Table of contents

Acknowledgements: .....	3
Abstract.....	5
Keywords .....	7
Chapter 1 .....	14
1.1 Introduction.....	14
1.1.1 Phosphors.....	14
1.1.2 Pulsed laser deposition.....	14
1.1.3 $Y_2SiO_5:Ce$ .....	15
1.2 Aim of this study .....	18
1.3 Layout of the thesis .....	19
References.....	19
Chapter 2 .....	21
Phosphors.....	21
2.1 Different phosphors .....	21
2.1.1 Band gap .....	21
2.1.2 Intra atomic .....	24
2.1.3 Different phosphor materials.....	24
2.1.4 Charge Transfer .....	25
2.2 Different luminescence .....	26
2.3 Phosphor research being done.....	27
2.4 Yttrium silicate doped with cerium ( $Y_2SiO_5:Ce$ ) .....	28
References.....	30
Chapter 3 .....	32
Pulsed laser deposition (PLD).....	32
3.1 Description of the technique .....	32
3.1.1 History .....	32
3.1.2 Four stage process:.....	33
3.1.2.1. Laser ablation of the target material and creation of a plasma: .....	33
3.1.2.2. Dynamic of the plasma: .....	34
3.1.2.3. Deposition of the ablation material on the substrate: .....	35

3.1.2.4. Nucleation and growth of the film on the substrate surface: .....	35
3.1.3 Advantages of PLD: .....	36
3.1.4 Disadvantages of PLD:.....	36
3.2 Process Parameters .....	37
3.2.1 The ambient pressure: .....	38
3.2.2 The laser fluence: .....	41
3.2.3 The substrate temperature:.....	42
References.....	43
Chapter 4 .....	46
The luminescent mechanism of $Y_2SiO_5:Ce$ .....	46
4.1 Introduction.....	46
4.2 CL and PL of the $Y_2SiO_5:Ce$ powder .....	46
4.3 Luminescent mechanism of $Y_2SiO_5:Ce$ .....	47
4.3.1 Excitation .....	47
4.3.2 Gaussian Peak Fit.....	50
4.3.3 Luminescent mechanism.....	53
4.4 Degradation of the $Y_2SiO_5:Ce$ powder.....	56
4.5 Conclusion .....	60
References.....	60
Chapter 5 .....	62
Characterization of the $Y_2SiO_5:Ce$ thin films: Part one.....	62
5.1 Introduction.....	62
5.2 Experimental procedure.....	63
5.2.1 The growth of $Y_2SiO_5:Ce$ thin films .....	63
5.2.2 Characterization of the $Y_2SiO_5:Ce$ thin films: SET 1 and 2 .....	64
5.3 Results and Discussions .....	65
5.3.1 SEM/BSE and EDS .....	65
5.3.2 AFM.....	70
5.3.3 Comparison: SET1 and 2 .....	81
5.4 Conclusion .....	84
References.....	85

<b>Chapter 6 .....</b>	<b>86</b>
<b>Crystal structure and luminescent properties of the Y<sub>2</sub>SiO<sub>5</sub>:Ce thin films: Part two.....</b>	<b>86</b>
<b>6.1 Introduction.....</b>	<b>86</b>
<b>6.2 Experimental Procedure .....</b>	<b>86</b>
<b>6.2.1 Characterization of the Y<sub>2</sub>SiO<sub>5</sub>:Ce thin films: SET 1 and 2 .....</b>	<b>86</b>
<b>6.2.2 Characterization of the Y<sub>2</sub>SiO<sub>5</sub>:Ce thin films: SET 3.....</b>	<b>87</b>
<b>6.2.3 CL and PL spectrometry for the thin films: SET 1 and 2.....</b>	<b>87</b>
<b>6.3 Results and Discussion.....</b>	<b>87</b>
<b>6.3.1 XRD .....</b>	<b>87</b>
<b>6.3.2 CL Scanning .....</b>	<b>89</b>
<b>6.3.3 CL measurements.....</b>	<b>91</b>
<b>6.3.4 PL measurements .....</b>	<b>93</b>
<b>6.3.5 Comparison: SET1 and 2 .....</b>	<b>95</b>
<b>6.4 Conclusion .....</b>	<b>98</b>
<b>References.....</b>	<b>99</b>
<b>Chapter 7 .....</b>	<b>101</b>
<b>CL degradation and APPH depth profiles of PLD thin films: Part three .....</b>	<b>101</b>
<b>7.1 Introduction.....</b>	<b>101</b>
<b>7.2 Experimental Procedure .....</b>	<b>104</b>
<b>7.2.1 Rutherford Backscattering (RBS) .....</b>	<b>104</b>
<b>7.2.2 Auger peak to peak height (APPH) depth profiles .....</b>	<b>104</b>
<b>7.2.3 Degradation.....</b>	<b>104</b>
<b>7.3 Results and discussions.....</b>	<b>104</b>
<b>7.3.1 RBS .....</b>	<b>104</b>
<b>7.3.2 APPH depth profiles .....</b>	<b>105</b>
<b>7.3.3 CL degradation: Area 1.....</b>	<b>106</b>
<b>7.3.4 CL Degradation Area 2 .....</b>	<b>109</b>
<b>7.4 Conclusion .....</b>	<b>112</b>
<b>Reference .....</b>	<b>113</b>
<b>Chapter 8 .....</b>	<b>114</b>

<b>XPS before and after electron degradation: Part four</b> .....	114
<b>8.1 Introduction</b> .....	114
<b>8.2 Experimental Procedure</b> .....	115
<b>8.2.1 Characterization</b> .....	115
<b>8.2.2 Peak fits</b> .....	115
<b>8.3 Results and Discussions</b> .....	115
<b>8.3.1 SXI</b> .....	115
<b>8.3.2 XPS</b> .....	116
<b>8.4 Conclusion</b> .....	130
<b>References</b> .....	131
<b>Chapter 9</b> .....	133
<b>Conclusion and future work</b> .....	133
<b>9.1 Conclusion</b> .....	133
<b>9.1.1 Luminescent mechanism</b> .....	133
<b>9.1.2 Thin films: Part one</b> .....	133
<b>9.1.3 Thin films: Part two</b> .....	134
<b>9.1.4 Thin films: Part three</b> .....	135
<b>9.1.5 Thin films: Part four</b> .....	135
<b>9.2 Future work</b> .....	136
<b>Direct continuation of nano-thin films:</b> .....	136
<b>9.2.1 More PLD process parameters</b> .....	136
<b>9.2.2 Off axis geometry</b> .....	136
<b>9.2.3 Heating and cooling luminescent properties</b> .....	137
<b>9.2.4 Characterization</b> .....	137
<b>Future Phosphor Research:</b> .....	137
<b>9.2.5 Nano-technology</b> .....	137
<b>9.2.6 Luminescence</b> .....	138
<b>9.2.7 Modern luminescence spectroscopy:</b> .....	138
<b>Appendix A</b> .....	140
<b>Publications</b> .....	140
<b>Proceedings</b> .....	142

<b>Conference participation.....</b>	<b>143</b>
<b>South African Institute of Physics .....</b>	<b>143</b>
<b>International conferences and other .....</b>	<b>143</b>

# Chapter 1

Chapter 1 serves as the introduction chapter on a research study done on blue emitting  $\text{Y}_2\text{SiO}_5:\text{Ce}$  nano phosphor thin films. It shortly introduces the 1) phosphor phenomenon, 2) the technique used for the growth of the thin films investigated in this thesis (pulsed laser deposition (PLD)) and 3) give some background information on the  $\text{Y}_2\text{SiO}_5:\text{Ce}$  material itself. It then concludes with the aim of this research study and provides the layout of the thesis. More detailed background, characterization, results and discussions are found in the chapters to follow. The results on the morphological and luminescent properties, obtained through changes made to some process parameters during PLD, delivered promising results. These results will add to the contribution towards the modern evolving display- and nano- technology.

## 1.1 Introduction

### 1.1.1 Phosphors

The most recent phosphor research delivered promising results for several new applications. Different phosphors with different dopants and thus different colours and luminescent properties were investigated [1, 2]. The investigations are mainly focused on the preparation methods (such as sol-gel, combustion and PLD) of phosphor powders as well as thin films, degradation, enhancing the luminescence, long afterglow as well as on nano-phosphors [3, 4].

### 1.1.2 Pulsed laser deposition

PLD is a well known fast and effective technique to grow phosphor thin films for possible application in optical displays. Thin film phosphors have some advantages over powders in the field emission display (FED) environment, such as a reduction of light scattering and a good thermal contact between the screen and the faceplate [5, 6] but the intensity is still a great problem.

Particle formation is, however, a major drawback of PLD and it usually is the main limiting factor in this application field. High performance electronic and optical devices require particle free films. The formation and emission of the particles strongly depend on the type of material used as the target and it is based on various physical phenomena such as the dislodgement of uniformities protruding from the target surface, gas phase clustering of the evaporated material due to supersaturation (in high gas pressures) and the generation of liquid phase droplets. Particles can therefore be in the vapour, liquid or solid phase [7, 8].

One of the solutions to the particle formation problem is optimization of the laser process parameters such as the ambient pressure (oxygen), laser fluence, laser pulse frequency, number of pulses, substrate temperature and the target to substrate distance. Surface morphology and thickness can be controlled by varying the growth parameters [6, 7]. As mentioned before, optical devices require phosphor displays and thus the need for better and more efficient luminescent intensities of the phosphors. The luminescent intensity of phosphor thin films can strongly depend on the surface morphology. A rougher surface would increase the intensity due to a lesser effect of total internal reflection if compared to a smooth thin film surface [5].

### 1.1.3 $\text{Y}_2\text{SiO}_5:\text{Ce}$

The main purpose of *this* phosphor research study is therefore to contribute to the improvement of the luminescent intensity of the phosphors used in electronic and optical display devices such as FEDs and plasma displays (PDs) [9, 10]. Cerium doped yttrium silicate ( $\text{Y}_2\text{SiO}_5:\text{Ce}$ ) is one of many phosphor materials under investigation. It is a blue emitting (double shoulder peak between 400 and 500 nm) rare earth phosphor that can be an alternative for the traditional ZnS phosphor used in cathode ray tubes (CRTs).

Light emission in rare earth phosphors is due to characteristic luminescence in the atom itself.  $\text{Ce}^{3+}$  (Trivalent Cerium) has only one electron in the 4f shell, with an electron configuration of  $[\text{Xe}].4f^1.5d^1.6s^2$ . The 4f energy level splits into the  $^2F_{5/2}$  and the  $^2F_{7/2}$  levels due to the electron having the ability to exhibit a  $+ 1/2$  or  $- 1/2$  spin [11, 12]. The

primary electrons get scattered throughout the host crystal, eventually transferring energy to the  $\text{Ce}^{3+}$  ion (situated in the band gap of the host material) resulting in excitation of the  $4f^1$  electron. The luminescence photon energy depends strongly on the structure of the host crystal through the crystal-field splitting of the  $4f$  state [13].

If an atom in a crystal is surrounded by ions, there exists a “crystal field” due to the interactions of the ions on the atom. Due to the symmetric effects, this crystal field causes the energy levels of the atom to split. A splitting of energy levels (“crystal field splitting”) occurs because the orientation of the “d” orbital wave function will increase the electron energy when the orbital is located in a region of high electron density [14].

$\text{Y}_2\text{SiO}_5:\text{Ce}$  is highly stable physically and chemically with respect to time and temperature as compared with other well-studied phosphor materials like ZnS and CdS [15]. Fully detailed descriptions about the transitions and energy levels, monoclinic crystal structure and the two different phases ( $X_1$  and  $X_2$ ) can be found in section 2.4 and 4.3. It is studied by many physicists for its polymorphous nature and interesting properties related to its luminescence when doped with various rare earth ions [15, 17, 17].

Ouyang *et al.* [18] investigated rare-earth-doped transparent yttrium silicate thin film phosphors for colour displays. They have reported on the luminescence of the as-deposited amorphous  $\text{Y}_2\text{O}_3\text{-SiO}_2$  doped with  $\text{Eu}^{3+}$ ,  $\text{Tb}^{3+}$  and  $\text{Ce}^{3+}$  thin films (prepared by magnetron sputtering). Two broad band peaks were found for  $\text{Y}_2\text{Si}_2\text{O}_7:\text{Ce}$ . One located in the blue region at 420 nm and the other in the red region at 642 nm. Eu doped films emitted at 622 nm (red) and Tb doped films at 542 nm (green). Annealing above 800 °C increased the luminescence intensity about 5-10 times. The reason for this emission was ascribed to the crystal field splitting effects. A conclusion was made that the primary colours needed for a full colour display could therefore be achieved by doping with  $\text{Eu}^{3+}$ ,  $\text{Tb}^{3+}$  and  $\text{Ce}^{3+}$

Another investigation was done on improving the efficiency of a blue emitting phosphor by an energy transfer from  $Gd^{3+}$  to  $Ce^{3+}$  by Bosze *et al.* [19].  $Gd^{3+}$  improves the efficiency by transferring energy to  $Ce^{3+}$ , and makes this phosphor  $((Y_{1-m-n}Ce_mGd_n)_2SiO_5)$  a more promising candidate for low-voltage field emission flat panel displays. Low voltage PL and CL measurements were made in order to find the optimum concentrations for  $Gd^{3+}$  that yielded the most luminous efficient phosphor. It was found that for PL, co-activating with  $Gd^{3+}$  did not improve the efficiency since  $Gd^{3+}$  does not absorb at Ce excitation energy (358 nm). For CL however, co-activating did improve the efficiency since  $Gd^{3+}$  was sufficiently excited and the optimum composition was found to be  $(Y_{0.8425}Ce_{0.0075}Gd_{0.15})_2SiO_5$ .

Karar *et al.* [15] prepared nano-crystalline silica capped yttrium silicate doped with cerium with a sol-gel process and investigated the PL properties. The material showed blue luminescence (437 nm) at room temperature and a small enhancement upon annealing. The PL intensities of these nano-crystalline samples were found to be much stronger than similar bulk samples. It was reported that annealing related PL enhancement is attributed to the formation of the optimum nano-crystalline size required for strong luminescence from nano-particles due to the doped rare earth ions and quantum confinement related effects. They also suggested that nano- $Y_2SiO_5$  has a relatively more intense blue emission than the nano- $Y_2Si_2O_7$  phase which is attributed to the position of the 5d level of  $Ce^{3+}$  in the energy band.

Degradation of the CL intensity of  $Y_2SiO_5:Ce$  phosphor powder was investigated in a previous study done by Coetsee *et al.* [20]. Auger electron spectroscopy (AES), X-ray photoelectron spectroscopy (XPS) and CL spectroscopy were used to monitor changes in the surface chemical composition and luminous efficiency of commercially available  $Y_2SiO_5:Ce$  phosphor powder. The degradation of the CL intensity for the powder was consistent with a well-known electron-stimulated surface chemical reaction (ESSCR) model. It was shown with XPS and CL that the electron stimulated reaction led to the formation of a silicon dioxide ( $SiO_2$ ) layer on the surface of the  $Y_2SiO_5:Ce$  phosphor powder. XPS also indicated that the Ce concentration in the surface layer increased

during the degradation process and the formation of  $\text{CeO}_2$  and  $\text{CeH}_3$  were also part of the degradation process. The CL intensity first decreased until about  $300 \text{ C.cm}^{-2}$  and then increased due to an extra peak arising at a wavelength of 650 nm. This extra peak was attributed to the newly formed  $\text{SiO}_2$  layer that contains some defect levels.  $\text{SiO}_2$  has a band gap and the electron beam irradiation can break the Si-O bonds and cause intrinsic defects [21, 22]. Skuja *et al.* [23, 24] reported two peaks for  $\text{SiO}_2$  at 1.9 eV (650 nm) and 2.7 eV (459 nm) with a theory that the two peaks are related to intrinsic defects involving broken Si-O bonds. Fully detailed results and discussions can be found in section 4.3.

## 1.2 Aim of this study

The aim of this study was to investigate the following aspects concerning the  $\text{Y}_2\text{SiO}_5\text{:Ce}$  phosphor thin films:

1. Investigation and construction of a more plausible luminescent mechanism for  $\text{Y}_2\text{SiO}_5\text{:Ce}$  by doing Gaussian peak fittings on the powder's cathode- (CL) and photoluminescent (PL) spectra.
2. Ablating  $\text{Y}_2\text{SiO}_5\text{:Ce}$  phosphor thin films onto Si (100) substrate with the use of the KrF (248 nm) excimer laser in PLD.
3. Changing process parameters during PLD, (such as gas pressure (vacuum ( $5 \times 10^{-6}$  Torr),  $1 \times 10^{-2}$  Torr and 1 Torr  $\text{O}_2$  pressure), different gas species (oxygen ( $\text{O}_2$ ), argon (Ar) and nitrogen ( $\text{N}_2$ )), laser fluence ( $1.6 \pm 0.1 \text{ J.cm}^{-2}$  and  $3.0 \pm 0.3 \text{ J.cm}^{-2}$ ) and substrate temperature (400 and 600 °C)) to investigate the effect on the surface morphology and luminescent intensity.
4. Characterization of the thin films (scanning electron microscopy (SEM), energy dispersive spectroscopy (EDS), atomic force microscopy (AFM) and x-ray diffraction (XRD)).
5. Monitoring the CL and PL results to find the most luminescent effective process parameters for the growth of  $\text{Y}_2\text{SiO}_5\text{:Ce}$  phosphor thin films.

6. A degradation study on one of the thin films in order to investigate the chemical changes on the surface of the thin films and a depth profiling study to monitor the CL intensity during sputtering.
7. XPS and Gaussian-Lorentz peak fits to identify any chemical changes during degradation.

### 1.3 Layout of the thesis

*Chapter 1* includes the introduction and aim of this study, with *chapter 2* explaining some phosphor fundamentals and briefing on the yttrium silicate phosphor used in this research study. *Chapter 3* describes the pulsed laser deposition technique and the effects of some process parameters (ambient pressure, laser fluence and substrate temperature). Discussions on the luminescent mechanism and degradation of the phosphor powder can be found in *chapter 4*. *Chapter 5* contains the thin film growth procedures as well as results and discussions for surface morphology analysis done with SEM/BSE, EDS and AFM. *Chapter 6* contains the analysis on the crystal structure and also CL scans and CL and PL measurements. *Chapter 7* contains the degradation studies and depth profile analysis. *Chapter 8* includes XPS and peak fitting data for chemical change identification. The conclusion and future work is outlined in *chapter 9* and *Appendix A* contains the publications and conference participation.

### References

1. J. J. Dolo, J. J. Terblans, B. F. Dejene, O. M. Ntwaeaborwa, E. Coetsee and H. C. Swart, Phys.Stat.Sol. (c), **5(2)** (2008) 594.
2. H. C. Swart, J. J. Terblans, O. M. Ntwaeaborwa, E. Coetsee, B. M. Mothudi and M. S. Dhlamini, Nucl. Instr. and Meth. B, **267 (16)** (2009) 2630.
3. H. C. Swart, E. Coetsee, J. J. Terblans, J. M. Fitz-Gerald and J. R. Botha, EJSSNT, **7** (2009) 369.
4. B. M Mothudi, O. M. Ntwaeaborwa, J. R Botha and H. C. Swart, Physica B, accepted June 2009.

5. K. T. Hillie and H. C. Swart, *Appl. Surf. Sci.*, **183** (2001) 304.
6. K. T. Hillie, C. Curren and H. C. Swart, *Appl. Surf. Sci.*, **177** (2001) 73.
7. L. Chen, Particles generated by pulsed laser ablation, in D. B. Chrisey, G. K. Hulber (Eds), *Pulsed Laser Deposition of Thin Films*, John Wiley & Sons, Inc, New York, (1994) chap. no. 6, p. 167.
8. E. Gyorgy, I. N. Mihailescu, M. Kompitsas and A. Giannoudakos, *Appl. Surf. Sci.*, **195** (2002) 270.
9. X. W. Sun and H. S. Kwok, *Appl. Phys. A, Mat. Sci. and Proc.*, **69** (1999) 39.
10. P. H. Holloway, J. Sebastian, T. Trottier, S. Jones, H. C. Swart and R. O. Peterson, *Mat. Res. Soc. Symp. Proc.*, **424** (1997) 425.
11. E. J. Bosze, G. A. Hirata, J. McKittrick and L. E. Shea, *Mat. Res. Soc. Symp.*, **508** (1998) 269.
12. H. C. Swart and K. T. Hillie, *Surf. Interface Anal.*, **30** (2000) 383.
13. S. Shionoya and W. M. Yen, *Phosphor Handbook*, CRC Press LLC, Boca Raton, (1999) p. 4, 21, 49, 61, 85, 178, 186.
14. <http://scienceworld.wolfram.com/> [Accessed 13 February 2006].
15. N. Karar and H. Chander, *J. Phys. D: Appl. Phys.*, **38** (2005) 3580.
16. Q. Y. Zhang, K. Pita, S. Buddhudu, and C. H. Kam, *J. Phys. D: Appl. Phys.*, **35** (2002) 3085.
17. E. J. Bosze, G. A. Hirata, and J. McKittrick, in: *Proc. Mater. Res. Soc.*, **558** (1999) 15.
18. X. Ouyang, A. H. Kitai and R. Siegele, *Thin Solid Films*, **254** (1995) 268.
19. E. J. Bosze, G. A. Hirata, L. E. Shea-Rohwer and J. McKittrick, *J. of Lumin.*, **104** (2003) 47.
20. E. Coetsee, J. J. Terblans and H. C. Swart, *J. of Lumin.*, **126** (2007) 37.
21. E. Paparazzo, *Surface Sci.*, **234** (1990) L253.
22. X. Liu, J. C. H. Phang, D. S. H. Chan and W. K. Chim, *J. Phys. D, Appl. Phys.*, **32** (1999) 1563.
23. L. N. Skuja and W. Entzian, *Phys. Stat. Sol. (a)*, **96** (1986) 191.
24. L. N. Skuja, A. N. Streletsky and A. B. Pakovich, *Solid State Comm.*, **50** (1984) 1069.

## Chapter 2

### Phosphors

This chapter gives a brief description on the basic principles of phosphors and the emission mechanism of the two basic types of phosphor materials. It also mentions some literature on the phosphor research being done and a basic description of the  $\text{Y}_2\text{SiO}_5\text{:Ce}$  phosphor material with the energy levels involved during luminescence.

#### 2.1 Different phosphors

A phosphor is a substance or material that exhibits the phenomenon of luminescence. It consists of a host material, which is normally either an insulator or semiconductor with a wide band gap, to which a dopant (usually a rare earth) is added as activator for conduction or luminescence. The host materials are typically [oxides](#), [nitrides](#) and [oxynitrides](#), [sulfides](#), [selenides](#), [halides](#) or [silicates](#) of [zinc](#), [cadmium](#), [manganese](#), [aluminum](#), [silicon](#), or various [rare earth](#) metals. Phosphors can be divided into 2 main categories: i) band gap and ii) intra atomic.

##### 2.1.1 Band gap

In solid state materials there are different crystal structures and lattices with each atom in the lattice having electrons that can exist in discrete electronic energy levels and bonding states. All of these energy levels and bonding states coalesce throughout the lattice and forms *energy bands* (combines all atoms in the lattice). The discreteness of the electronic energy levels therefore restricts the electrons to certain *energy bands*. This results in energy bands having high (conduction) and low (valence) energy states with an energy range in between (Fig. 1). This energy range is called the “band gap” or “energy gap” ( $E_g$ ) and relates to the energy difference (in electron volts) between the top of the valence band and the bottom of the conduction band. Electrons are forbidden to exist in this energy gap. The energy gap differs from material to material and electrons can get

excited across this band from the lower energy bands (valence) to the higher (conduction) bands.

In conductors (metals) (see Fig. 2(a)), the valence and conduction band overlaps slightly, so conduction and transition occur effortlessly. In semiconductors the bands are separated with a small gap in between (smaller than 3 eV) and with insulators the separation between the bands are very wide [1]. For electrons to be able to get excited from the valence to the conduction band in semiconductors and insulators, absorption of extra energy is required. The electrons in the valence band can therefore get excited to higher energy bands via energy transferred from an external source such as photons. If an electron is excited to a higher state an electronic hole (or unoccupied state) is left behind in the valence band and these holes react as positively charged particles. In semiconductors the electrons in the conduction band and holes in the valence band contribute to electrical conductivity.

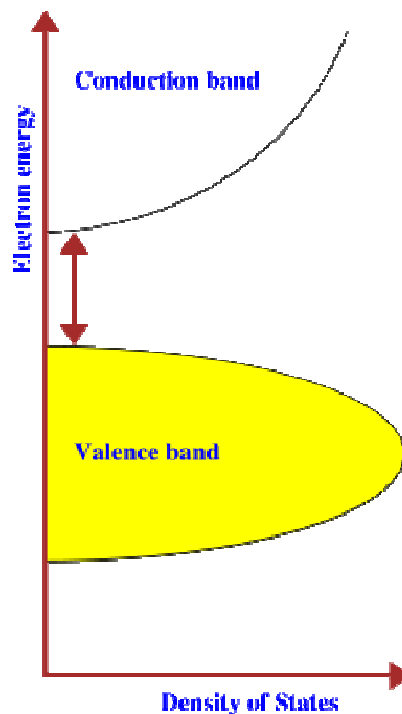


**Figure 1: An illustration of the band gap [1].**

Semiconductors are very useful for construction of electronic devices as their conductivity can be modified by adding impurities into their crystal structures. This

process of adding impurities is called doping and extreme caution is needed during this process. The materials chosen as suitable dopants depend on the atomic properties of both the dopant and the material to be doped. In general, dopants that produce the desired controlled changes are classified as either electron acceptors or donors. Doping a semiconductor crystal introduces allowed energy states within the band gap but very close to the energy band that corresponds with the dopant type (Fig. 2(b)). In other words, donor impurities create states near the conduction band while acceptors create states near the valence band [2].

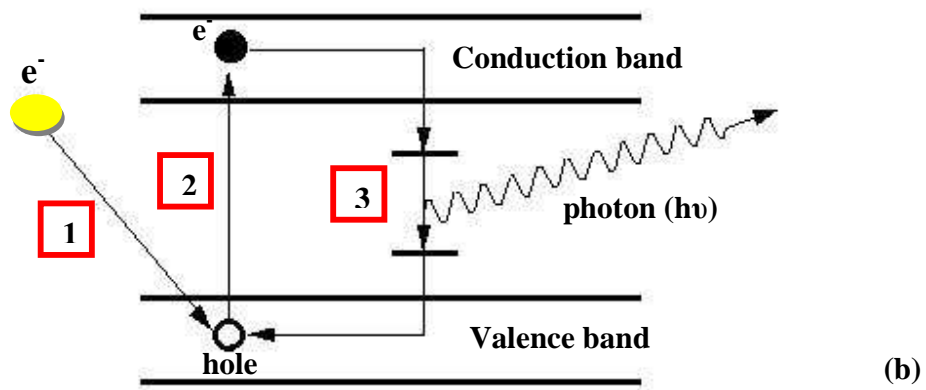
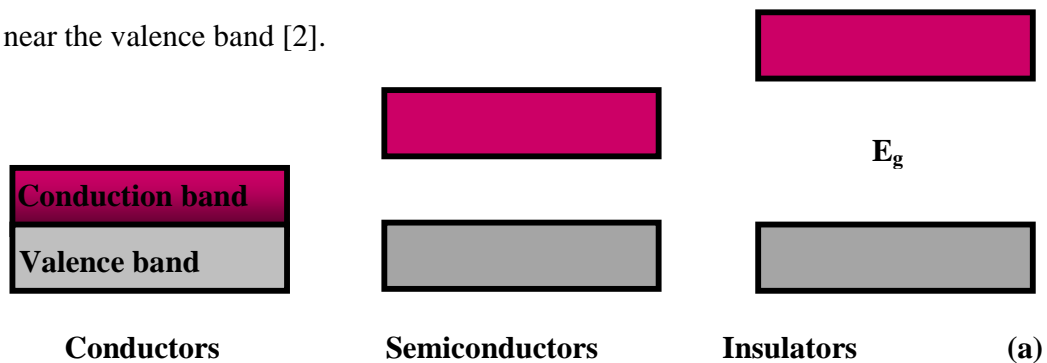


**Figure 2: Schematic diagram indicating a) the  $E_g$  difference between conductors, semiconductors and insulators and b) band gap luminescence.**

These *states* in the band gap, created by the dopant, creates the opportunity for conduction, excitation, transition and relaxation to occur due to lesser energy needed for the electrons to get excited in the band gap to lower energy levels than the conduction

band. *Band gap luminescence* therefore includes a mechanism with 3 main processes (Fig. 2b)): 1 – absorption of energy from an external source, such as an electron beam, to electrons in the valence band, 2 – excitation of these electrons from the valence to the conduction band and 3 – emission of photons as relaxation of the excited electrons occur to lower bands in the band gap. A *band gap phosphor* would thus be classified as a phosphor emitting photons via a mechanism that includes excitation and relaxation to and from the conduction and valence band (and acceptor and donor levels close to the conduction and valence band).

### 2.1.2 Intra atomic

*Intra atomic* literally means *within an atom* and can sometimes be referred to as *characteristic*. If the host lattice is doped with either transition (3d) or rare-earth (4f) metal ions, some of the host lattice's cations can be substituted. In this specific case the excitation of the electrons in the valence band will then be to higher energy levels in the dopant's ions (which is partially filled). Relaxation will then be to either lower energy levels in the dopant's ions or to the valence band (or energy levels close to the valence band). *Intra atomic luminescence* therefore includes the same 3 main processes for band gap luminescence, with the difference in that the excitation and relaxation occurs in the dopant's (rare-earth or transition ion) energy levels, which is situated inside the band gap of the host material. A *characteristic phosphor* would therefore be a phosphor emitting photons via a mechanism where the transitions occur in the dopant's electrical energy levels. Fig. 3 shows a schematic diagram of intra atomic luminescence.

### 2.1.3 Different phosphor materials

Different phosphor materials emit photons at different energies and therefore different colours. The following is just a few examples of different phosphor materials and the colour of emission:

- ZnS:Cu,Al, green - for television screens
- ZnS:Ag,Cl or ZnS:Zn, blue - for display tubes
- (Zn,Cd)S:Ag or (Zn,Cd)S:Cu, yellow-green - for display tubes
- ZnS:Ag, blue – for television screens

- $\text{Zn}_2\text{SiO}_4:\text{Mn}$ , yellowish-green - for display tubes
- $\text{MgF}_2:\text{Mn}$ , orange - for radar screens
- $\text{Gd}_2\text{O}_2\text{S}:\text{Eu}$ , red - for high X-ray absorption
- $\text{Y}_3\text{Al}_5\text{O}_{12}:\text{Tb}$ , yellow-green - for projection tubes [3]
- $\text{SiO}_2:\text{PbS}$ , red – for television screens (Fig. 4a))
- $\text{Y}_2\text{SiO}_5:\text{Ce}$ , blue – field emission displays (Fig. 4b))
- $\text{SrAl}_2\text{O}_4:\text{Eu}^{2+},\text{Dy}^{3+}$ , green – for long afterglow (Fig. 4c))

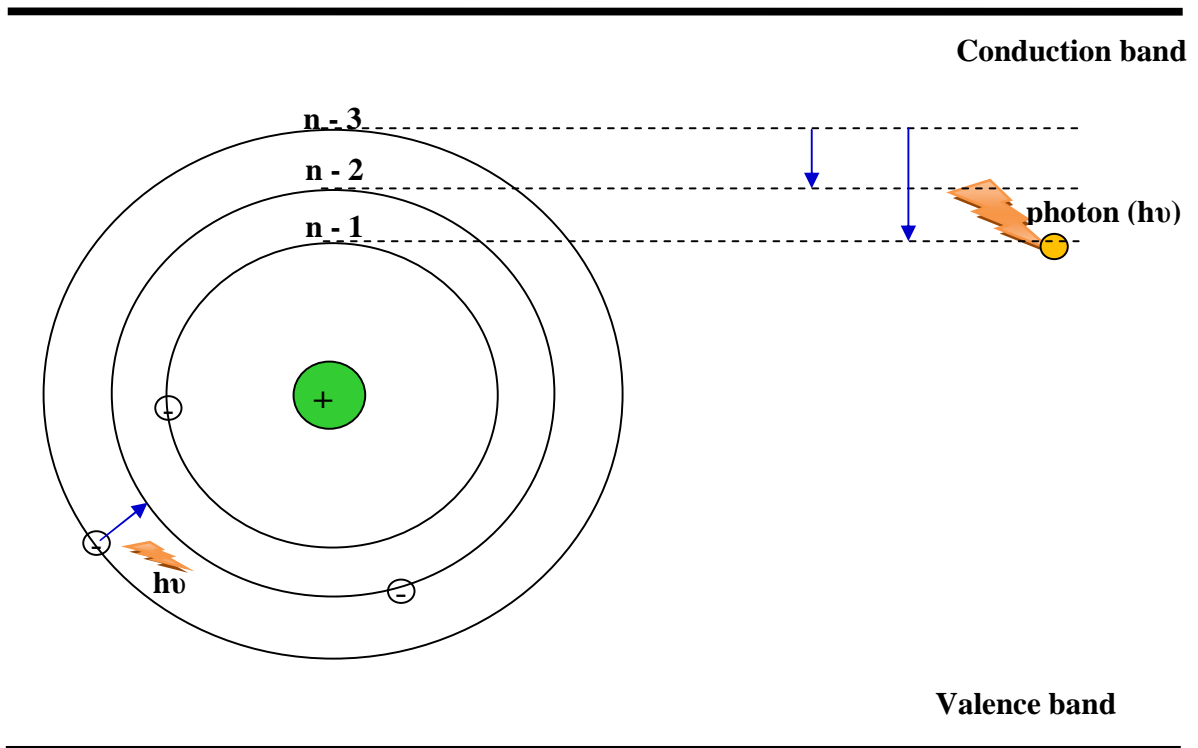


**Figure 3: Schematic diagram illustrating intra atomic luminescence.**

#### 2.1.4 Charge Transfer

Energy and charge transfer are also mechanisms that could lead to luminescent enhancement and was reported by some researchers on different phosphor materials [4]. In the next paragraphs a brief introduction on some charge transfer mechanisms that could be possible during luminescence of the  $\text{Y}_2\text{SiO}_5:\text{Ce}$  phosphor material are mentioned.

During preparation methods of the  $\text{Y}_2\text{SiO}_5\text{:Ce}$  phosphor material, as is also the case with all other phosphor materials, there exist the possibility of defects being created in the lattices. Some of these defects are oxygen vacancies. These vacancies are positive when compared to the regular  $\text{O}^{2-}$  site and they can electrostatically attract electrons from nearby ions and form positive and neutral centres. In  $\text{Ce}^{3+}$  doped  $\text{Y}_2\text{SiO}_5$ , for example the only source of electrons available are the  $\text{Ce}^{3+}$  ions. The charge imbalance is therefore stabilized by a transfer of electrons from the  $\text{Ce}^{3+}$  centres resulting in the formation of  $\text{Ce}^{4+}$  centres. These defects or oxygen vacancies and  $\text{Ce}^{4+}$  centres are for some electrostatic reason very close to each other and the distances between them vary. This variation can therefore explain some luminescent bands and structures that differ from the standard luminescent bands or emission peaks [4].

Another possibility is the process of cross relaxation. This is a process where an excited Ce ion transfers some of its energy to a neighbour Ce ion. The transfer occurs between the 5d and the two different 4f energy levels, e.g.  ${}^2\text{D} + {}^2\text{F}_{7/2} \rightarrow {}^2\text{D} + {}^2\text{F}_{5/2}$ .  ${}^2\text{D}$  is the lowest excited state and the transition to the  ${}^2\text{F}_{7/2}$  state, which is the high-energy transition, can either produce a photon or be absorbed by a neighboring Ce ion and excite it to the  ${}^2\text{D}$  state. The transition from the  ${}^2\text{D}$  to the  ${}^2\text{F}_{5/2}$ , which is the low energy transition, does not provide sufficient energy for a neighbouring Ce ion in the ground state to get excited. The transition to the  ${}^2\text{F}_{5/2}$  are therefore more likely to produce a photon [5].

## 2.2 Different luminescence

There are different kinds of luminescence such as chemoluminescence (emission of light as a result of a chemical reaction), bioluminescence (also light emission from a chemical reaction but by a living organism like a firefly), crystalloluminescence (light emission during crystallization), electroluminescence (luminescence as an electrical current pass through a material), cathodoluminescence (emission of light when a material like a phosphor is bombarded with an electron beam generated by an electron gun),

mechanoluminescence (a result from any mechanical action on a solid), photoluminescence (light emission by the absorption of photons and), phosphorescence (type of photoluminescence where the material do not immediately emits light during excitation), fluorescence (type of photoluminescence with immediate emission of photons) and radioluminescence (luminescence that is produced in a material by the bombardment of ionizing radiation such as beta particles) [6]. Cathodoluminescence and photoluminescence are the two forms of luminescence mostly used during phosphor research.

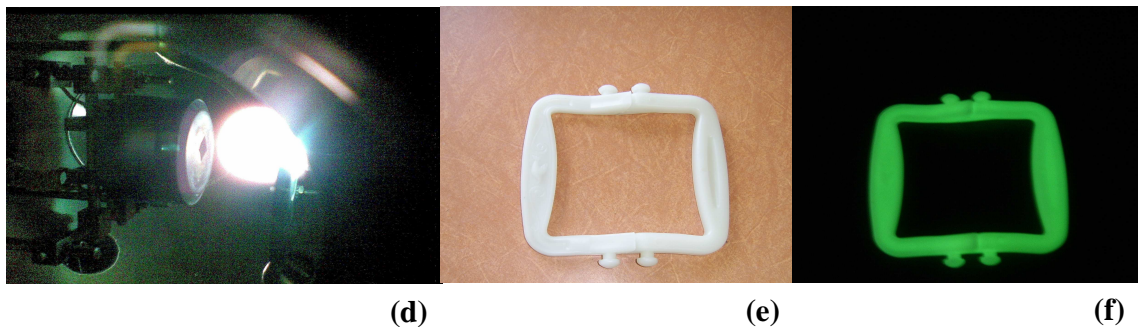
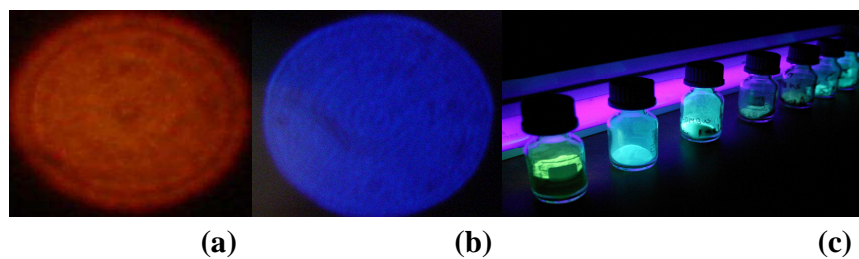


**Figure 4: Digital photos taken; for three different phosphors, a)  $\text{SiO}_2\text{:PbS}$  red, b)  $\text{Y}_2\text{SiO}_5\text{:Ce}$  blue and c)  $\text{SrAl}_2\text{O}_4\text{:Eu}^{2+},\text{Dy}^{3+}$  green emission; d) plasma plume during the growth of  $\text{Y}_2\text{SiO}_5\text{:Ce}$  thin films; long afterglow phosphor  $\text{SrAl}_2\text{O}_4\text{:Eu,Dy}$  mixed with a polymer in the shape of handle bars e) absorption of sunlight, f) phosphorescence during night time.**

### 2.3 Phosphor research being done

Intensive phosphor research has been done on different phosphor materials as the lighting industry develops and the need for improvement expands. Just a few research aspects on the phosphor field:

- Synthesizing the phosphor powders by different techniques (like the sol gel and combustion methods) and growing thin films (with PLD, Fig.4d) are sample preparation techniques that delivered promising results.
- Investigating the luminescent intensities, afterglow and degradation of these as-synthesized phosphors yielded new research fields that exhibit room for improvement.
- Annealing of the samples, changing dopant concentrations, as well as different dopants are also investigated.
- Nano-phosphor particles were a result of some of these synthesized techniques and thin films grown and this added to nano-technology.
- Mixing some of the long afterglow phosphors with polymer materials to investigate the application need of these long afterglow materials (Fig.4e) and f).

## 2.4 Yttrium silicate doped with cerium ( $\text{Y}_2\text{SiO}_5:\text{Ce}$ )

$\text{Y}_2\text{SiO}_5:\text{Ce}$  and other oxide phosphors, have better thermal and chemical stability compared to some sulfides which are currently used in the screens of some displays.  $\text{Y}_2\text{SiO}_5:\text{Ce}$  has a very complicated crystal structure and luminescent mechanism and intense research need to be done to fully understand the setup. From literature it is found that  $\text{Y}_2\text{SiO}_5:\text{Ce}$  has two different monoclinic crystal structures. A low temperature (synthesized at temperatures less than 1190 °C)  $X_1$  - phase (much weaker luminescent intensity [7], with space group  $P2_1/c$ ) and a high temperature (synthesized at temperatures above 1190 °C with a melting temperature at 1980 °C)  $X_2$  - phase (space group  $B2/c$ ). In each of these two phases there are two possible  $\text{Y}^{3+}$  sites in the  $\text{Y}_2\text{SiO}_5$  matrix [7, 8]. These two sites are contributed to the difference in coordination numbers (CN). During the preparation method of  $\text{Y}_2\text{SiO}_5:\text{Ce}$  the activator  $\text{Ce}^{3+}$  (radius of 0.106 nm) can easily substitute  $\text{Y}^{3+}$  (radius of 0.093 nm) thus also resulting in the two different crystallographic sites. The notation A1 and A2 are given to the two sites in the  $X_1$  - phase with CN of 9 and 7. B1 and B2 are denoted to the  $X_2$  - phase with CN of 6 and 7.

A1 with the CN of 9 means that there are 8 oxygens bonded to yttrium and silicon and only 1 that is bonded to only yttrium. CN of 7 means that 4 oxygens are bonded to yttrium and silicon and 3 are bonded to only yttrium. Both B1 and B2 have two oxygens atoms that are only bonded to yttrium [4, 9]. The phosphor used in this study is  $X_1$  - phase as indicated by the XRD results (see chapter 6) and emission spectra [9].

Luminescence in  $Y_2SiO_5:Ce$  occurs due to characteristic transitions (in the  $Ce^{3+}$  ion itself).  $Y_2SiO_5$  has a wide band gap of about 7.4 eV (insulator) so doping it with an activator such as Ce creates an energy level structure inside the wide band gap where the 5d to 4f transition takes place. Splitting of the 4f energy level into the  $^2F_{5/2}$  and  $^2F_{7/2}$  energy levels is due to the  $4f^1$  electron in  $Ce^{3+}$  having the ability to exhibit a  $+1/2$  and  $-1/2$  spin [10, 11]. This creates the expectation of a luminescent spectrum with two main peaks in the blue region (between 400 and 500 nm). However; reports on broad band and double shoulder spectra have been found see Fig. 5a). Part of this research study therefore reports on i) the investigation that was done on the luminescent properties and complex crystal structure (Fig. 5b)) of  $Y_2SiO_5:Ce$  powder and ii) the construction of a more plausible luminescent mechanism.

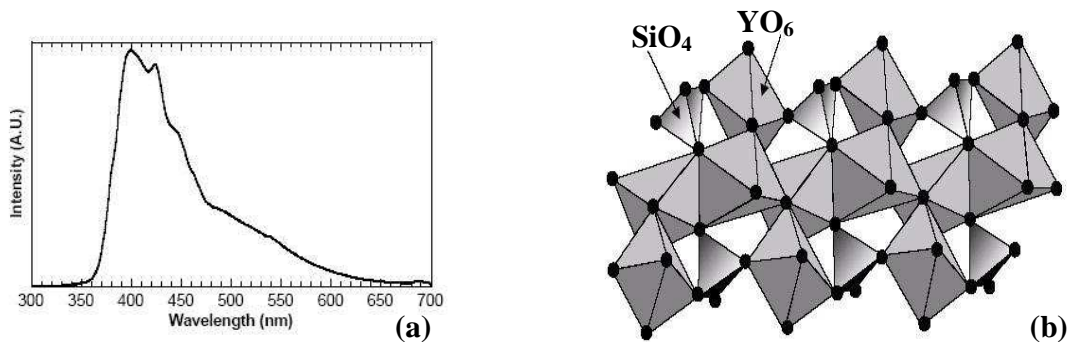
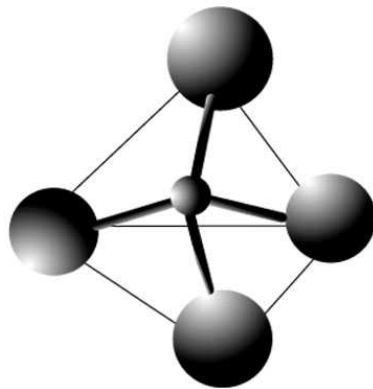
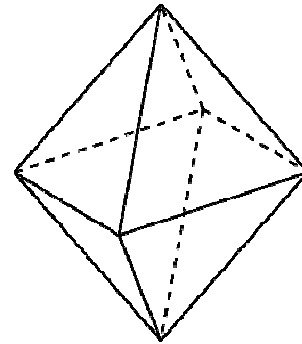


**Figure 5: a)  $(Y_{1-x}Ce_x)_2SiO_5$  emission spectra from Bosze *et al.* [12] and b) schematic crystal structure of  $Y_2SiO_5$  [13].**

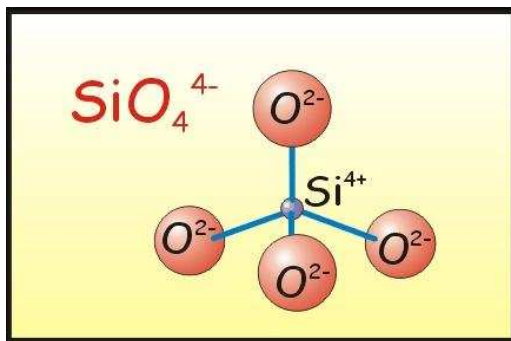
Figure 6 shows the  $SiO_4$  and  $YO_6$  tetra- and octahedron structures that forms the complicated monoclinic crystal structure of  $Y_2SiO_5$  as seen from Fig. 5b).



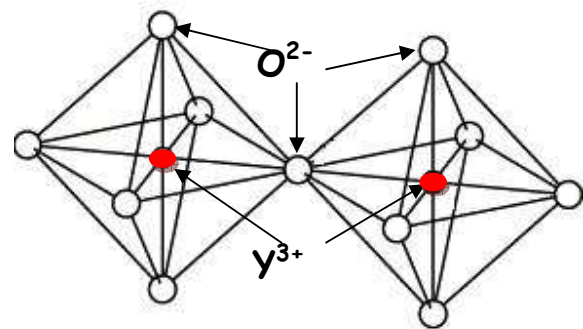
**Tetrahedron**



**Octahedron**



**SiO<sub>4</sub> Tetrahedron**



**Two YO<sub>6</sub> Octahedrons**

**Figure 6: Schematic diagrams illustrating the SiO<sub>4</sub> and YO<sub>6</sub> tetra- and octahedron structures of Y<sub>2</sub>SiO<sub>5</sub> [14, 15, 16].**

## References

1. <http://www.answers.com/topic/band-gap> [Accessed 4 February 2009].
2. <http://en.wikipedia.org/wiki/Semiconductor> [Accessed 4 February 2009].
3. <http://en.wikipedia.org/wiki/Phosphor> [Accessed 4 February 2009].
4. T. Aitasalo, J. Holsa, M. Lastusaari and J. Niittykoski, F. Pelle, *Opt. Mater.*, **27** (2005) 1511.
5. N. Taghavinia, G. Lerondel, H. Makino and T. Yao, *Thin Solid Films*, **503 (1-2)** (2006) 190.

6. <http://en.wikipedia.org/wiki/Luminescence> [Accessed 6 February 2009].
7. H. Jiao, F. Liao, S. Tian and X. Jing, *J. Electrochem. Soc.*, **151** (7) (2004) 39.
8. J. Wang, S. Tian, G. Li, F. Liao and X. Jing, *J. Electrochem. Soc.*, **148** (6) (2001) 61.
9. E. J. Bosze, G. A. Hirata, L. E. Shea-Rohwer and J. McKittrick, *J. Lumen*, **104** (1-2) (2003) 47.
10. P. H. Holloway, J. Sebastian, T. Trottier, S. Jones, H. C. Swart and R. O. Peterson, *Mater. Res. Soc. Symp. Proc.*, **424** (1997) 425.
11. K. T. Hillie and H. C. Swart, *Appl. Surf. Sci.*, **183** (2001) 304.
12. E. J. Bosze, G. A. Hirata and J. McKittrick, *Proc. Mater. Res. Soc.*, **558** (1999) 15.
13. Reactions for Yttrium Silicate High-k Dielectrics, James Joseph Chambers, Ph. D thesis, 2000 p. 33, 41.
14. M. Yoshino<sup>a</sup>, Y. Liua, K. Tatsumib, I. Tanakab, M. Morinagaa and H. Adachib, *Solid State Ionics*, **162** (2003) 127.
15. <http://www.uraniumminerals.com/Tutorials/Silicates/Silicates.htm> [Accessed 6 July 2009].
16. [http://academic.brooklyn.cuny.edu/geology/powell/core\\_asbestos/geology/silicates/intro\\_min/tet\\_roll/tetra\\_roll.htm](http://academic.brooklyn.cuny.edu/geology/powell/core_asbestos/geology/silicates/intro_min/tet_roll/tetra_roll.htm) [Accessed 6 July 2009].

## Chapter 3

### Pulsed laser deposition (PLD)

This chapter gives a short description of the pulsed laser deposition (PLD) technique used for the growth of the thin films. It also explains the effect of some process parameters during the growth technique.

#### 3.1 Description of the technique

The principle of PLD is a very complex physical phenomenon. This is in contrast with the simplicity of the basic setup of the PLD system; see Fig.1. It is a technique used for growing thin films and it basically involves the evaporation of a target material with short and intensive laser pulses (typically 30 ns pulses with energy in the range of 0.1 – 1 J and a frequency of 1 – 20 Hz). These high powered laser pulses are focussed onto a target inside a vacuum chamber. The ablation process can however occur in ultra high vacuum or in the presence of some background gas. Evaporation of the target material forms a plasma plume which expands and flows towards a substrate such as a silicon wafer mounted inside the chamber. The particles in the plume condense onto a heated substrate and a thin film is grown.

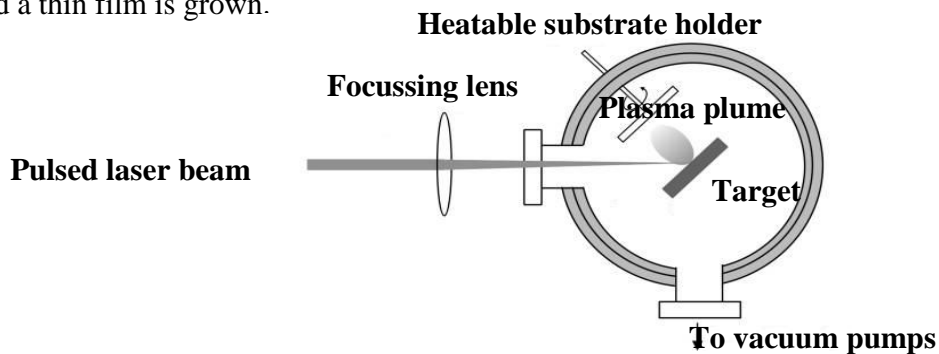


Figure 1: Schematic diagram of a PLD system setup [1].

#### 3.1.1 History

The history of PLD started with the stimulated emission process postulated by Einstein in 1916. The laser assisted thin film growth started soon after Maiman constructed the first

optical maser (a rod of ruby as the lasing medium) in 1960. In 1962, Breech and Cross used a ruby laser to vaporize and excite atoms from a solid surface. Three years later (1965), Smith and Turner used the ruby laser to deposit thin films and this marked the very beginning of the development of the PLD technique. The deposited thin films were still inferior to thin films grown with other techniques such as chemical vapour deposition and molecular beam epitaxy, but in the early 80's a group of researchers in the former USSR achieved remarkable results on manufacturing thin-film structures using laser technology.

The breakthrough came in 1987 when Dijkkamp and Venkatesan used PLD to successfully grow a high-temperature superconductive material ( $\text{YBa}_2\text{Cu}_3\text{O}_7$ ), which was of more superior quality than films grown with other techniques. Since then the technique of PLD was used to fabricate high quality crystalline films, such as ceramic oxides, nitride films, metallic multilayers and various superlattices. This led to rapid development of laser technology in the 1990's such as lasers having higher repetition rate and shorter pulse durations than the early ruby lasers. This ensured the growth of well defined thin films with complex stoichiometry [2, 3].

### **3.1.2 Four stage process:**

The process of PLD can generally be divided into four stages:

1. Laser ablation of the target material and creation of a plasma
2. Dynamic of the plasma
3. Deposition of the ablation material on the substrate
4. Nucleation and growth of the film on the substrate surface.

#### **3.1.2.1. Laser ablation of the target material and creation of a plasma:**

As the laser pulse is absorbed by the target, energy is first converted to electronic excitation and then to thermal, chemical and mechanical energy resulting in evaporation, ablation, plasma formation and exfoliation. The evaporation of the bulk material is

caused by Coulomb explosion and there are different mechanisms related to the laser-target interaction. The incident laser pulse penetrates the surface of the material within the penetration depth which is dependent on the laser wavelength and index of refraction of the target material at the applied laser wavelength. (This typically is in the region of 10 nm for most materials).

A process called electronic sputtering is the main mechanism that causes vaporization of the target material in PLD. An averaged electrical field is generated by the incident photons from the laser light and this is sufficiently strong enough to remove the electrons from the bulk material of the penetrated volume [2, 4]. Electron-hole-pairs are created and a direct consequence of the electron-lattice interactions is an increase in the lattice temperature followed by the desorption of particles. This process occurs within 10 ps of a ns laser pulse and the material is vaporised due to the target surface that gets heated up. The temperature of the generated plasma plume is typically 10 000 K.

The other mechanisms such as hydrodynamic (melting of the target surface and ejection of molten droplets) and exfoliation (target surface cannot reach melting point, thermal stresses are not released through melting so it leads to cracking of the target and ejection of flakes) sputtering can cause nonuniform erosion of the target, causing the formation of cones and craters or the detachment of flakes or droplets and can usually be determined from the topography of the target after sputtering [2, 4].

#### **3.1.2.2. Dynamic of the plasma:**

A layer of high-pressure vapour particles is produced near the surface of the target. The vaporised particles expel away from the target parallel to the normal vector of the target's surface towards the substrate. This jet of particles expands and forms a plasma plume in accordance with the cosine law [2, 4]. The plume can contain a variety of particles such as atoms, ions, electrons and atomic clusters. The temperature of the particles is high and atoms in the plume can easily be ionized as there is plenty of thermal energy available.

The spatial distribution of the plume is dependent on the background pressure inside the PLD chamber. In vacuum, the plume is very narrow and forward directed, almost no scattering occurs with the background gasses. There is also an intermediate region of the plume where a splitting between the high and low energetic particles can be observed. At high background pressures more collisions and scattering of the particles in the plume occur. The increase in scattering due to the high background pressure leads to a reduction of kinetic energies of the particles (the particles get slowed down). The visibility of the plume is a result of fluorescence and recombination processes occurring in the plasma [2, 4].

#### **3.1.2.3. Deposition of the ablation material on the substrate:**

The quality of the deposited films is determined by this stage. Highly energetic particles ablated from the target can damage the substrate surface by sputtering off atoms and by causing defects in the deposited film. A collision region is formed between the particles emitted from the target and sputtered species from the substrate. This serves as a condensation source of particles [2].

#### **3.1.2.4. Nucleation and growth of the film on the substrate surface:**

The growth of the thin films is considered by theoretical nucleation and growth models. There are three predictable modes: three-dimensional growth of islands (Volmer-Weber nucleation and growth), two-dimensional growth of monolayers (Frank-van der Merwe) and the formation of full monolayers followed by the growth of separate three-dimensional islands (Stranski-Krastinov) [4]. The thermodynamics of the surface energies of the film and the substrate determines which mode dominates the growth of the film.

The three-dimensional growth involves a number of processes taking place after the particles have arrived on the substrate. Some of these processes are atom deposition on substrate, re-evaporation from substrate, cluster (island) nucleation, diffusion to cluster, atom deposition of cluster, re-evaporation from cluster and dissociation of cluster.

If the film surface energy is low and the substrate energy is high it is more likely for the film to grow as complete monolayers instead of three-dimensional islands. The atomic processes are essentially the same as for the three-dimensional growth, except that the thickness of the islands corresponds to only one monolayer.

The third possible mode begins with complete monolayers. Islands start to form after 1-5 monolayers and the reason for this could be that the lattice stress is higher on the surface of the deposited monolayers than on the bare substrate. It is sometimes assumed that nucleation occurs on random sites, homogeneously on the whole substrate surface, but in practice the surface of the substrate is not uniform enough to ensure homogeneous nucleation. There are always defects and dislocation intersections providing more favourable nucleation sites [4].

### **3.1.3 Advantages of PLD:**

There are a number of advantages of PLD over other film deposition methods:

- i – It is a versatile technique. A wide range of materials such as oxides, metal, semiconductors and even polymers can be grown by PLD.
- ii – It has the ability to maintain target composition in the deposited thin films, keeping the stoichiometry of the target.
- iii – Relatively high deposition rates can be achieved at moderate laser fluences.
- iv – Deposition can occur in both inert and reactive background gasses.
- v – The use of a carousel enables the growth of multilayer films without breaking the vacuum.

### **3.1.4 Disadvantages of PLD:**

- i – The generation of particulates during the deposition process, which is not ideal for the application field.
- ii – The non-uniform layer thickness.
- iii – The ablation plume cross section is generally small and this limits the sample size.
- iv – The deposition of novel materials usually involves a period of optimization of deposition parameters [5, 6].

### 3.2 Process Parameters

The generation of particles during PLD is a major limiting factor during the deposition of thin films. The presence of the particles formed in the thin film inhibits the more widespread application of PLD. Phosphor thin films are an alternative to phosphor powders in the optical display fields (FEDs, liquid crystal displays (LCDs)). The reason for this is even though the powders are much more efficient, the particle size may limit resolution of the display. Table 1 shows some comparison between the powders and thin films.

<i>Property</i>	<i>Thin film phosphor</i>	<i>Phosphor powder</i>
Efficiency	Poor	Excellent
Resolution	< 1 $\mu\text{m}$	5 – 10 $\mu\text{m}$
Screen contrast	Excellent	Good
Lifetime	Good	Poor
Mechanical stability	Excellent	Good
Thermal stability	Excellent	Good

**Table 1: A comparison between phosphor thin films and powders for displays [7].**

However; the growth of these thin films with PLD results in thin films with different surface morphologies than what is needed for optimum use in the display field. The ideal thin film surface should be uniform and smooth with no loose or big micron particles that can be detrimental to the display systems. One solution to address this major problem would be modifications to the surface by optimization of the process parameters. Some of these parameters are:

1. The ambient pressure
2. the laser fluence and
3. the substrate temperature.

Intensive research on optimization of process parameters has also been done with guidelines and consensus available from literature; basically each material analysed produces different results. In the end a basic structure can be proposed in order to grow the best phosphor thin film for optimum use in displays.

The particles generated by PLD can basically be classified in three categories, depending on whether the original matter, when just ejected from the surface, is in the solid, liquid or vapour state. In general, the particles formed from the vapour state are in nano - meter range while the other two states are in micron or submicron range. The shape of the particles formed from the liquid state tends to be spherical, from the solid they tend to be irregular in shape and they may be formed spherical or polyhedral from the vaporised state. It is however difficult to establish a correlation between deposition parameters and the size and shape of particles generated [8].

### **3.2.1 The ambient pressure:**

An ambient is deliberately introduced during PLD to form particles with a desired size. Ultrafine particles can be formed with particle diameters in the range of a few nano - meters to a few tens of nano - meters. An example is research done by Matsunawa *et al.* [9] on the production of ultrafine powders of various metals (Fe, Ni, and Ti) in Ar and He ambient. The decrease in ambient pressure resulted in a decrease in particle size.

The ambient pressure therefore determine the mean free path length, the kinetic energy, the resident stay time of the particles in the plume and therefore the size of the particles adhering onto the substrate. At a pressure of the order of 1 mTorr, the mean free path length is approximately 5 cm. At a higher pressure of about 100 mTorr the path length becomes 0.05 cm. The increased collisions decreases the kinetic energies of the particles, slowing them down, increasing their stay time in the plume as they move slower and this gives them enough time to nucleate and grow into bigger nano – particles. An increase in the gas pressure would then increase the particle sizes as a result of increased collisions between the gas particles and the particles in the plume [10, 11, 12].

Scharf and Krebs [11] studied the influence of inert gas pressure on deposition rate during PLD. The deposition rates of permalloy (Py) and silver (Ag) were monitored during the deposition in inert helium (He), neon (Ne), Ar and xenon (Xe) gas. They have reported that under ultrahigh vacuum, resputtering from the film surface occurs due to the

presence of energetic particles in the plasma plume. With increasing gas pressure, a reduction of the particle energy is accompanied with a decrease of resputtering and a rise in the deposition rate. At higher gas pressures, scattering of ablated material out of the deposition path between target and substrate was observed, and this led to a decrease in the deposition rate. The maximum deposition rate was obtained in a He pressure of about 300 mTorr. Their results were interpreted as follows:

At very high gas pressures the number of gas atoms in the deposition channel is much higher than the number of ablated particles. The plasma expansion leads to a shock front between the plasma plume and the surrounding gas. The shock front acts like a dynamic pressure and hinders the expansion of the plasma plume towards the substrate. This effect is not so strong at the sides of the plume so the plume expands sideways and therefore results in a reduction in deposition rate on the substrate.

Sturm, Fahler and Krebs [13] presented a similar model while investigating the PLD of metallic systems (Ag, Fe and Fe/Ag) in low pressure (30 mTorr) Ar gas. Time-of-flight (TOF) and deposition rate measurements showed a reduction of particle energy with increasing Ar pressure. They explained their results by the scattering of a dense cloud of ablated material in a diluted gas. They have also assumed that the Ar gas atoms are at rest relative to the ablated ions and atoms in the plume, which are much faster (by a factor of about 30 and 5 respectively). A dense cloud of ablated particles therefore has to move through the almost static and diluted arrangements of Ar atoms.

The ions (for example Ag ions) in the plume collide with Ar atoms and the Ar atoms themselves get scattered out of the flight path of the ablated material between the target and the substrate. Thus as the colliding Ar atoms are removed from the flight path, the following slower ions and atoms fly through a significantly reduced Ar atom density and have a higher probability to reach the substrate. In other words, as the faster ions and atoms are scattered and not deposited they open a channel for the deposition of the slower particles. This model is however valid for metals only for pressures below 75 mTorr since the number of ablated ions has to be higher than that of the gas atoms in the

relevant volume. In oxide materials the ablation rate is ten times higher, therefore the above model should be even more suitable.

A comparison between Ar and O<sub>2</sub> ambient were investigated by Long *et al.* [14] while analysing the growth and characteristics of titanium dioxide (TiO<sub>2</sub>) thin films grown on Si (100) substrates by PLD. The XRD results showed that an increase in O<sub>2</sub> pressure to 225 mTorr resulted in an amorphous ((004)-oriented anatase phase) TiO<sub>2</sub> film. At the same pressure conditions (37.5 mTorr) the films ablated in Ar gas resulted in a (110)-oriented rutile phase TiO<sub>2</sub> layer. This was ascribed to the high ambient pressure that decreased the kinetic energy of the particles in the plume but that the reduction of kinetic energy in Ar gas was smaller than in O<sub>2</sub>. Thus the plasma was prevented to reach the substrate and to form a good crystalline layer in both cases but the surface mobility of the reduced ablated species that did reach the substrate in Ar gas was much higher and resulted in the rutile phase film.

Shen *et al.* [12] reported on large grains that formed by agglomeration of particles as the ambient Ar pressure increased to 375 mTorr. PLD was used to fabricate bismuth doped ZnSe films on Si (100) substrate in an Ar ambient and the SEM images showed that the agglomerated particles became larger as the ambient pressure increased. Similar results were found when ZnSe films were prepared in a N<sub>2</sub> ambient. This was also explained by the increased collisions which lead to the formation of larger particles during the flight of the ablated species toward the substrate.

The effect of N<sub>2</sub> pressure on the two-step method (PLD and anneal) deposition of GaN films were studied by Liu *et al.* [15]. They have mentioned that the collisions and scattering of the ablated species by N<sub>2</sub> molecules before they reach the substrate will influence the status, amount and kinetic energy of the ablated particles that arrive at the substrate surface. At low N<sub>2</sub> pressures (1.1 mTorr, 5.6 mTorr) the collision rate is low and the incident particles have such high kinetic energies that they are re-sputtered from the sapphire (0001) substrate and result in a poor thin film. Increasing the pressure to 11 mTorr increased the collisions in the plume and also reduces the number of particles

arriving at the substrate. Those particles also have too low energies to migrate to the right positions for good crystalline films but after annealing of this film, the particles on the surface achieve higher mobility and formed high orientation films.

### **3.2.2 The laser fluence:**

The laser fluence consists of two variables: the laser energy or power and the laser spot size. Tighter focus at constant laser power increases the particles' number density. In general, there exist a threshold value below which the particles are barely visible, for example for YBCO materials the threshold fluence for the occurrence of particles is about  $0.9 \text{ J/cm}^2$  (when a XeCL 308 nm excimer laser with 20 ns pulses are used) [8]. Above the threshold fluence, the particle number density increases with increasing fluence and decrease again at higher fluence indicating saturation.

Tong *et al.* [16] reported on the effect of increased laser fluence on the structural and optical characteristics of CdS thin films grown onto Si (111) and quartz substrates. XRD results showed that an increase in the laser incident energy from 0.5 mJ/pulse to 1.2 mJ/pulse lead to more intense and sharper CdS diffraction peaks. This means that the crystalline quality of the films improved with increased fluence. The increased energy cause an increase in plasma density and ion energy, an enhancement of mobility of the deposited atoms on substrate surface and this result in better orientation and thus improved crystallinity. Too high laser fluence may lead to too high plasma density and the growth of bulky grains. The size of the particles and the number of cluster particles can therefore be increased with increased laser incident energy and thus also improve the PL intensity.

The improvement of crystallization with increased laser fluence ( $1.8 - 2 \text{ J/cm}^2$ ) was also showed by Fang *et al.* [17].  $\text{CaCu}_3\text{To}_4\text{O}_{12}$  (CCTO) thin films were grown on Pt/Ti/SiO<sub>2</sub>/Si substrates by PLD and results showed that a low fluence lead to low kinetic energies of the particles ejected from the target as well as a low particle density. This resulted in a discontinuity of the grain growth of CCTO films and a degradation of dielectric properties.

### 3.2.3 The substrate temperature:

The substrate temperature also plays a significant role during PLD and influences the kinetic energies of the particles on the substrate surface. Cho *et al.* [18] noted during the investigation of optical properties of sol-gel derived  $\text{Y}_2\text{O}_3:\text{Eu}^{3+}$  thin film phosphors for display applications, that an increase in the substrate temperature improved the crystallinity and luminescent intensities of thin film phosphors.

This was also reported by Kang *et al.* [19] while investigating the effect of substrate temperature on structural, optical and electrical properties of ZnO thin films deposited by PLD. The substrate temperature not only affects the crystallinity but it can also influence the thin film composition. XRD results showed a constraint in the growth of the crystal due to low atomic mobility at a deposited temperature of 100 °C. An increase to 500 °C supplied the atoms on the substrate surface with more thermal energy and thus increased their surface mobility that lead to better crystallization. However too high temperatures such as 700 °C can decrease the crystallinity of the thin films due to desorption and dissociation of atoms.

AFM images showed nano - metre sized grains and at 100 °C substrate temperature there was a mixture of small grains and large grains [19]. As the substrate temperature increased to 500 °C larger and more uniform grains formed that increased the surface roughness. At 700 °C a decrease in the surface roughness was however observed. The intensity of the UV emission peak also increased at increased substrate temperatures to 500 °C. A decrease in intensity was observed as the temperature increased to 700 °C. So the increased substrate temperature definitely has an effect of a rougher surface morphology that can influence optical properties.

Figure 2 shows images of plasma plumes created by PLD. The colour of the plume is

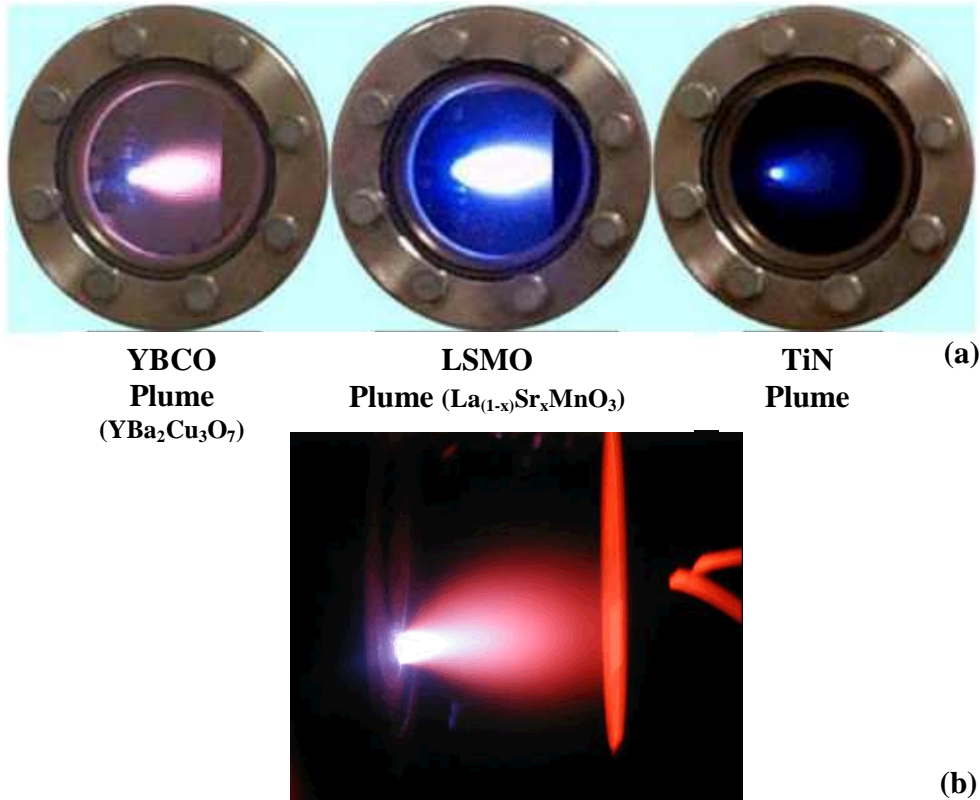


**Figure 2: a) Examples of plasma plumes formed during PLD and b) also showing a heated substrate holder typically in the order of 700 °C [20, 21].**

mainly a fluorescence result from the type of material being ablated and the length and volume of the plume is dependent on the ambient pressure. The more the ambient pressure the smaller the plume and visa versa [20].

## References

1. <http://www.chm.bris.ac.uk/laser/ashfold/ablation.htm> [Accessed 9 February 2009].
2. [http://en.wikipedia.org/wiki/Pulsed\\_laser\\_deposition](http://en.wikipedia.org/wiki/Pulsed_laser_deposition) [Accessed 9 February 2009].
3. <http://pulsedlaser.net/2.html> [Accessed 9 February 2009].
4. <http://www.orc.tut.fi/PLD-report%20PULSAR-project.pdf> [Accessed 9 February 2009].

5. T. J. Jackson and S. B. Palmer, *J. Phys. D: Appl. Phys.*, **27** (1994) 1581.
6. <http://www.andor.com/learn/applications/?docid=66> [Accessed 9 February 2009].
7. S. L. Jones, D. Kumar, K. G. Cho, R. Singh and P. H. Holloway, *Displays*, **19** (1999) 151.
8. L. Chen, Particles generated by pulsed laser ablation, in D. B. Chrisey, G. K. Hulber (Eds), "Pulsed Laser Deposition of Thin Films", John Wiley & Sons, Inc, New York, (1994) chap. no. 6, p. 167.
9. A. Matsunawa, S. Katayama, A. Susuki and T. Ariyasu, *Trans. J. Welding Res. Inc.*, **15** (1986) 61.
10. Krebs, M. Weisheit, J. Faupel, E. Suske, T. Scharf, C. Fuhse, M. Stormer, K. Sturm, M. Seibt, H. Kijewski, D. Nelke, E. Panchenko and M. Buback, "Pulsed Laser Deposition (PLD) – a Versatile Thin Film Technique", B. Kramer, *Advances in Solid State Physics*, Springer Berlin/Heidelberg, **43** (2003) 101.
11. T. Scharf and H. U. Krebs, *Appl. Phys. A*, **75** (2002) 551.
12. Y. Shen, N. Xu, W. Hu, X. Xu, J. Sun, Z. Ying and J. Wu, *Solid State Electron.*, **52** (2008) 1833.
13. K. Sturm, S. Fahler and H. Krebs, *Appl. Surf. Sci.*, **154-155** (2000) 462.
14. H. Long, G. Yang, A. Chen, Y. Li and P. Lu, *Thin Solid Films*, **517** (2008) 745.
15. M. Liu, B. Y. Man, C. S. Xue, H. Z. Zhuang, H. C. Zhu, X. Q. Wei and C. S. Chen, *Appl. Phys. A*, **85** (2006) 83.
16. X. L. Tong, D. S. Jiang, L. Liu, Z. M. Liu, M. Z. Luo, *Optics Communications*, **270** (2007) 356.
17. L. Fang and M. Shen, *J. Crystal Growth*, **310** (2008) 3470.
18. J. Y. Cho, K. Ko and Y. R. Do, *Thin Solid Films*, **515** (2007) 3373.

19. S. J. Kang, Y. H. Joung, H. H. Shin and Y. S. Yoon, *J. Mater. Sci: Mater. Electron*, **19** (2003) 1073.
20. [http://resources.edb.gov.hk/physics/articleIE/pld/pld\\_c.htm](http://resources.edb.gov.hk/physics/articleIE/pld/pld_c.htm) [Accessed 17 February 2009].
21. <http://www.geocities.com/xsrao/research.htm> [Accessed 17 February 2009].

## Chapter 4

### The luminescent mechanism of $\text{Y}_2\text{SiO}_5:\text{Ce}$

The luminescent mechanism and degradation of the  $\text{Y}_2\text{SiO}_5:\text{Ce}$  powder are outlined in this chapter. It was constructed by using the powder's luminescent PL and CL spectra and Gaussian fits.

#### 4.1 Introduction

As was mentioned in section 2.4 (chapter 2),  $\text{Y}_2\text{SiO}_5:\text{Ce}$  is a blue emitting phosphor that has two different monoclinic crystal structures ( $X_1$  and  $X_2$  - phase) [1]. In each of these two phases there are two possible  $\text{Y}^{3+}$  sites [1, 2] that are attributed to the difference in coordination numbers (CN) (9 and 7).  $\text{Ce}^{3+}$  has only one electron in the 4f shell, with an electron configuration of  $[\text{Xe}].4f^1.5d^1.6s^2$ . Splitting of the 4f energy level into the  $^2F_{5/2}$  and  $^2F_{7/2}$  energy levels is due to the  $4f^1$  electron in  $\text{Ce}^{3+}$  having the ability to exhibit a  $+1/2$  and  $-1/2$  spin [3, 4].

Luminescence in  $\text{Y}_2\text{SiO}_5:\text{Ce}$  occurs due to characteristic transitions (in the  $\text{Ce}^{3+}$  ion itself). The primary electrons get scattered throughout the host crystal during excitation, eventually transferring energy to the  $\text{Ce}^{3+}$  ion (situated in the band gap of the host material). This results in a luminescent spectrum with two main peaks in the blue region (between 400 and 500 nm). However; there are reports on broad band and double shoulder spectra [1, 2, 3, 4]. This part of the thesis therefore reports on i) an investigation of the luminescent properties of  $\text{Y}_2\text{SiO}_5:\text{Ce}$  powders, and ii) the construction of a plausible luminescent mechanism.

#### 4.2 CL and PL of the $\text{Y}_2\text{SiO}_5:\text{Ce}$ powder

Commercially available  $\text{Y}_2\text{SiO}_5:\text{Ce}$  standard phosphor powder from Phosphor Technology (UK) were investigated with CL and PL. CL spectroscopy was investigated

by using 2 keV electrons, a beam current density of  $52 \text{ mA}\cdot\text{cm}^{-2}$  in ultra high vacuum (UHV) of  $3 \times 10^{-9}$  Torr. The CL measurements were made in an UHV chamber with a PHI model 549 system and the data were collected with an Ocean Optics S2000 spectrometer. PL measurements were done with a HeCd laser ( $\lambda = 325 \text{ nm}$ ) and a Varian Cary Eclipse fluorescent spectrophotometer equipped with a xenon flash lamp ( $\lambda = 325 \text{ nm}$ ). The least square method was used to perform Gaussian peak fits.

### 4.3 Luminescent mechanism of $\text{Y}_2\text{SiO}_5\text{:Ce}$

#### 4.3.1 Excitation

The excitation spectrum of the  $\text{Y}_2\text{SiO}_5\text{:Ce}$  phosphor powder measured at an emission wavelength of 433 nm shows the presence of three main peaks (Fig. 1a)). A linear least square method was used to fit Gaussian peaks to the measured excitation data. Three main peaks situated at 246, 305 and 357 nm were clearly identified. Cooke *et al.* [5] also reported on a PL excitation spectrum for hydrothermally prepared  $\text{Y}_2\text{SiO}_5\text{:Ce}$  nanophosphor powders that crystallize in the  $X_1$  - phase from the  $X_2$  - phased bulk material. The bulk ( $X_2$ ) PL excitation spectra showed three excitation peaks at 265, 310 and 356 nm and the nano ( $X_1$ ) particles showed only a main excitation peak at 366 nm. The excitation spectra (not showed) for different PL emission peaks (emission peaks at 420, 425, 430, 435 and 440 nm) were also investigated. There was no difference in the position of the three main excitation peaks. There was only a slight decrease in intensity.

Aitasalo *et al.* [4] studied the luminescent properties of  $X_1\text{-Y}_2\text{SiO}_5\text{:Ce}$  that was prepared by a sol-gel method and reported on the excitation spectra from the A1 site with two peaks at about 285 and 365 nm. The observation was contributed to the fact that the  $5d^1$  configuration should be split into five different components and that there is a probability that some of the bands overlap with another band since the band width of the observed bands (the two peaks observed) is large. It could also be that the other three bands are situated at higher energy levels.

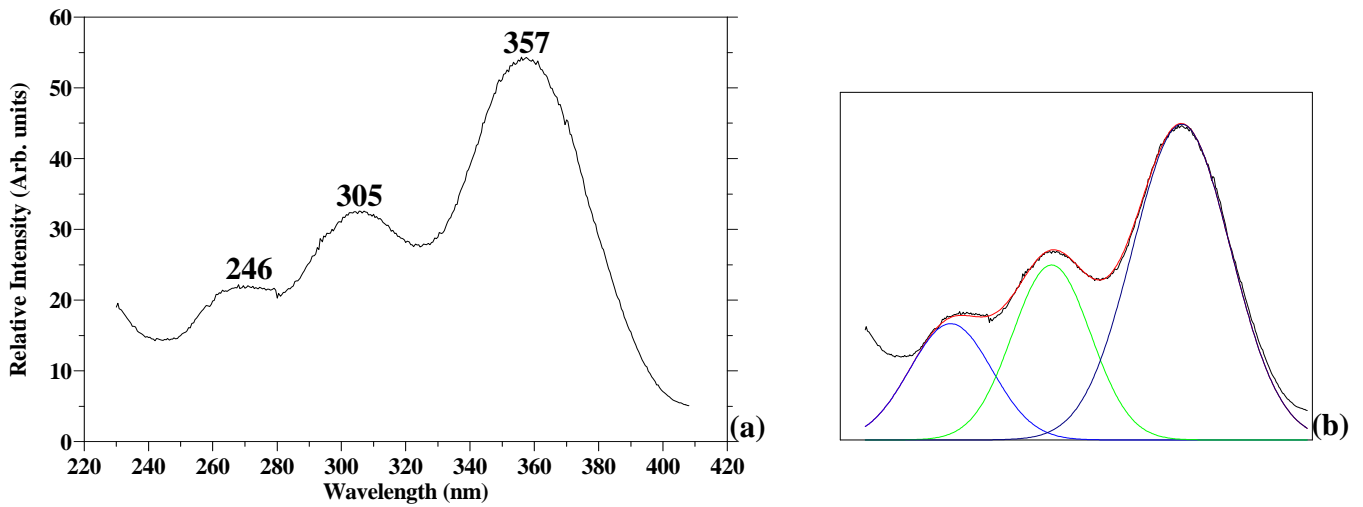


**Figure 1: a) Excitation spectrum and b) Gaussian peak fitting of the Y<sub>2</sub>SiO<sub>5</sub>:Ce phosphor powder. Spectrum excited with a xenon flash lamp.**

Wang *et al.* [2] studied the influence of rare earth elements (Sc, La, Gd and Lu) on the luminescent properties of the blue X<sub>2</sub>-Y<sub>2</sub>SiO<sub>5</sub>:Ce FED phosphor powder. The excitation spectra also showed three peaks at 270, 300 and 360 nm that were ascribed to the transitions from the 4f<sup>1</sup> ground state (<sup>2</sup>F<sub>5/2</sub>) to different crystal field components of the 5d excited states. The splitting of the energy levels (4f and 5d) (crystal field splitting) occurs because of the interactions of the ions and atoms with each other in the crystal field. This effect differs from crystal field to crystal field, depending on the type of materials and crystal structures. For BaMgAl<sub>10</sub>O<sub>17</sub>:Eu<sup>2+</sup>, the emission spectrum consists of a wide band peaking at 450 nm (blue emission), which corresponding to the 5d→4f transitions of the Eu<sup>2+</sup> [6]. The excitation spectrum monitoring at 450 nm emission consists of two wide bands peaking at about 254 and 310 nm, respectively [6]. Zhang *et al.* [6] observed the two peaks for BaMgAl<sub>10</sub>O<sub>17</sub>:Eu<sup>2+</sup> at 230 and 310 nm, respectively. These two peaks were attributed to the field splitting of the Eu<sup>2+</sup> d-orbital [6, 7]. The excitation spectrum of bulk Y<sub>2</sub>O<sub>2</sub>S:Eu<sup>3+</sup> is a wide band with two peaks which are attributed to charge-transfer (CT) transitions. The one at 266 nm corresponds to O–Eu CT band, and the other at 325 nm to the S–Eu charge-transfer band [8]. It is well-known that the CT band is sensitive to the ligand environment (the bonding energy between the central ion and ligand ions). The systematic behavior in the energy bands leads to the

transfer of an electron from the valence band to a trivalent lanthanide. The final state in the transition is the ground state of the divalent lanthanide ion. In the  $Y_2O_2S$  crystal, there are two anions, one is  $O^{2-}$  and the other is  $S^{2-}$  therefore; there are two charge-transfer transitions from the 2p orbital of  $O^{2-}$  to the 4f orbital of  $Eu^{3+}$  and from the 3p orbital of  $S^{2-}$  to the 4f orbital of  $Eu^{3+}$ , respectively [8].

The three peaks in Fig. 1a) might therefore be due to the excitation to three *different* energy levels in either the host's band gap (other luminescent centres) or to energy levels in the  $5d^1$  configuration in the  $Ce^{3+}$  ion inside the band gap, or both. The higher excitation peak (357 nm) in this case may most probable be due to the CT of electrons from the 2p orbital of  $O^{2-}$  to the 4f orbital of  $Ce^{3+}$  and the other two peaks due to the 5 d field splitting. Emission spectra for each excitation band obtained, indicated the familiar broad band emission of  $Y_2SiO_5:Ce$  as can be seen in Fig. 2.

There was a definite increase in intensity as the excitation energy was decreased. No major changes in the broad peak shape or the peak positions for the different emission peaks were measured. The difference in intensity between the high and low energy excitation can be ascribed to the excitation of the electrons to different energy impurity levels in the host band gap itself (defect levels closer to the conduction band). The relaxation to lower levels of these higher excited electrons will either be non-radiative or will relaxed to the 5d state in the  $Ce^{3+}$  ion itself and then further relax radiatively to the 4f level, resulting in the low intensity emission peak. The low excitation energy may lead to excitation directly to the 5d state. This low excitation energy may not be enough for excitation to the higher energy levels close to the conduction band in the host's band gap but high enough for excitation to the 5d levels of the  $Ce^{3+}$  ion.

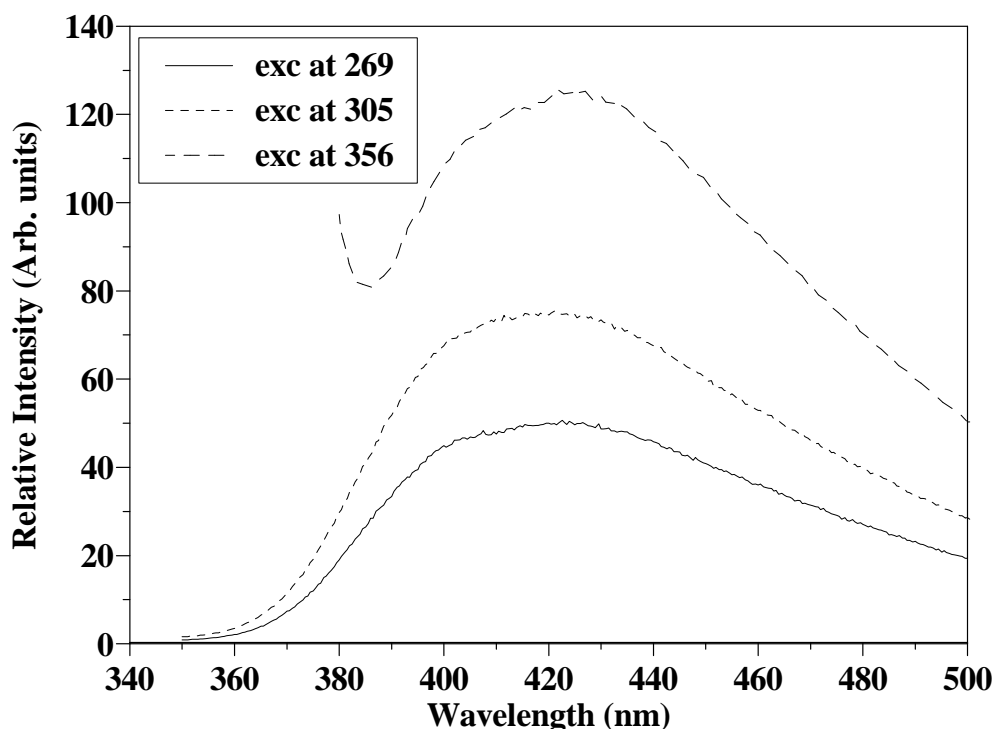


**Figure 2: Broad PL emission peaks for the different excitation energies as indicated.**

#### 4.3.2 Gaussian Peak Fit

Fig. 3 shows the CL and PL emission spectra from the  $Y_2SiO_5:Ce$  powders. The primary electrons are scattered throughout the host crystal and eventually a fraction of these electrons will transfer their energy to the  $Ce^{3+}$  ion. Gaussian peak fits were done in order to explain the broadness of the emission spectra in more detail. The broadness of the emission peak is ascribed to emission from more than one energy level. The CL and PL spectra show emission in the same range with a higher PL intensity due to larger area of excitation. Fig. 4 show possible Gaussian curve fits for the emission data showed in Fig. 3. A different number of peaks were used as indicated. First, two peaks were fitted as a solution for the broad spectra, then three and then four peaks. The peak positions and peak position differences are tabulated in table 1.

Fig. 4a) and d) show the results for two fitted peaks. The transferred energy difference from the  $5d$  to the  $^2F_{5/2}$  and  $^2F_{7/2}$  levels of the  $4f$  energy level is expected to be about  $2000\text{ cm}^{-1}$  [1]. The difference between these two peak positions is, however,  $3095$  or  $3336\text{ cm}^{-1}$

<sup>1</sup> (Table 1) which is larger than the expected  $2000\text{ cm}^{-1}$ . Clearly the luminescence can therefore not be ascribed to only these two peaks. The transitions from only 1 5d level to two 4f levels are therefore ruled out.

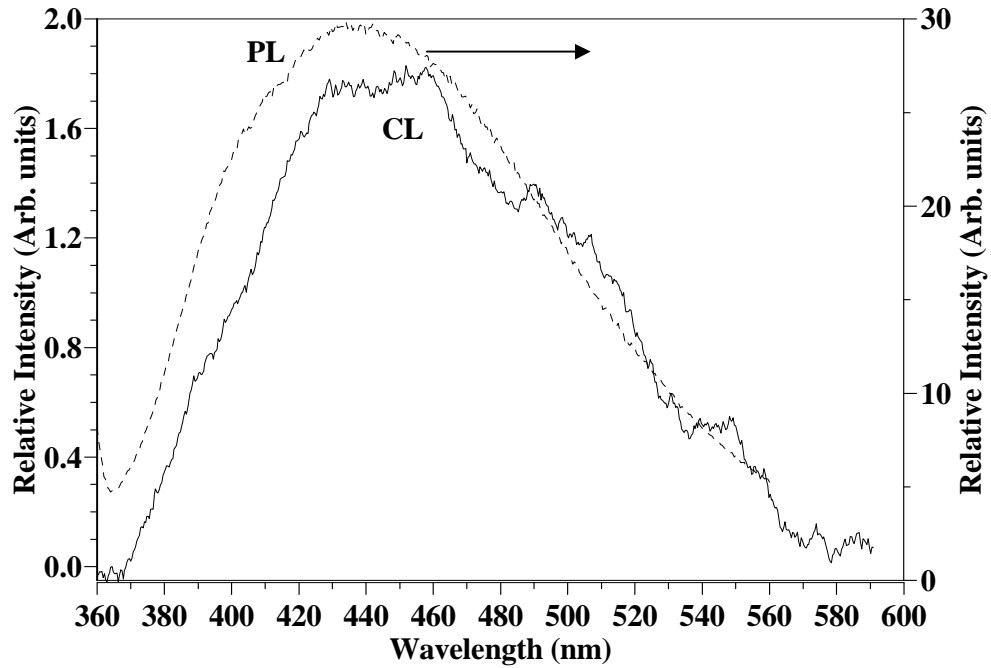


**Figure 3: CL (2 keV energy electrons, beam current of  $20\ \mu\text{A}$ ) and PL (xenon flash lamp,  $\lambda = 325\text{ nm}$ ) spectra of the  $\text{Y}_2\text{SiO}_5:\text{Ce}$  powders.**

Fig. 4b) and e) shows a difference of  $2210$  and  $2172\text{ cm}^{-1}$  between peaks 2 and 3 respectively. This could be assigned to the 5d to  ${}^2\text{F}_{5/2}$  and  ${}^2\text{F}_{7/2}$  transition with a third additional peak 1 in both cases (PL and CL), that may be attributed to an independent luminescent centre. For the linear least square method, the FWHM (full width half maximum) of the fitted peaks should theoretically be the same (it is the same emitting 5d to 4f), but due to the complex host matrix and crystal field splitting effect this value cannot be a fixed parameter [2]. Wang *et al.* [2] also found, while doing Gaussian peak fits on the  $\text{X}_2$  - phase of  $\text{Y}_2\text{SiO}_5$  (3 peaks as a resolution), that the FWHM value of the peaks are not the same and that further research was required.

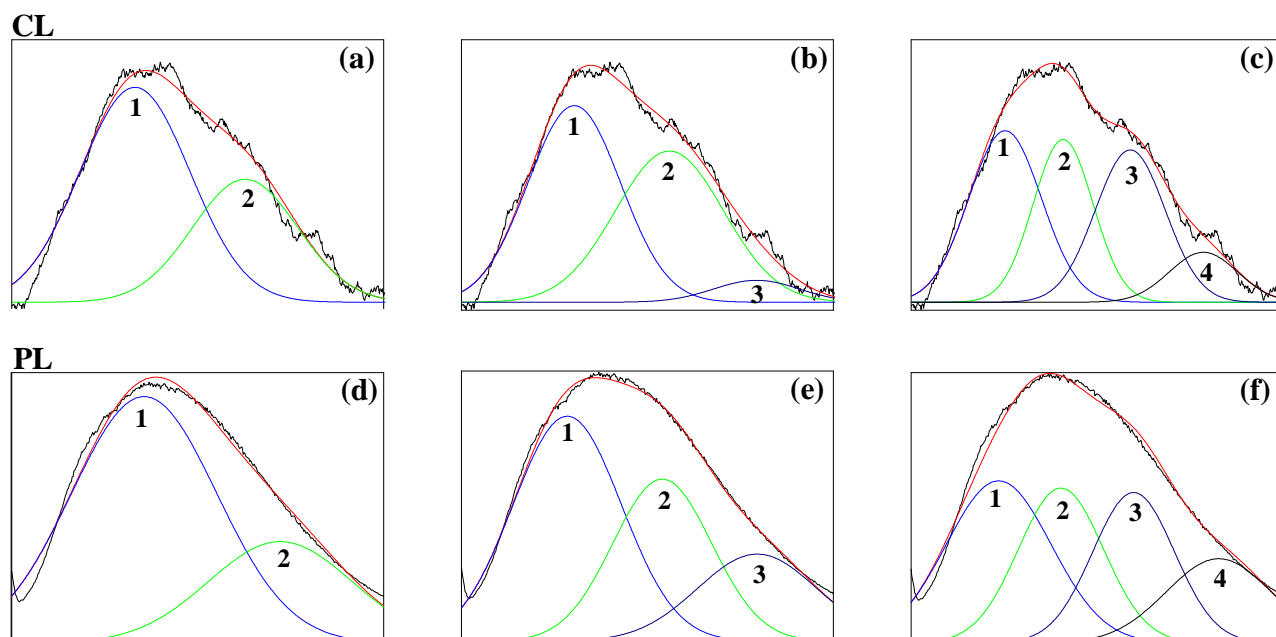


**Figure 4: Gaussian peak fits for the CL a) – c) and PL d) – f) spectra for the  $\text{Y}_2\text{SiO}_5:\text{Ce}$  powders.**

Since the  $\text{Ce}^{3+}$  ion can occupy two different sites in the host matrix due to the different coordination numbers there could be four emission peaks as in Fig. 4c) and f). The peak differences between 1 and 2, 2 and 3 and 3 and 4 are all close to  $2000\text{ cm}^{-1}$ . However the closest value is between 1 and 2 and 2 and 3 for both cases. A plausible explanation could be that peaks 1 and 2 are from one site, A1, and peaks 3 and 4 from the other A2 site [1]. Aitasalo *et al.* [4] reported on a luminescent spectrum for the A1 site with a broad peak at  $22470\text{ cm}^{-1}$  (445 nm) while studying the delayed luminescence of  $\text{Ce}^{3+}$  doped  $\text{X}_1$  form of  $\text{Y}_2\text{SiO}_5$  powder. Jiao *et al.* [1] measured a difference of  $1900\text{ cm}^{-1}$  and  $1500\text{ cm}^{-1}$  for the difference between 1 and 2 and 3 and 4, respectively. These are of the same order as the CL results in this study of  $1945$  and  $1574\text{ cm}^{-1}$ . It is also of the same order for the PL results for the difference of peak 1 and 2 ( $1843\text{ cm}^{-1}$ ) but not for peak 3 and 4.

**Table 1: Peak positions and peak position differences for the curve fits in Fig. 3.**

Peak	Position (nm)	Position (cm <sup>-1</sup> )	Peak position difference (cm <sup>-1</sup> )
a) 1	436	22936	
a) 2	504	19841	3095
b) 1	428	23364	
b) 2	484	20661	2703
b) 3	542	18450	2211
c) 1	418	23923	
c) 2	455	21978	1945
c) 3	496	20161	1817
c) 4	538	18587	1574
d) 1	430	23256	
d) 2	502	19920	3336
e) 1	415	24096	
e) 2	464	21552	2544
e) 3	516	19380	2172
f) 1	407	24570	
f) 2	440	22727	1843
f) 3	480	20833	1894
f) 4	525	19048	1785

Lin *et al.* [9] observed peak differences of 1540 and 1360 cm<sup>-1</sup> between the two 4f levels in the X<sub>1</sub> and X<sub>2</sub> - Y<sub>2</sub>SiO<sub>5</sub> phase (also powders) while investigating the crystal structure dependence of the luminescence of rare earth ions (Ce<sup>3+</sup>, Tb<sup>3+</sup>, Sm<sup>3+</sup>) in Y<sub>2</sub>SiO<sub>5</sub>. The values differ notably from 2000 cm<sup>-1</sup> and was ascribed to the presence of Ce<sup>3+</sup> in different sites in the host lattices.

#### 4.3.3 Luminescent mechanism

Aitasalo [4] also reported on reducing preparation conditions that could probably result in oxygen vacancies (intrinsic traps) in the  $\text{Y}_2\text{SiO}_5$  lattice. These vacancies are positively charged and can electrostatically attract electrons from a nearby ion and form the so-called positive  $\text{F}^+$  and neutral F centres. The only source of readily available electrons is the other  $\text{Ce}^{3+}$  ions and thus some  $\text{Ce}^{4+}$  centres are created. This mechanism therefore supports the fact that there exist  $\text{Ce}^{4+}$  ions (much smaller than  $\text{Ce}^{3+}$ ) in the host lattice. While investigating the delayed luminescence, two bands were found in the spectrum and were ascribed to the two types of emitting  $\text{Ce}^{4+}$  centres: those close to the F defects (emission at 575 nm) and those close to the  $\text{F}^+$  defects (emission at 479 nm) centres [4]. This observation should be noted and could be possible during the growth of the thin films and even during the preparation methods of the powders. Oxygen vacancies could be created that could lead to charge transfer and  $\text{Ce}^{4+}$  ions and this could result in additional luminescent centres that could contribute to the broadness of the emission spectrum.

Not all bonds between the  $\text{Ce}^{3+}$ ,  $\text{Y}^{3+}$  and  $\text{O}_2^-$  ligands in the lattice are of the same length. This creates the possibility for Jahn-Teller distortion and leads to emission from the 5d to the 4f levels to become distorted. The Jahn-Teller distortion describes the geometrical distortion of non-linear molecules under certain situations [3]. If the emission gets distorted then this could also result in a broad emission spectrum.

Energy transfer from the A2 to the A1 site is also a possibility that should not be ignored. Aitasalo showed that emission from only the A1 site due to energy transfer from the A2 site completely dominated the emission spectrum. This kind of transfer was also observed at 15 K in  $\text{X}_1 - \text{Y}_2\text{SiO}_5:\text{Eu}^{3+}$  [4].

The luminescent properties of  $\text{Y}_2\text{SiO}_5$  have been studied for some time now but no definite proof could be given for the splitting of the 5d level. Only results with presumptive explanations could be provided. The first excited state in a  $\text{Ce}^{3+}$  ion is a 5d state with two closely-disposed terms  $^2\text{D}_{3/2}$  and  $^2\text{D}_{5/2}$ . In the free  $\text{Ce}^{3+}$  ion the energy difference between the 5d and 4f is about 6.3 eV (196 nm). In a crystalline environment

the splitting of the 5d level could take place due to the effect of the surrounding crystal field. This could result in lowering of the “centre of gravity” of the 5d structure, especially in oxygen containing matrices, to a value of 4.3 eV (287 nm) [10]. Transition and emission can easily occur because now the centre of the 5d level is at relatively low energy [11]. A plausible explanation for the broad band emission would thus be transition from different 5d levels [12, 13]. As mentioned before,  $\text{Y}_2\text{SiO}_5$  has a very complicated crystal structure so emission from all neighbour  $\text{Ce}^{3+}$  ions (differently orientated in the structure) could result in transition with energies just slightly lower or higher than the ion close to it. The net effect is as if the broad curve gets “coloured in” with peaks to the left and right of a maximum intensity point.

All of the above-mentioned possibilities should be considered while investigating the luminescent properties of  $\text{Y}_2\text{SiO}_5:\text{Ce}$  and during the curve fitting process. A strong influence would be the preparation method of the sample material used as the phosphor (powders or thin films) as this could lead to defects and oxygen vacancies, together with the crystal field effect and different orientation of the ions in the crystal structure.

Fig. 5 shows a schematic illustration of the possible emission transitions and luminescent mechanisms that could explain the 4 fitted peaks in Fig. 4. The most plausible explanation according to our excitation and emission results is that the two different sites of the  $\text{Ce}^{3+}$  ion (A1 and A2) in the host matrix are responsible for the two sets of visible peaks (peak set 1 and 2 as well as peak set 3 and 4). The difference in orientation of the neighbour ions in the crystal structure will be responsible for the broadening of the band emission. The emission peaks are from the 5d levels to the splitted  $^2\text{F}_{5/2}$  and  $^2\text{F}_{7/2}$  energy levels of the 4f energy levels of the two different sites. The excitation spectrum clearly indicated that other defect levels are also present in the matrix. Some of the excited electrons captured in the defect levels may transfer their energy to the electrons in the 4f levels during the de-excitation process. These electrons are then excited to the 5d levels. Electrons from the excited 5d levels will then be de-excited radiatively to the 4f levels.

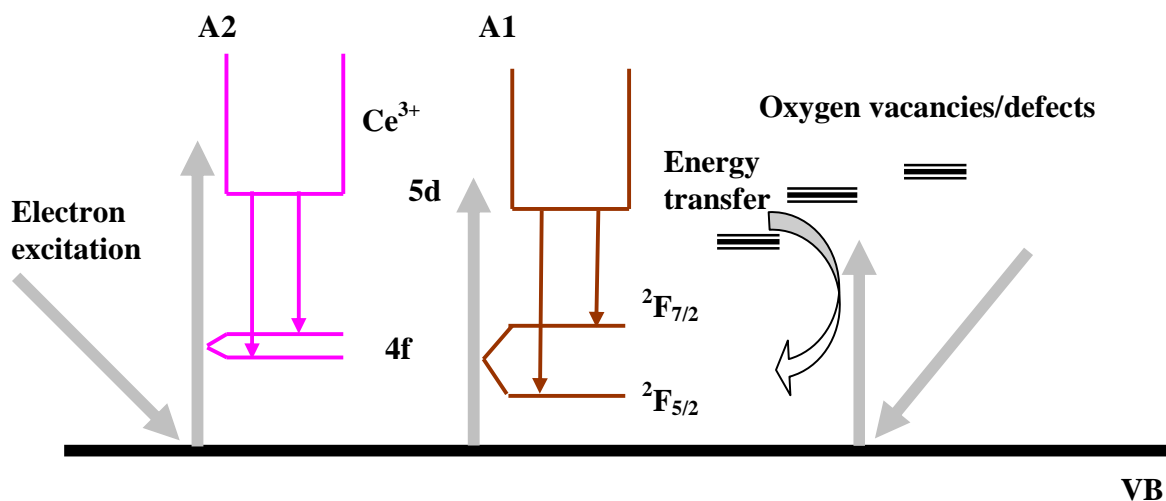


**Figure 5: The schematic illustration of the luminescent mechanism of the  $Y_2SiO_5:Ce$  phosphor powders.**

#### 4.4 Degradation of the $Y_2SiO_5:Ce$ powder

A degradation study that was done on the  $Y_2SiO_5:Ce$  powder by Coetsee *et al.* [14] at a previous stage, included AES, CL and XPS analysis. The powder was irradiated for 24 hr with an electron current density of  $26 \text{ mA}\cdot\text{cm}^{-2}$  in an  $O_2$  pressure of  $1 \times 10^{-6}$  Torr. The CL intensity was monitored (450 nm) and the chemical changes on the surface analysed with XPS. The CL intensity first decreased and then increased after about  $300 \text{ C}\cdot\text{cm}^{-2}$  electron dose. The increase in the CL intensity was due to a second peak arising between 600 and 700 nm and the bright blue colour of the  $Y_2SiO_5:Ce$  changed to a whitish colour after 24 hours (see Fig. 6). This indicated that a chemical reaction occurred on the surface (due to ESSCR) during the degradation process which was then analysed with XPS.

XPS showed an extra shoulder at the high binding energy side of the Si 2p peak, a much broader O 1s peak, an increase in the Ce 3d peak, and a slight shift in the Y 3d peak after degradation.

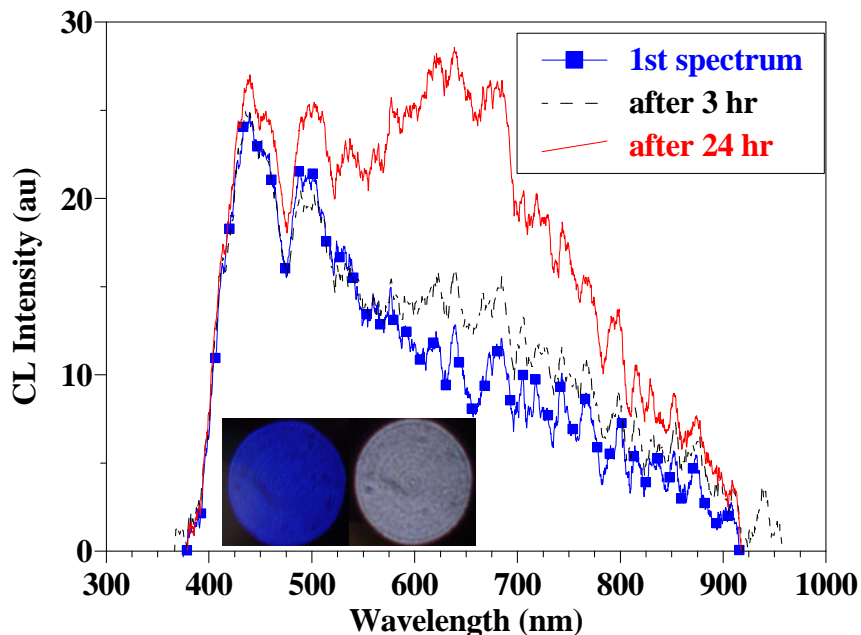


**Figure 6: CL intensity against wavelength for the light emitted from the powders before and after 3 and 24 hr electron bombardment. The insets show digital images of the bright blue colour before and the whitish colour after degradation.**

Fig. 7 and 8 shows the measured and fitted XPS results for the Si 2p and O 1s peaks after degradation. The Si peak position for the  $Y_2SiO_5$  chemical state was measured at 101.3 eV before degradation. The extra Si peak measured at 103.3 eV was attributed to the silica ( $SiO_2$ ) chemical state after degradation [15]. The O 1s peak was measured at 530.4 eV before degradation. The XPS fitted results showed peaks at 529, 530.4, 532.1 and 533.6 eV that correlate well with  $CeO_2$  [16], the  $Y_2SiO_5:Ce$  O 1s peak measured in this study before degradation and the last two peaks with  $SiO_2$  [17, 18], respectively.

The Ce 3d peaks before degradation were at 881.7 and 885.4 eV and after degradation it was at 882.7 and 886.5 eV (results not shown here), which is in agreement with Ce in the  $CeO_2$  oxidation stage [19] and  $CeH_3$  [20]. The Y 3d 157.6 and 159.2 eV peak intensities

before degradation (results not shown here) decreased due to the coverage of the  $Y_2SiO_5$  with  $SiO_2$ ,  $CeO_2$  and  $CeH_3$  without a distinct shift in binding energy position. It must be pointed out that there was a slight shift in the Y 3d peak to 157.1 eV which might be an

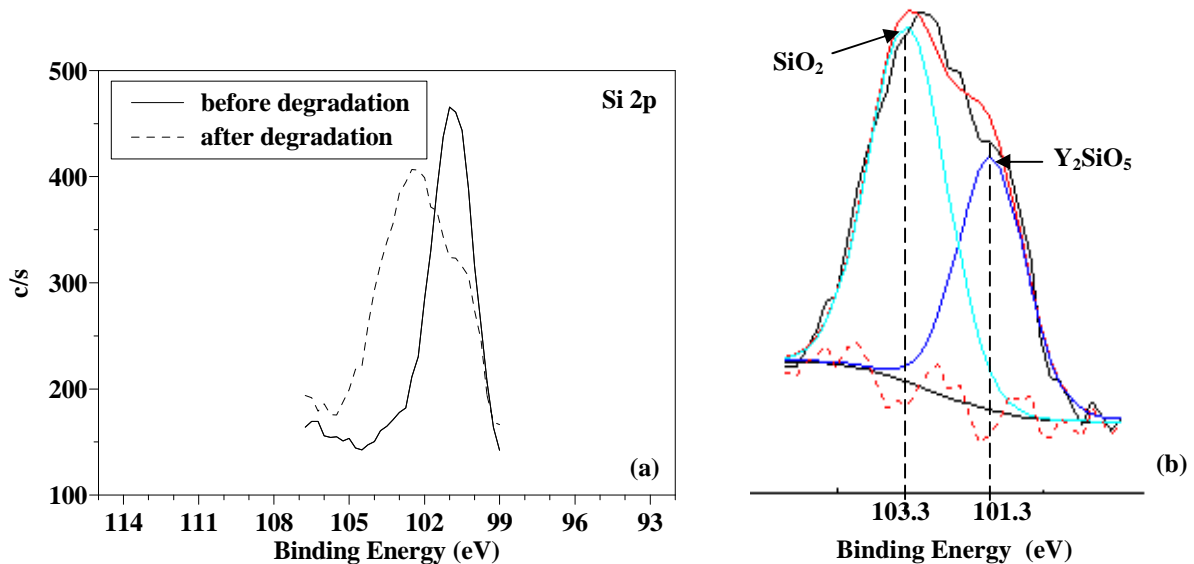


**Figure 7: (a) Measured XPS results for the Si 2p peak before and after 24 hr degradation, (b) fitted results for Si 2p in the  $Y_2SiO_5$  and in the  $SiO_2$  chemical state.**

The surface reaction on  $Y_2SiO_5:Ce$  is consistent with the well known ESSCR model [22, 23]. The ESSCR mechanism explains the formation of  $SiO_2$  plus  $CeO_2$  and  $CeH_3$ , whereby the electron beam dissociates the oxygen gas, as well as water vapour from the background gases into atomic species, which then react with the surface atoms to form a different chemical layer. The increase in CL intensities indicates that the newly formed layer is luminescent and thus contributing to the emission peak between 600 and 700 nm.

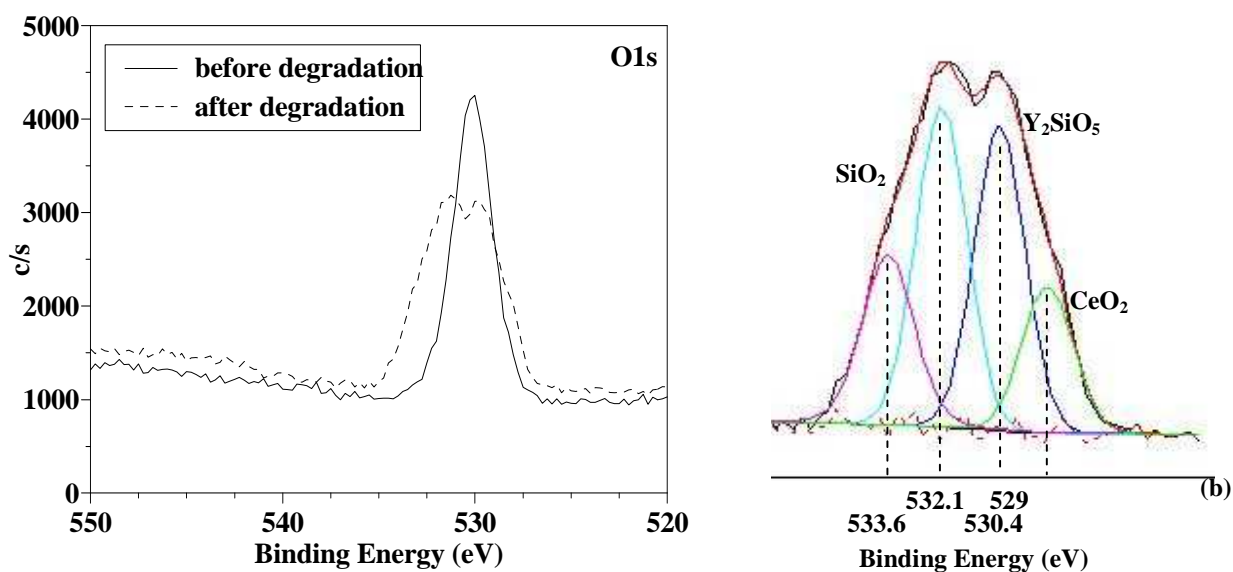


**Figure 8: (a) Measured XPS results for the O 1s peak before and after 24 hr degradation, (b) fitted results for O 1s after degradation in the  $\text{SiO}_2$ ,  $\text{Y}_2\text{SiO}_5$  and  $\text{CeO}_2$  chemical state.**

$\text{SiO}_2$  has a band gap and the electron beam irradiation can break the Si-O bonds and cause intrinsic defects [16, 24]. Skuja *et al.* [25, 26] reported two peaks for  $\text{SiO}_2$  at 1.9 eV (650 nm) and 2.7 eV (459 nm) with a theory that the two peaks are related to intrinsic defects involving broken Si-O bonds. A definite contribution from the  $\text{SiO}_2$  1.9 eV defect leads to the increase in the CL intensity between 600 and 700 nm, thus also resulting in the change in colour. There could be a very low intensity contribution from the 2.7 eV defect to the peak emission between 400 and 500 nm, which results in the increase in the intensity in that region. Violet/blue light emission (379.5 nm) was previously observed at room temperature from thin  $\text{CeO}_2$  films deposited on Si (111) [27]. No evidence of emission in the 600 to 700 nm range for  $\text{CeO}_2$  was found.

The formation of the luminescent  $\text{SiO}_2$  layer on the surface of the  $\text{Y}_2\text{SiO}_5:\text{Ce}$  therefore leads to the degradation of the blue emitting  $\text{Y}_2\text{SiO}_5:\text{Ce}$  phosphor powders to a whitish light emitting phosphor.

## 4.5 Conclusion

CL and PL results were investigated and the ideal profiles for the Gaussian peak fits yielded four peaks that fit the broad band spectrum. The origin of these four peaks is due to the two different  $Ce^{3+}$  sites in the host matrix (A1 and A2) and the crystal field split of the 4f levels. Defect levels also play an important role in the excitation process. A better understanding of the luminescent mechanism creates opportunities for enhancement in the  $Y_2SiO_5:Ce$  phosphor application field. The degradation of the  $Y_2SiO_5:Ce$  phosphor powders investigated with AES and CL spectroscopy first resulted in a decrease in CL intensity measured at 450 nm and then an increase after about 300 C.cm<sup>-2</sup> due to the chemical change in the phosphor surface. XPS and CL indicated that the change in peak shape is due to the formation of a luminescent  $SiO_2$  layer on the surface which is formed according to the ESSCR mechanism. The emission of light from the  $SiO_2$  defect levels contributed to the CL intensity in the 600 to 700 nm wavelength range. The colour changed from blue to whitish during the degradation process.

## References

1. H. Jiao, F. Liao, S. Tian and X. Jing, *J. Electrochem. Soc.*, **151** (7) (2004) 39.
2. J. Wang, S. Tian, G. Li, F. Liao and X. Jing, *J. Electrochem. Soc.*, **148** (6) (2001) 61.
3. E. J. Bosze, G. A. Hirata, L. E. Shea-Rohwer and J. McKittrick, *J. Lumen*, **104** (1-2) (2003) 47.
4. T. Aitasalo, J. Holsa, M. Lastusaari and J. Niittykoski, *F. Pelle, Opt. Mater.*, **27** (2005) 1511.
5. D. W. Cooke, J. K. Lee, B. L. Bennett, J. R. Groves, L. G. Jacobsohn, E. A. McKigney, R. E. Muenchausen, M. Nastasi, K. E. Sickafus, M. Tang and J. A. Valdez, *Appl. Phys. Lett.*, **88** (2006) 103.
6. J. Y. Zhang, Z. T. Zhang, Z. L. Tang, Y. Tao, X. Long, X. Long, *Chem. Mater.*, **14** (2002) 3005.
7. P. Zhu, W. Di, Q. Zhub, B. Chenc, H. Zhu, H. Zhaoa, Y. Yang, X. Wang, *J. Alloys Comp*, **454** (2008) 245.

8. Z. Fu, Y. Geng, H. Chen, S. Zhou, H. K. Yang, J. H. Jeong, *Opt. Mater.*, (2008) doi:10.1016/j.optmat.2008.01.008.
9. J. Lin, Q. Su, H. Zhang and S. Wang, *Mater. Res. Bull.*, **31** (2) (1996) 189.
10. A. I. Kuznetsov, *Zhurnal Prikladnoi Spektroskopii*, **20** (5) (1974) 823.
11. X. Ouyang, A. H. Kitai and R. Siegele, *Thin Solid Films*, **254** (1995) 268.
12. Y. Liu, C. Xu, H. Matsui, T. Imamura and T. Watanabe, *J. Lumin.*, **87** (2000) 1297.
13. E. J. Bosze, G. A. Hirata and J. McKittrick, *Proc. Mater. Res. Soc.*, **558** (1999) 15.
14. E. Coetsee, J. J. Terblans and H. C. Swart, *J. Lumin.*, **126** (2007) 37.
15. M. Laczka, W. Beier and L. Stoch, *Glastechn. Berichte*, **62** (1989) 320.
16. E. Paparazzo, *Surface Sci.*, **234** (1990) L253.
17. D. Sprenger, H. Bach, W. Meisel and P. Gulich, *J. Non-cryst. Solids*, **126** (1990) 111.
18. T. A. Clarke and E. N. Rizkalla, *Chem. Phys. Lett.*, **37** (1976) 523.
19. D. D. Sarma and C. N. R., *J. Electron Spectrosc. Relat. Phenom.*, **20** (1980) 25.
20. L. Schlapbach, J. Osterwalder and H. C. Siegmann, *J. Less-Common Metals*, **88** (1982) 291.
21. Y. Uwamino, Y. Ishizuka, H. Yamatera, *J. Electron Spectrosc. Relat. Phenom.*, **34** (1984) 69.
22. J. Sebastian, S. Jones, T. Trottier, H. C. Swart and P. H. Holloway, *J. SID*, **3/4** (1995) 147.
23. P. H. Holloway, J. Sebastian, T. Trottier, S. Jones, H. C. Swart and R. O. Peterson, *Mat. Res. Soc. Symp. Proc.*, **424** (1997) 425.
24. X. Liu, J. C. H. Phang, D. S. H. Chan and W. K. Chim, *J. Phys. D, Appl. Phys.*, **32** (1999) 1563.
25. L. N. Skuja and W. Entzian, *Phys. Stat. Sol. (a)*, **96** (1986) 191.
26. L. N. Skuja, A. N. Streletsky and A. B. Pakovich, *Solid State Comm.*, **50** (1984) 1069.
27. F. Gao, G. Li, J. Zhang, F. Qin, Z. Yao, Z. Liu, Z. Wang, and L. Lin, *Chin. Phys. Lett.*, **18** (2001) 443.

## Chapter 5

### Characterization of the $\text{Y}_2\text{SiO}_5\text{:Ce}$ thin films: Part one

This chapter contains the experimental procedure, the growth of the different thin films, characterization and the results and discussions for SEM/backscattered electrons (BSE), EDS and AFM measurements for the thin films in SET1 and 2 in order to investigate surface morphology with different process parameters.

#### 5.1 Introduction

Particle formation is a major drawback of PLD and it usually is the main limiting factor in the application field of this deposition method. For example high performance electronic and optical devices require particle free films. The formation and emission of the particles strongly depend on the type of material used as the target and it is based on various physical phenomena such as the dislodgement of uniformities protruding from the target surface, gas phase clustering of the evaporated material due to supersaturation (in high gas pressures) and the generation of liquid phase droplets. Particles can therefore be in the vapour, liquid or solid phase [1].

One of the solutions to the particle formation problem is optimization of the laser process parameters such as the ambient pressure (oxygen), laser spot size, frequency, number of pulses and the substrate temperature. The ambient pressure during PLD can be characterized as either passive or active. The passive use is mainly to compensate for some loss of a constituent element such as oxygen or nitrogen in ceramics and the active use with either an inert or reactive gas is deliberately introduced to form particles with a desired size or composition. Incorporating an ambient during PLD can therefore create ultrafine particles with nano - meter size diameters. The particle sizes, however, do change as the ambient pressure changes [1].

The effect of the inert ambient pressure on the nature of the particles is most likely related to the increased collisions between the particles in the plume and the ambient as the pressure increases. Previous research that was done by Coetsee *et al.* [2, 3] on the growth of Y<sub>2</sub>SiO<sub>5</sub>:Ce thin films, resulted in non uniform thin films containing micron size spherically shaped particles with a broad CL emission band between 400 and 500 nm. This chapter therefore includes the investigation of the process parameters for PLD in order to reduce the particle sizes and to grow uniform thin films for optimal FED application.

## **5.2 Experimental procedure**

### **5.2.1 The growth of Y<sub>2</sub>SiO<sub>5</sub>:Ce thin films**

Commercially available Y<sub>2</sub>SiO<sub>5</sub>:Ce standard phosphor powder from Phosphor Technology (UK) were pressed into a pellet and annealed at 600 °C for 24 hr in vacuum to remove any water vapour that might be present in the powder. The Lambda Physik 248 nm KrF and the XeCl ( $\lambda = 308$  nm) excimer lasers were used to ablate three sets of thin films on silicon (Si) (100) substrates. The Si (100) substrates were cleaned in acetone for 5 min, in an ultrasonic water bath and then for another 5 min in methanol. The substrates were blown dry with nitrogen (N<sub>2</sub>) gas. Table 1 shows the different experimental parameters used for the growth of the different thin films.

For SETs 1 and 2 the vacuum base pressure was  $5 \times 10^{-6}$  Torr before the system was backfilled with the ambient to the desired pressure and in SET 3 the vacuum base pressure was  $3 \times 10^{-5}$  Torr. The target to substrate distance for SETs 1 and 2 was 4 cm and for SET 3 3.5 cm.

**Table 1: 3 Sets of thin films grown with different process parameters with PLD.**

<i>Thin film</i>	<i>Pressure (Torr) (O<sub>2</sub>)</i>	<i>Substrate Temperature (°C)</i>	<i>Frequency (Hz)</i>	<i>Fluence (J/cm<sup>2</sup>)</i>	<i>Pulses</i>	<i>Laser</i>
<b>SET1</b>						
5	Vacuum	600	8	3 ± 0.3	4000	KrF
2	1 x 10 <sup>-2</sup>	600	8	3 ± 0.3	4000	KrF
3	1	600	8	3 ± 0.3	4000	KrF
13	Vacuum	600	8	1.6 ± 0.1	4000	KrF
15	1 x 10 <sup>-2</sup>	600	8	1.6 ± 0.1	4000	KrF
17	1	600	8	1.6 ± 0.1	4000	KrF
9	Vacuum	400	8	3 ± 0.3	4000	KrF
6	1	400	8	3 ± 0.3	4000	KrF
<b>SET2</b>						
M4	0.455 O <sub>2</sub>	600	8	1.6 ± 0.2	4000	KrF
M9	0.455 N <sub>2</sub>	600	8	1.6 ± 0.2	4000	KrF
A3	0.455 Ar	600	8	1.6 ± 0.2	4000	KrF
<b>SET3</b>						
Uncoated	7.5 x 10 <sup>-3</sup> O <sub>2</sub>	400	10	2.7	6600	XeCl
Coated (SnO <sub>2</sub> )	7.5 x 10 <sup>-3</sup> O <sub>2</sub>	400	10	2.7	6600 + 1200	XeCl

**5.2.2 Characterization of the Y<sub>2</sub>SiO<sub>5</sub>:Ce thin films: SET 1 and 2**

SEM/BSE and EDS results were obtained with a Shimadzu Superscan SSX-550 system and AFM with the Shimadzu SPM – 9600 model (125 μm scanner) to determine surface morphology.

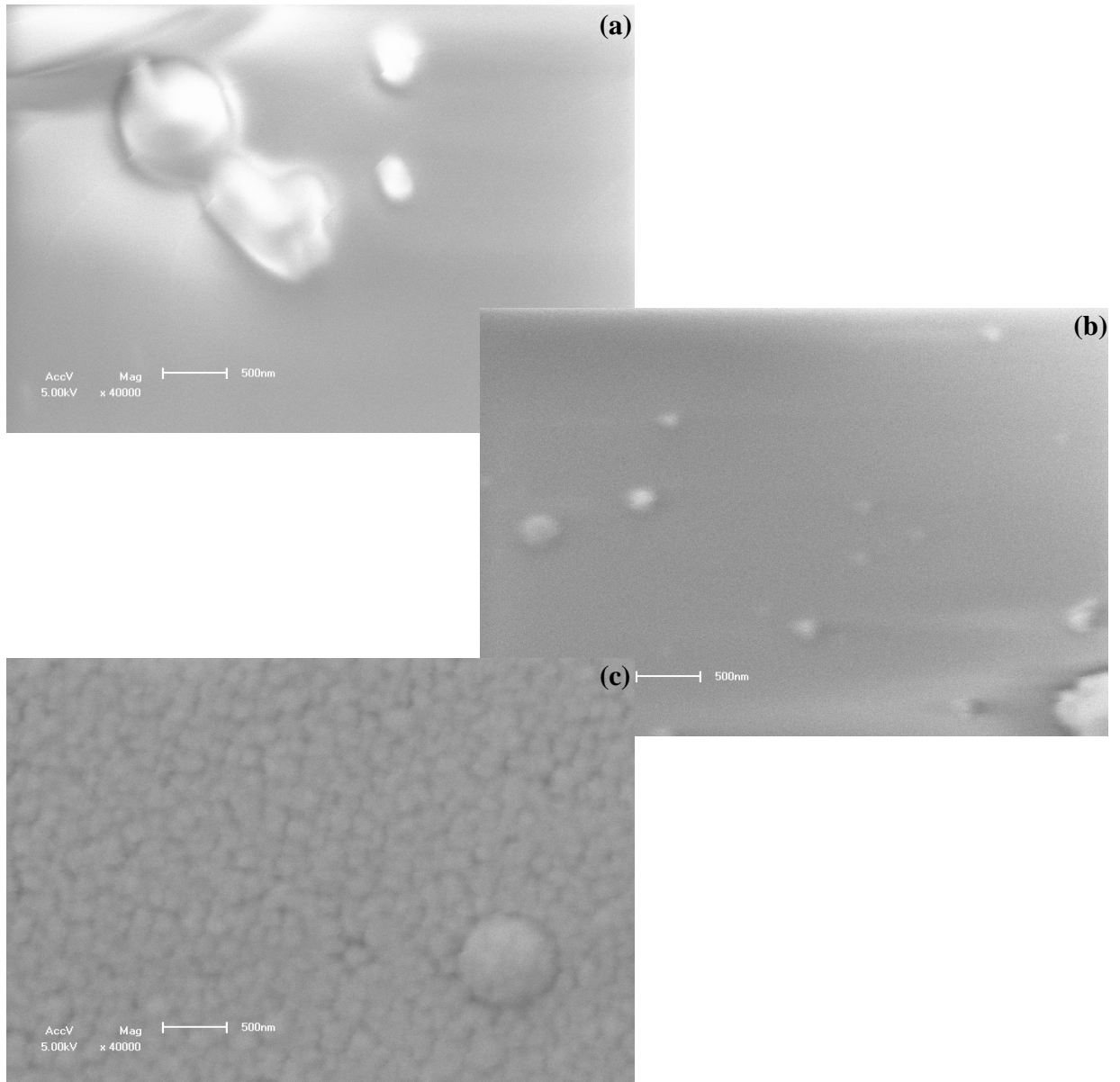
## 5.3 Results and Discussions

### 5.3.1 SEM/BSE and EDS

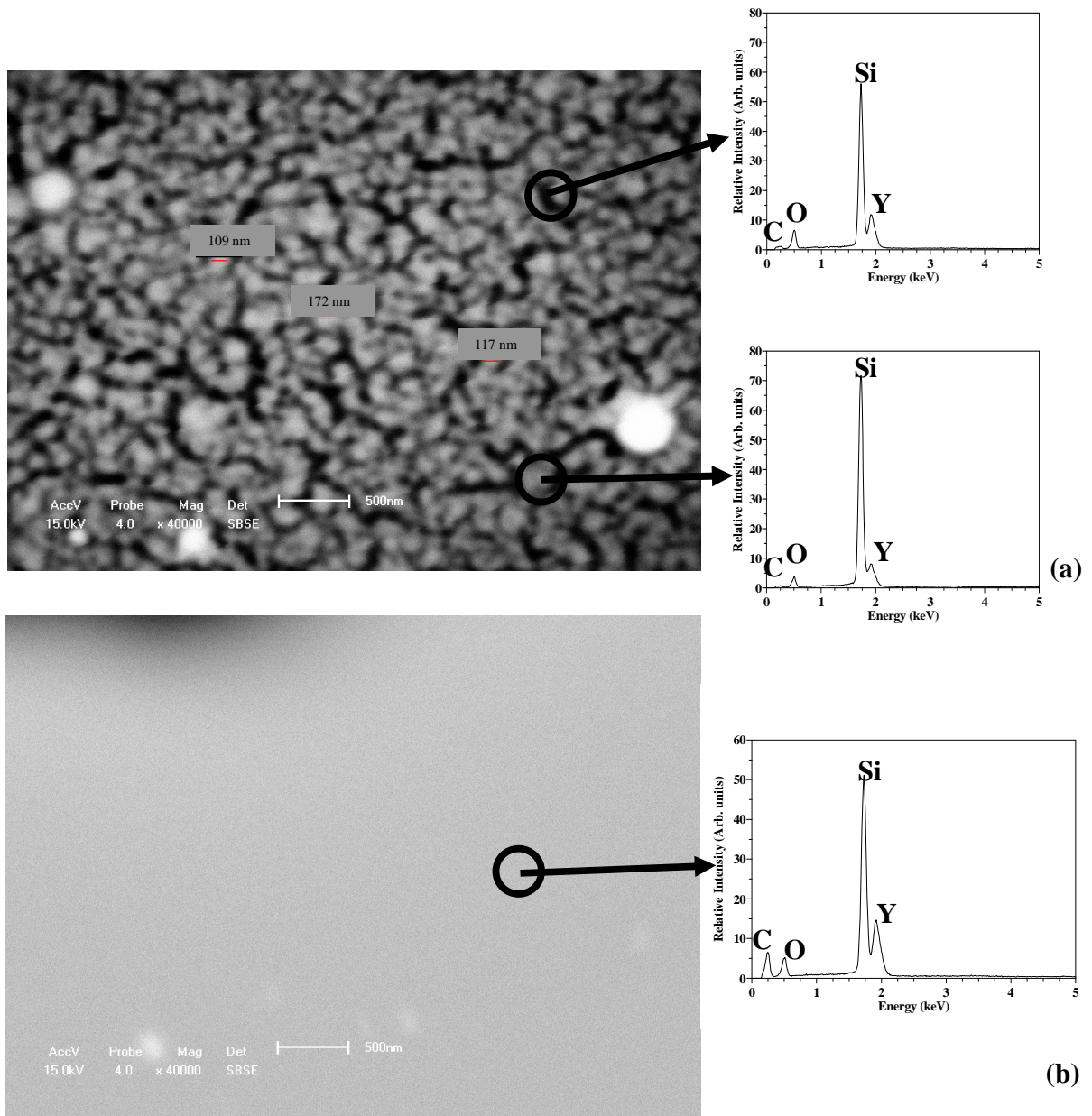
Fig. 1 shows the SEM images taken for the thin films ablated in a)  $5 \times 10^{-6}$  Torr (vacuum) (a lot of charging), b)  $1 \times 10^{-2}$  Torr O<sub>2</sub> and c) 1 Torr O<sub>2</sub> in SET1. The substrate temperature, pulse frequency, fluence and amount of pulses were kept constant at 600 °C, 8 Hz,  $3 \pm 0.3 \text{ J.cm}^{-2}$  and 4000 respectively. SEM images were done with 5 kV electron beam energy, magnification of x 40 000 and a scale of 500 nm. EDS analysis was done on all the thin films in SET1 and 2 but only the results for SET1 (Fig. 2a) 1 Torr O<sub>2</sub> and b)) vacuum are shown. EDS (BSE images taken and EDS analysis done with 15 kV energy beam) was done to indicate whether the Si (100) substrates was covered with the Y<sub>2</sub>SiO<sub>5</sub>:Ce phosphor layer. The SEM images for the lower fluence of  $1.6 \pm 0.1 \text{ J.cm}^{-2}$  SET1 can be seen in Fig. 3. Fig. 4 shows the two thin films ablated with  $3 \pm 0.3 \text{ J.cm}^{-2}$  fluence at 400 °C in a) vacuum and b) 1 Torr O<sub>2</sub>.

Fig. 5 shows the SEM images for SET2 thin films ablated at 450 mTorr O<sub>2</sub> a), N<sub>2</sub> b) and Ar c), at 600 °C and fluence of  $1.6 \pm 0.1 \text{ J.cm}^{-2}$ . EDS analysis done on *all* these thin films showed Y, Si, O and C on the surface areas which is an indication that the phosphor layer was successfully ablated onto the Si (100) substrate. All the thin films ablated in vacuum and 10 mTorr O<sub>2</sub> show a smooth layer with the SEM measurements. A rougher surface is however visible from the films ablated in 1 Torr O<sub>2</sub> and it looks like a spherically shaped nano - particle layer. From Fig. 5a) and c) ablation in 450 mTorr ambient show some layer on the substrate which is rougher than b). The existence of unwanted bigger micron size particles also occurs on all thin films.

These bigger unwanted micron particles can severely degrade the performance of electronic and optical devices and elimination can be done either with a mechanical approach of applying shadow mask, filters or doing off-axis ablation or by optimization of the process parameters [1]. These SEM images give a rough indication of the surface morphology but better imaging was obtained with AFM analyses.



**Figure 1: SEM images of the three thin films ablated in a) vacuum, b) 10 mTorr and c) 1 Torr O<sub>2</sub> ambient at 600 °C with a fluence of  $3 \pm 0.3 \text{ J.cm}^{-2}$  (5 kV beam energy, magnification of x 40 000 and a scale of 500 nm (FOV: 5 x 4  $\mu\text{m}$ )).**



**Figure 2: BSE images and EDS analysis of the thin films ablated with a fluence of  $3 \pm 0.3 \text{ J.cm}^{-2}$  in a) 1 Torr  $\text{O}_2$  and in b) vacuum at  $600 \text{ }^\circ\text{C}$ . (BSE images were done with a 15 keV beam energy, magnification of  $\times 40\,000$  and a scale of 500 nm (FOV:  $5 \times 4 \text{ }\mu\text{m}$ )). (Ce concentration below detection limit of EDS system.)**

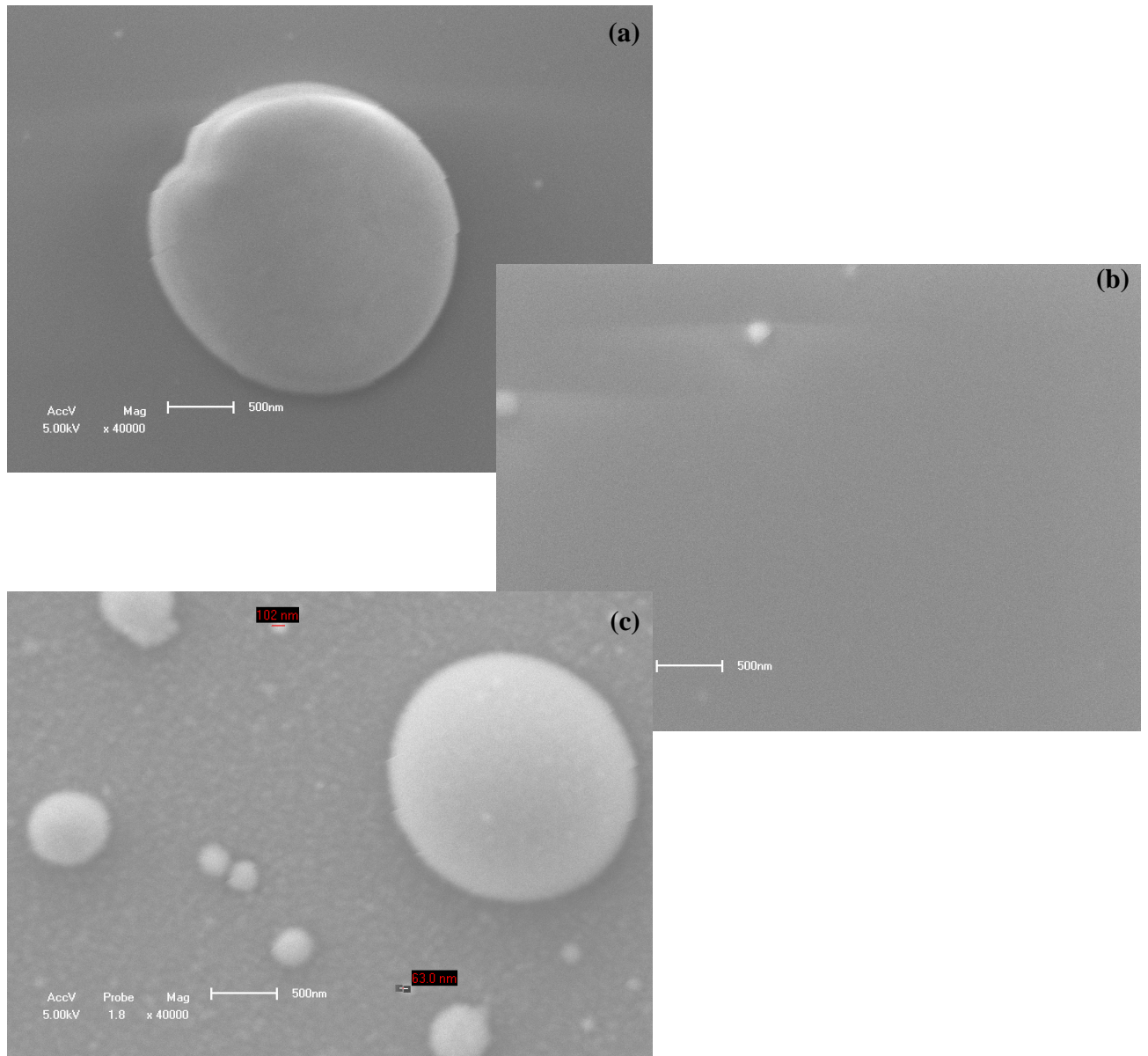


**Figure 3: SEM images of the three thin films ablated in a) vacuum, b) 10 mTorr and c) 1 Torr O<sub>2</sub> ambient at 600 °C with a fluence of  $1.6 \pm 0.1 \text{ J.cm}^{-2}$  (5 kV beam energy, magnification of x 40 000 and a scale of 500 nm (FOV: 5 x 4  $\mu\text{m}$ )).**

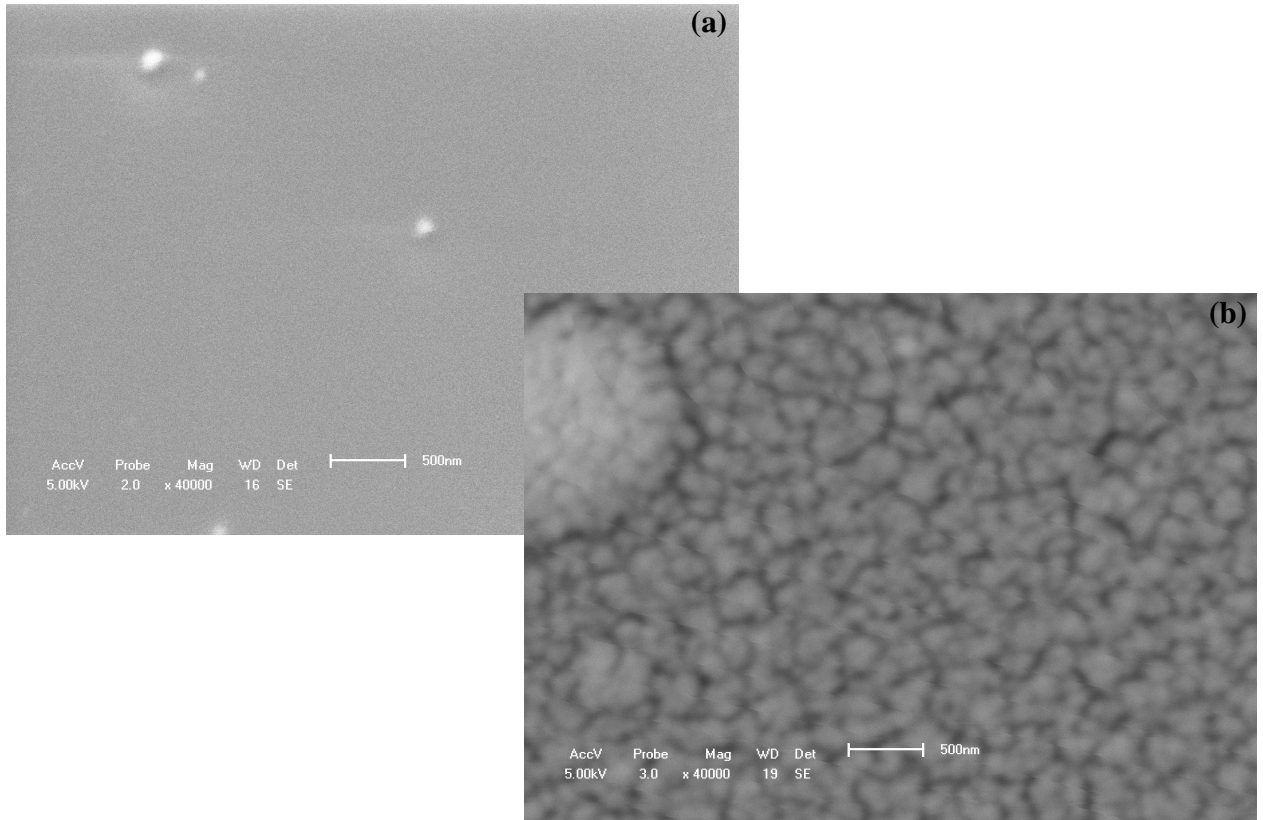


**Figure 4: SEM images of the two thin films ablated in a) vacuum, b) 1 Torr O<sub>2</sub> ambient at 400 °C with a fluence of  $3 \pm 0.3 \text{ J.cm}^{-2}$  (5 kV beam energy, magnification of x 40 000 and a scale of 500 nm (FOV: 5 x 4  $\mu\text{m}$ )).**

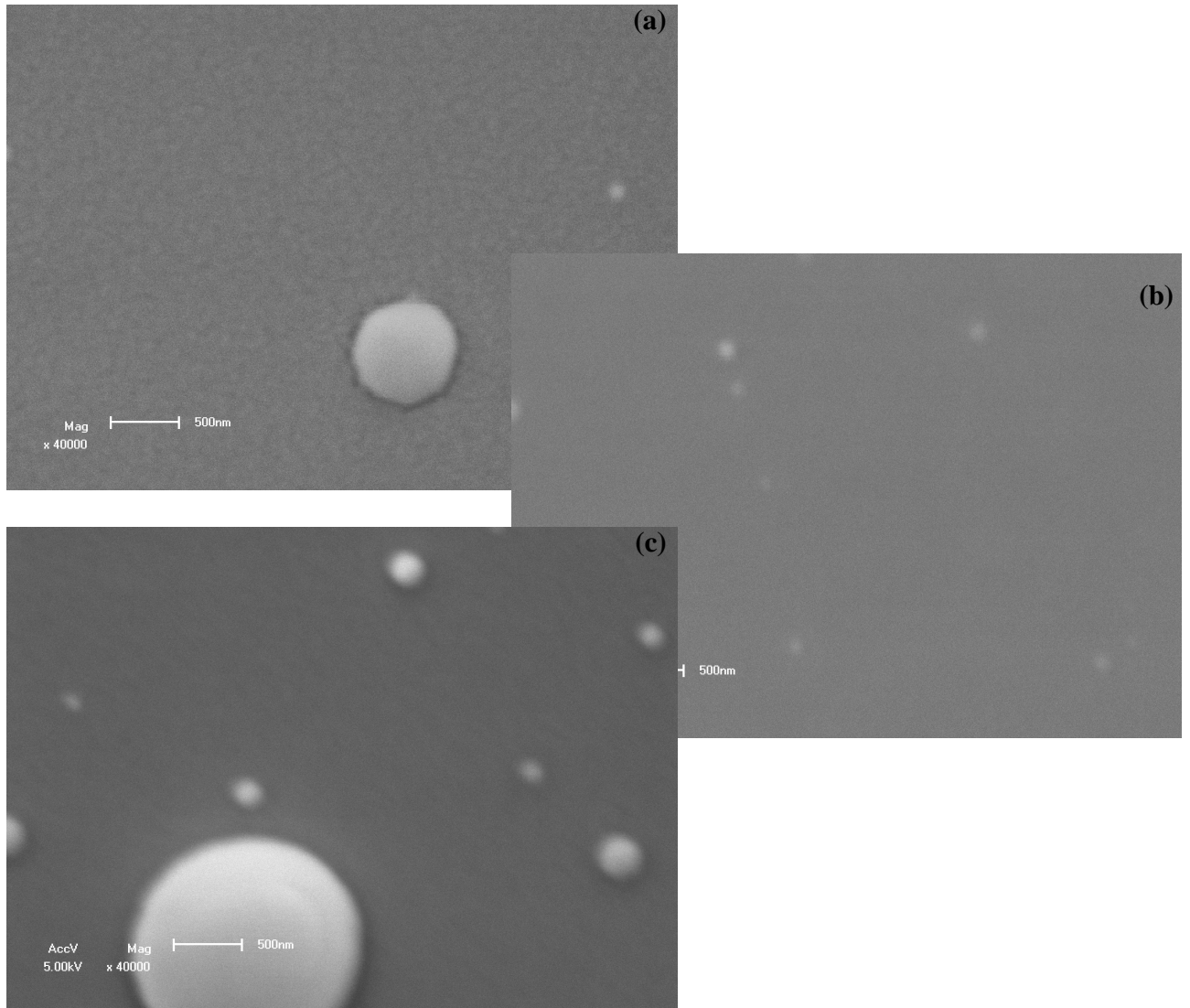
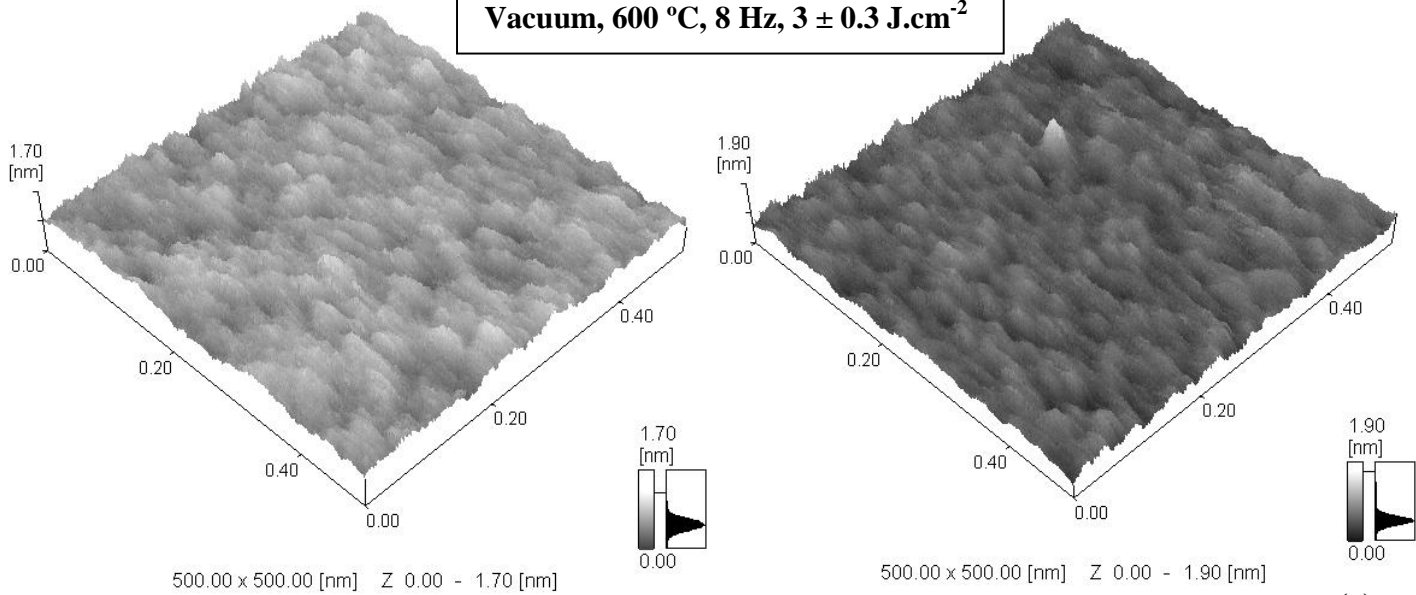


**Figure 5: SEM images of the three thin films ablated in 450 mTorr a) O<sub>2</sub>, b) N<sub>2</sub> and c) Ar ambient at 600 °C with a fluence of  $1.6 \pm 0.1 \text{ J.cm}^{-2}$  (5 kV beam energy, magnification of x 40 000 and a scale of 500 nm (FOV: 5 x 4  $\mu\text{m}$ )).**

### **5.3.2 AFM**

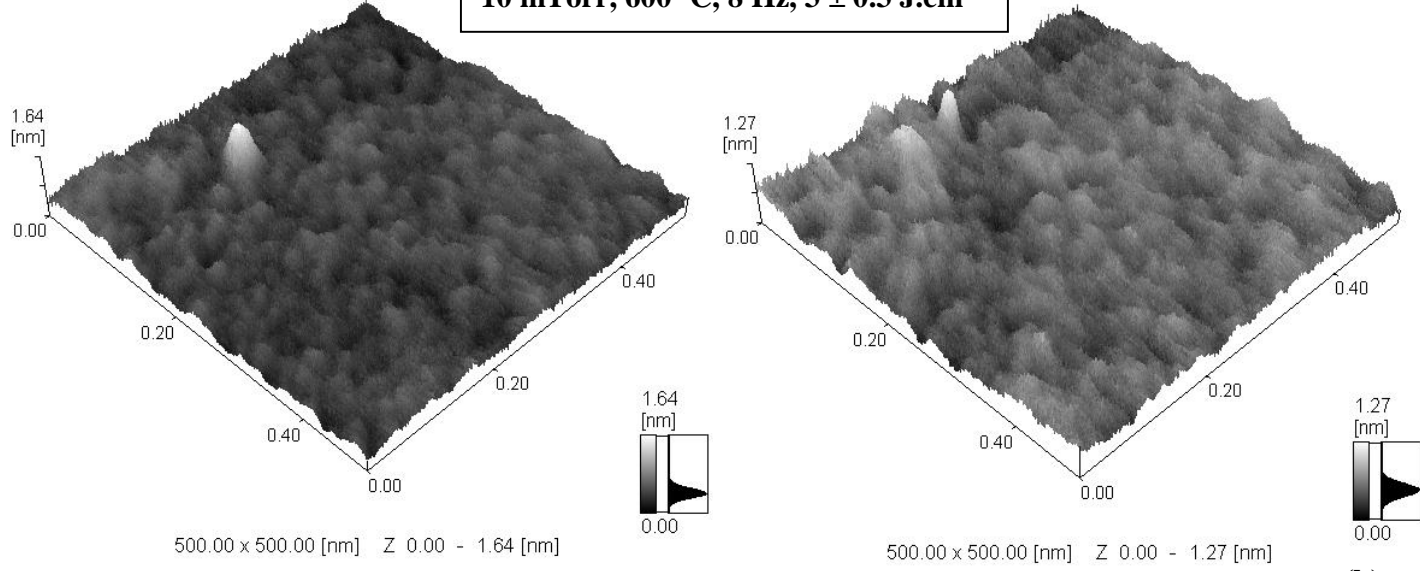
Fig. 6 shows 500 x 500 nm area scanned AFM 3D Height images for thin films in SET1 and 2 done in contact mode. Different areas on each thin film were scanned but only two areas are shown, in order to get a better picture of the surface morphology.

**Vacuum, 600 °C, 8 Hz,  $3 \pm 0.3 \text{ J.cm}^{-2}$**



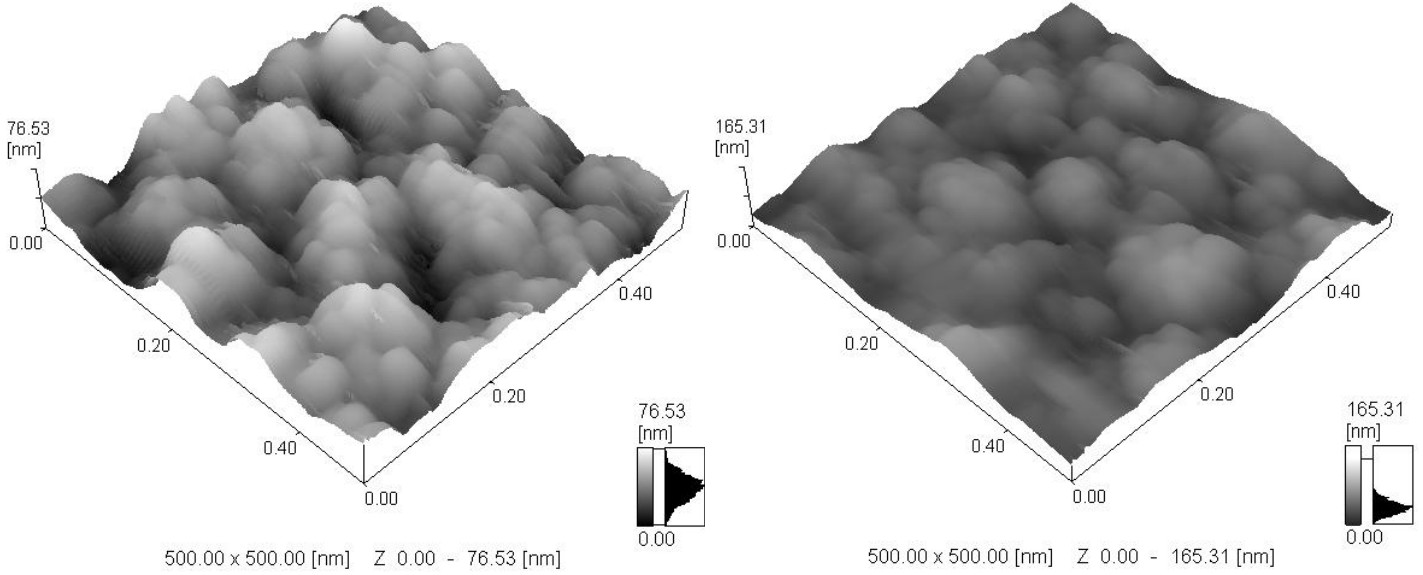
**(a)**

**10 mTorr, 600 °C, 8 Hz,  $3 \pm 0.3 \text{ J.cm}^{-2}$**



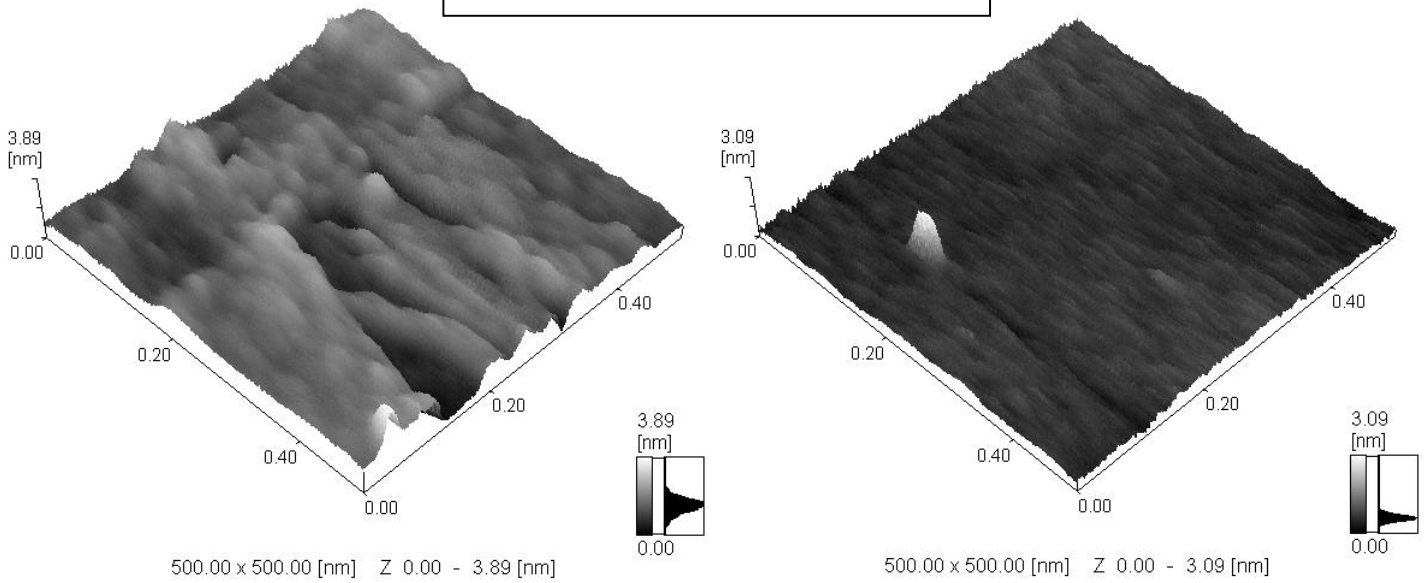
**(b)**

**1 Torr, 600 °C, 8 Hz,  $3 \pm 0.3 \text{ J.cm}^{-2}$**



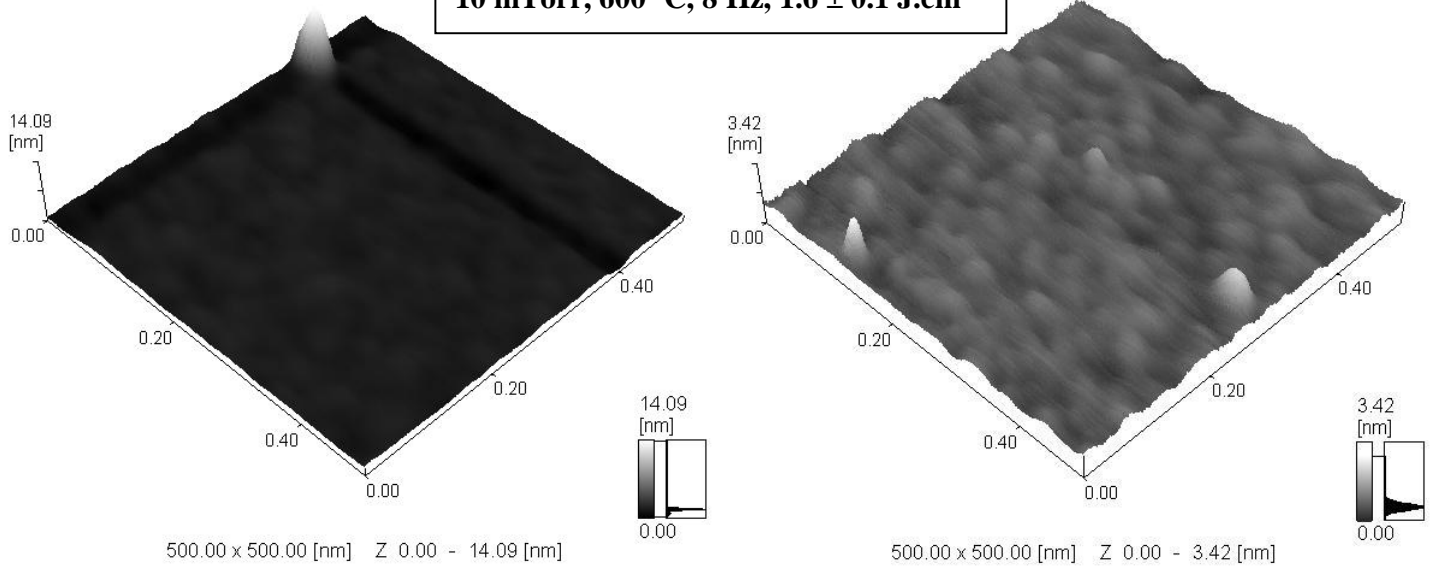
**(c)**

**Vacuum, 600 °C, 8 Hz,  $1.6 \pm 0.1 \text{ J.cm}^{-2}$**



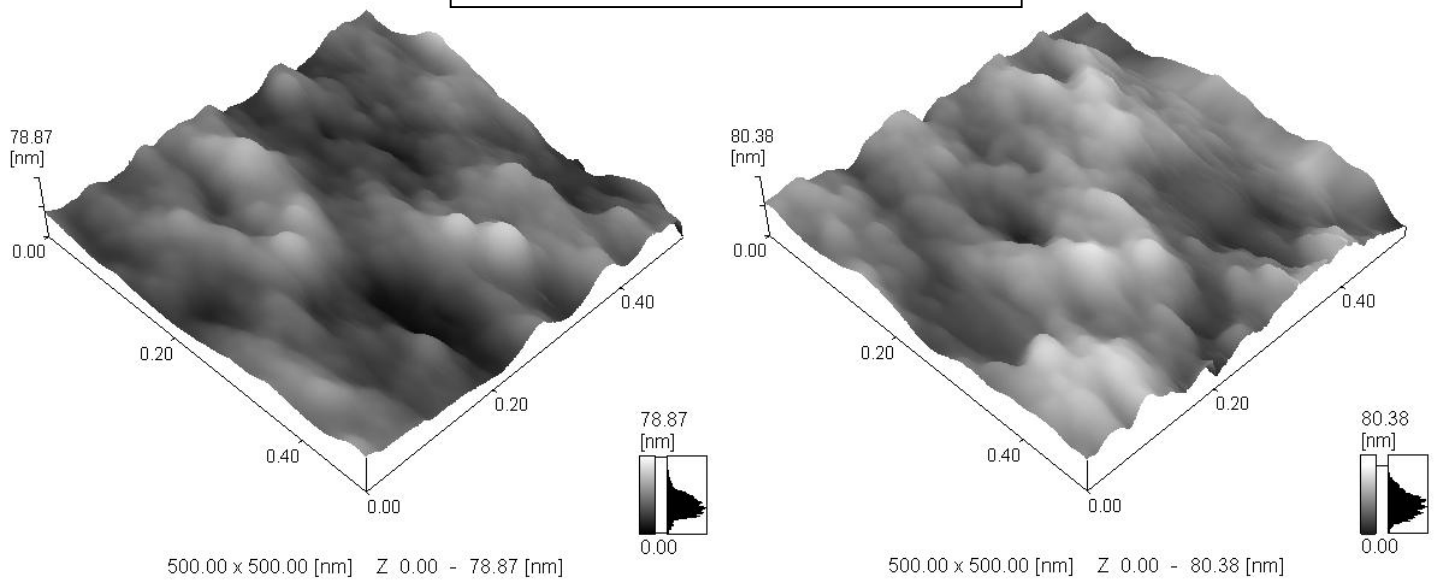
**(d)**

**10 mTorr, 600 °C, 8 Hz,  $1.6 \pm 0.1 \text{ J.cm}^{-2}$**



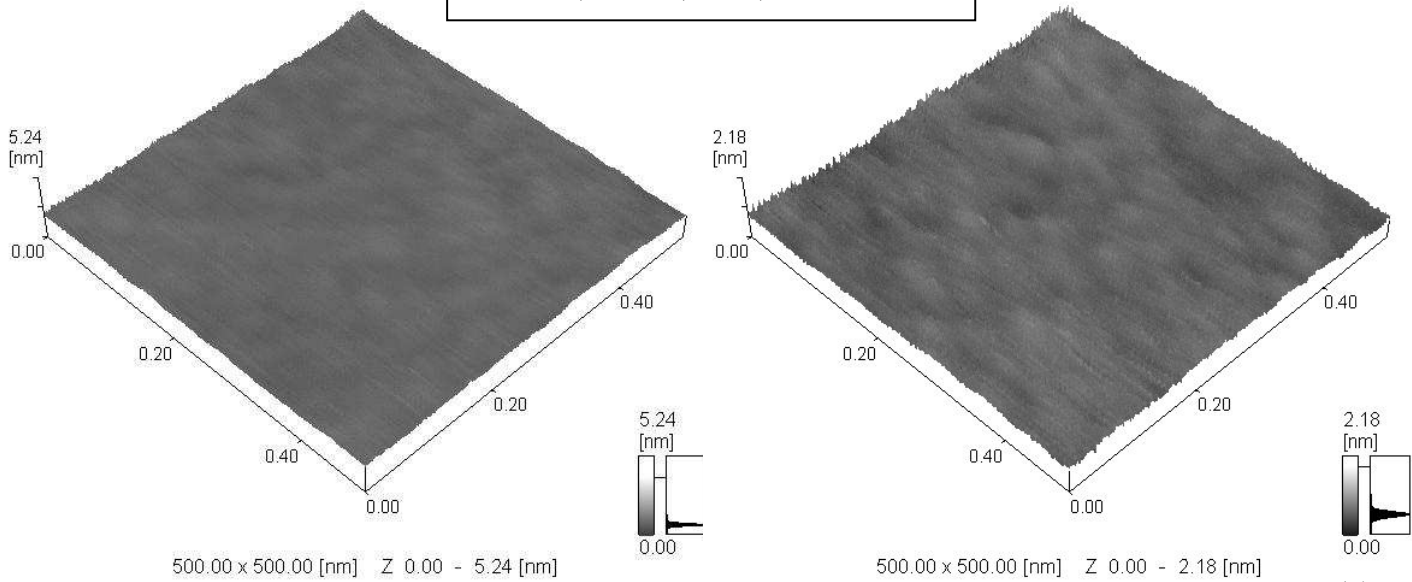
(e)

**1 Torr, 600 °C, 8 Hz,  $1.6 \pm 0.1 \text{ J.cm}^{-2}$**



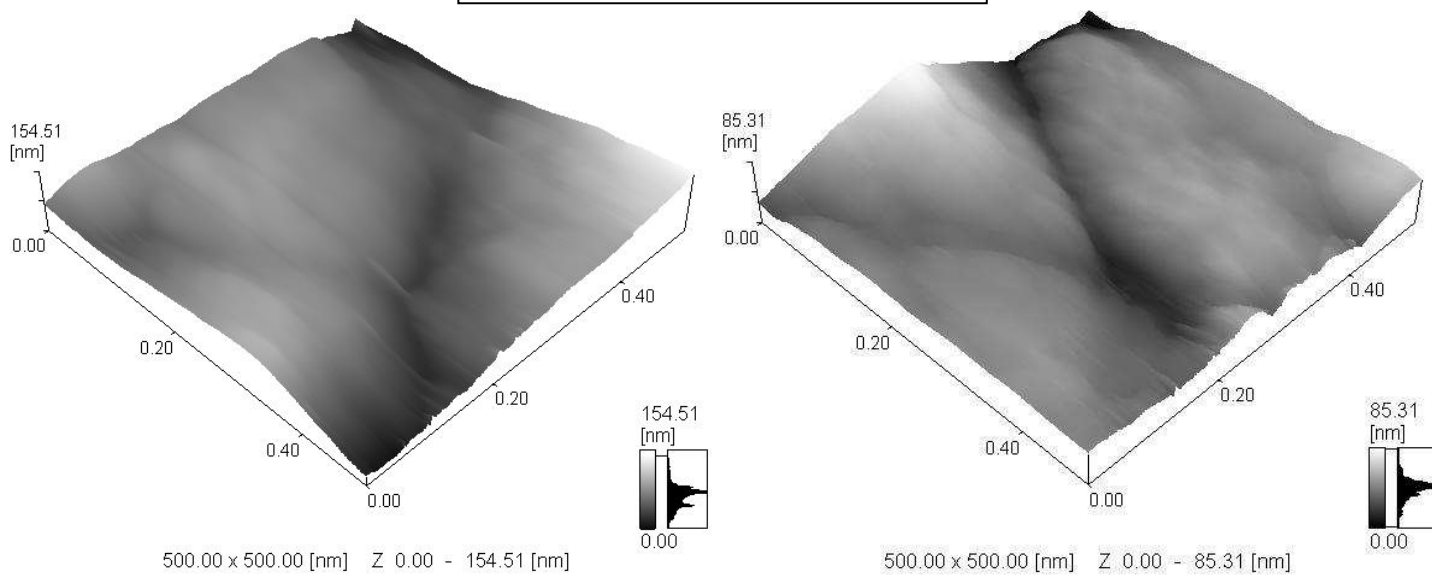
(f)

**Vacuum, 400 °C, 8 Hz,  $3 \pm 0.3 \text{ J.cm}^{-2}$**



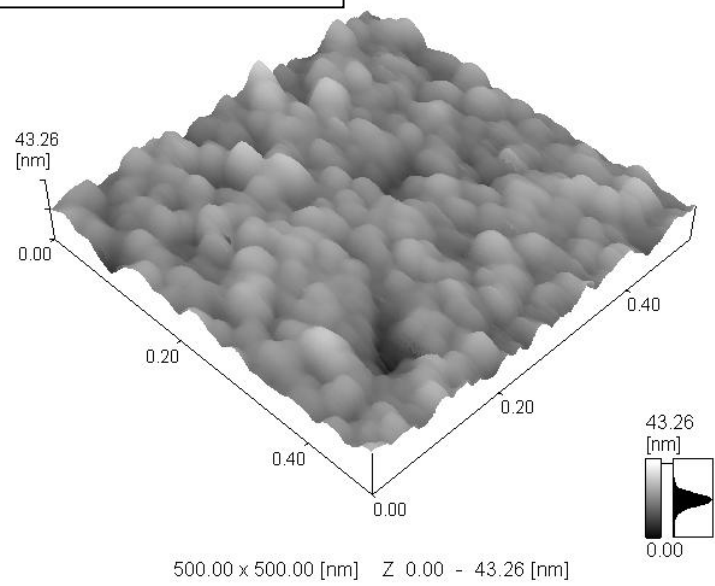
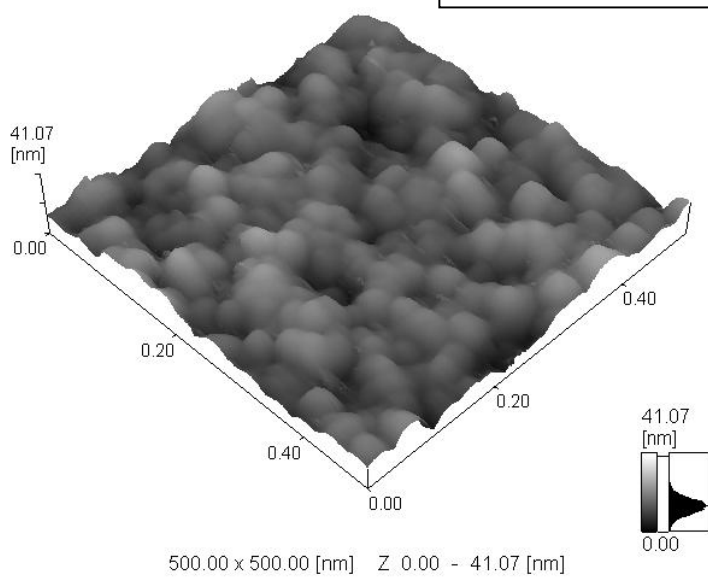
**(g)**

**1 Torr, 400 °C, 8 Hz,  $3 \pm 0.3 \text{ J.cm}^{-2}$**



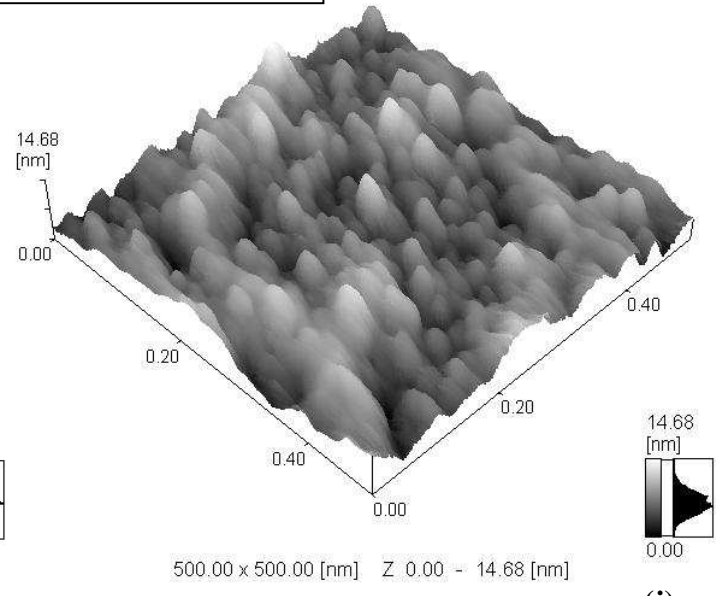
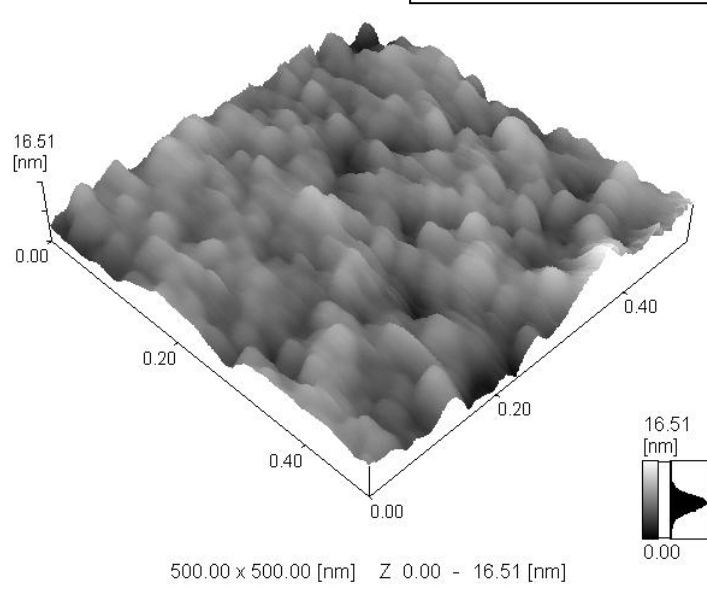
**(h)**

**455 mTorr O<sub>2</sub>, 600 °C, 8 Hz, 1.6 ± 0.2 J.cm<sup>-2</sup>**

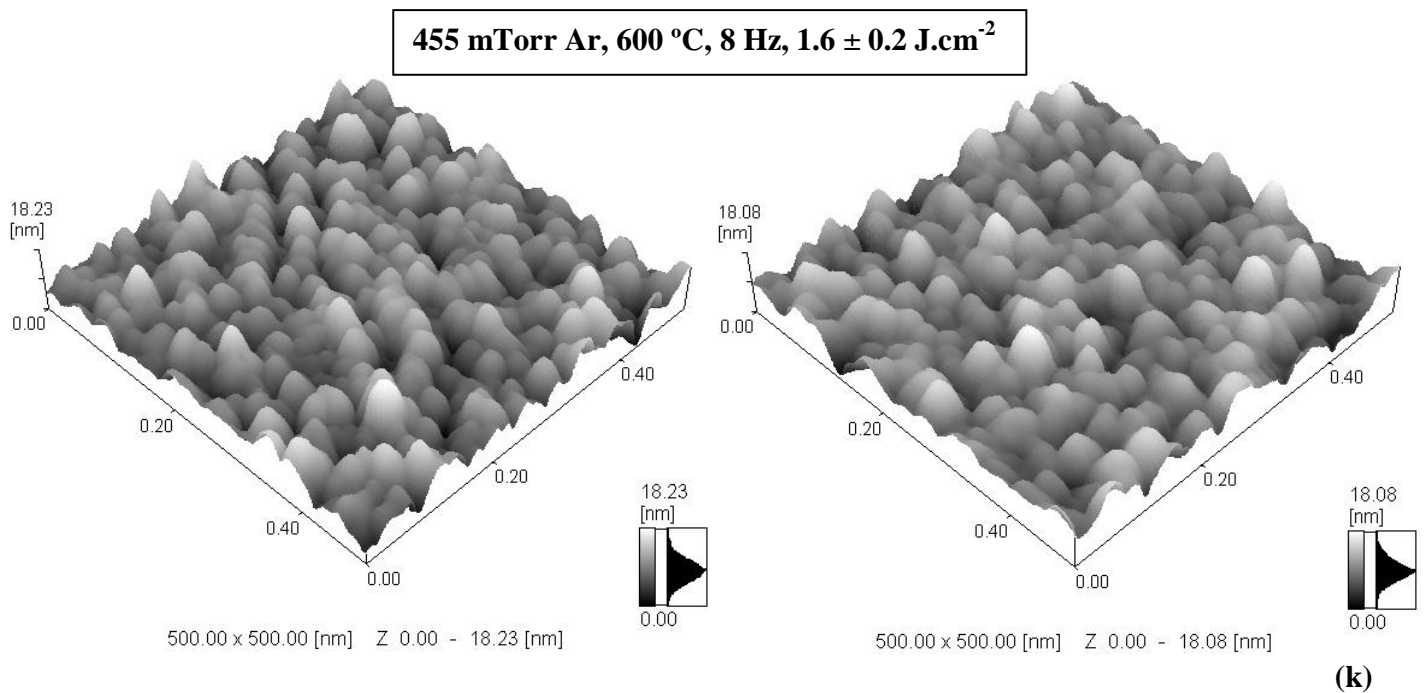


**(i)**

**455 mTorr N<sub>2</sub>, 600 °C, 8 Hz, 1.6 ± 0.2 J.cm<sup>-2</sup>**

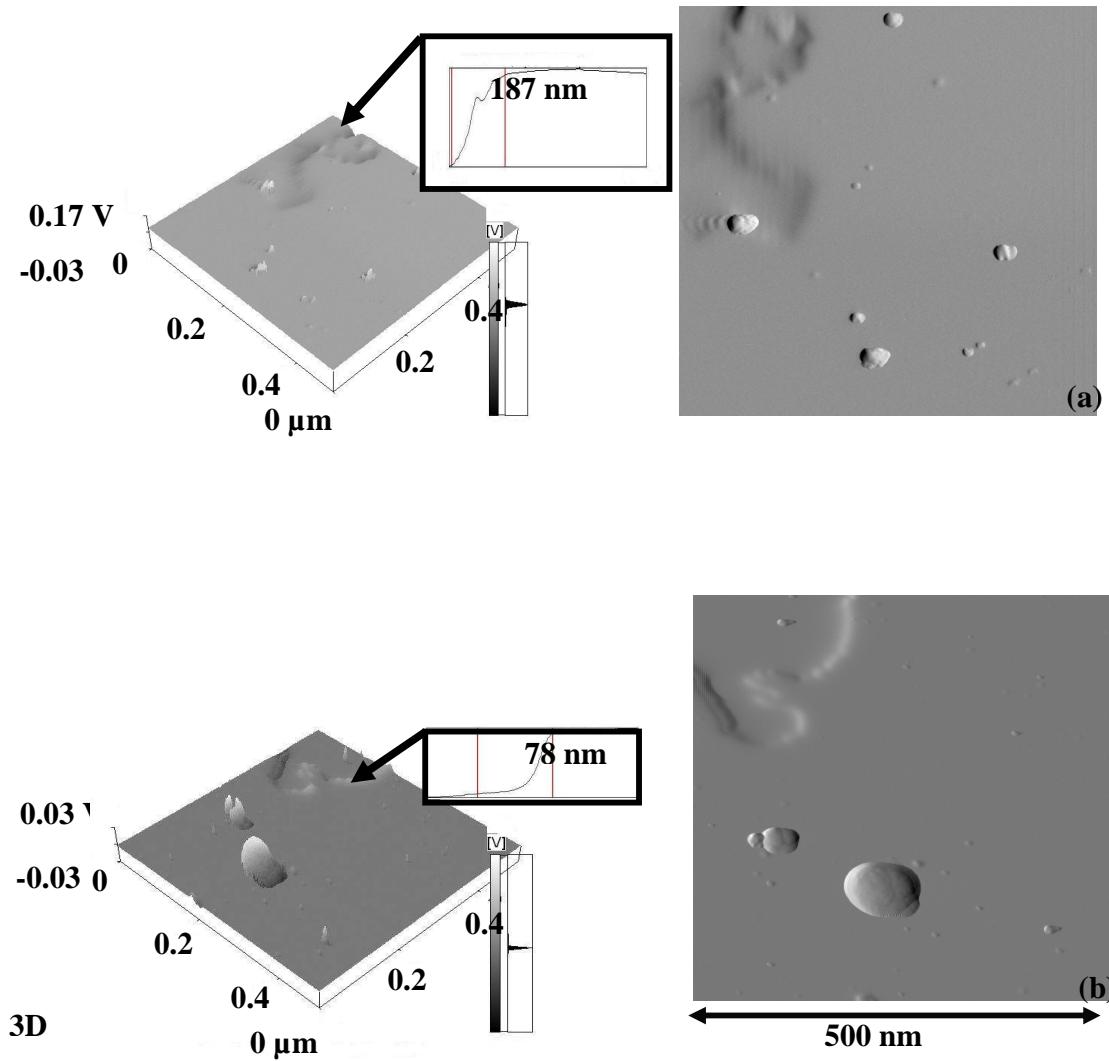


**(j)**



**Figure 6: 3D Height AFM images done in contact mode for the thin films in SET1 and 2 with a) – i) ablated in oxygen ambient, j) in nitrogen and k) in argon.**

It is clear from AFM images Fig. 6a), b), d), e), g) and j) that the thin films that appeared to be smooth and uniform from SEM images (Fig. 1a) and b), 3a) and b), 4a) and 5b)) either consist of a very thin layer of small nano - particles unevenly distributed or the surface layer covering the substrate can just be identified as *uniform* but with a rough surface area. Deflection images that was taken on these *uniform* thin films reflect very smooth surfaces, Fig. 7, and was used to indicate an estimation of the thickness of the thin films in Fig. 6a) and d) as a result of height profile. The growth process of the layers onto the substrate is an uneven process. The substrate surface in some cases is therefore not completely covered and the thin layer's thicknesses vary on different areas on the thin film. This is due to the fact that the target is rotating during the deposition process (in order to prevent destruction of the target by the powerful laser pulses) but the substrate is stationary. A solution to this problem could be to let the substrate rotate at the same speed as the target.



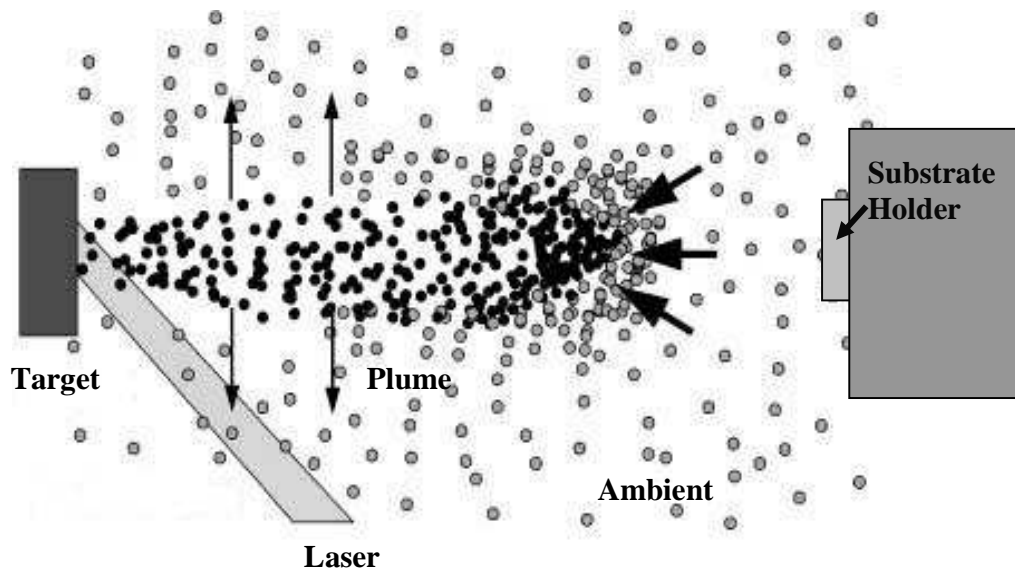
**Figure 7: Deflection 3D and 2D images of thin films in SET1 ablated in vacuum with a fluence of a)  $3 \pm 0.3$  and b)  $1.6 \pm 0.1 \text{ J.cm}^{-2}$  to show the rough estimation of the height of the thin films.**

Table 2 shows the surface roughness values for the thin films in Fig. 6.

**Table 2:  $R_{rms}$  values for the thin films in Fig. 6.**

<b><i>Figure 6</i></b>	<b><i>Left image (<math>R_{rms}(nm)</math>)</i></b>	<b><i>Right image (<math>R_{rms}(nm)</math>)</i></b>
<b>(a)</b>	0.13	0.12
<b>(b)</b>	0.12	0.12
<b>(c)</b>	12.26	13.29
<b>(d)</b>	0.39	0.16
<b>(e)</b>	0.72	0.19
<b>(f)</b>	10	11.1
<b>(g)</b>	0.09	0.08
<b>(h)</b>	20.84	11.57
<b>(i)</b>	3.94	3.77
<b>(j)</b>	1.83	2.07
<b>(k)</b>	2.72	2.55

The thin films ablated in vacuum and 10 mTorr ambient  $O_2$ , (Fig. 6a), b), d), e) and g)) show the same morphology. The low 10 mTorr ambient pressure would thus have minor affect on the kinetic energies and particle sizes of the particles in the plume. An increase in the pressure to 1 Torr  $O_2$  however shows a definite increase in particle size (Fig. 6c), f) and h)) and RMS roughness. The increased ambient pressure results in shorter mean free path lengths of the particles. This causes more collisions that reduce the kinetic energies and ensure longer residence stay time in the plume. This in turn enables longer time for nucleation, growth and agglomeration of the particles to occur as they adhere onto the substrate. Fig. 8 shows a schematic diagram of how the particles in the plume experience obstruction and collisions from the gas particles in a high ambient pressure.



**Figure 8: Schematic diagram to illustrate the interactions of the particles in the plume in a higher ambient pressure before they reach the substrate [4].**

The effect of the increased fluence that led to bigger particle and grain sizes can be seen from Fig. 6c) compared to Fig. 6f) [1, 5]. The SEM images in Figs. 1c) and 3c) clearly show that the sizes of the particles formed at lower fluence are smaller and also less agglomerated than the particles that were ablated with the higher fluence. The higher fluence therefore led to a thicker layer of nano - particles formed than at the lower fluence. The particle sizes of the higher fluence vary mainly between 130 to 140 nm (and bigger) and the lower fluence sizes vary between 50 and 60 nm. The higher fluence particles consist of smaller particles ranging from 5 to 30 nm as measured with AFM. The surface structure of the thin film ablated at 400 °C substrate temperature (Fig. 6h) and 4b)) is less compact (lesser agglomeration of particles than at 600 °C). A rough estimate of the number of particles/cm<sup>2</sup> for the 400 °C and the 600 °C samples is 3 x 10<sup>9</sup> particles/cm<sup>2</sup> compared to 4 x 10<sup>9</sup> particles/cm<sup>2</sup>. These bigger particles are however an agglomeration of smaller particles. The value for the lower fluence (Fig. 3c)) is of the order of 15 x 10<sup>9</sup> particles/cm<sup>2</sup>. The height measurements done at the interfaces of the regions not covered by the ablated thin films (Fig. 7a) and b)) show thicknesses of 187 and 78 nm, respectively. The higher fluence led to a thicker *uniform* thin film as expected. The increase in substrate temperature definitely resulted in a rougher surface

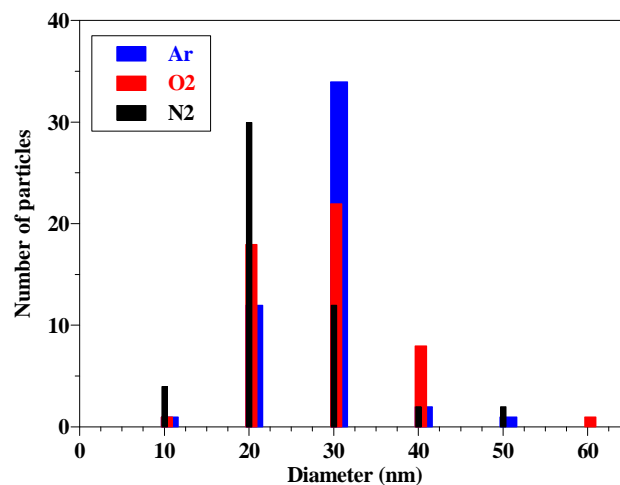
layer as can be seen from Fig. 6g) and a) and h) and c). More variations in the substrate temperature would be a future research project.

Fig. 6j) indicates that ablation in N<sub>2</sub> gas resulted in small particles of mostly 20 nm in diameter and the maximum height measured at 14.7 nm. Ablation in O<sub>2</sub> gas (Fig. 6i)) produced bigger particles of 20, 30 and 40 nm as well as an agglomeration of these particles into bigger size clusters of about 80 to a 100 nm. Fig. 6k), ablation in Ar gas, shows particle sizes of mostly 30 nm and maximum height of about 19.8 nm. The particles in Fig. 6k) are much more spherically defined and evenly distributed on the surface in comparison with the agglomerated particles in Fig. 6i).

As mentioned earlier, thin film morphology and other characteristic properties strongly depend on the gas pressure during PLD. The ambient particles interact with the particles in the plume and this has an effect on the particle sizes, amount and status as they arrive at the substrate [6]. The vaporised particles close to the target's surface have high kinetic energies due to energy transfer from the laser's ablation spot (having a temperature of about 5000 to 10 000 K [7]). In vacuum there is virtually no collisions between the ejected species before they reach the substrate and the particles could have a mean free path length of up to 5 cm. When a background gas is introduced of about 100 mT, the path length could decrease to 0.05 cm [1]. Colliding with the gas atoms and scattering in the plasma decreases the kinetic energies of the particles and delete "some sort of" disorder in the plume.

High background pressures act as a buffer and increases the resident stay time of the particles in the plume [1, 6]. It is possible that some of the vaporized particles that have high kinetic energies get scattered away either from the substrate or from the gas atoms in the plume. These fast moving particles get scattered out of the flight path of the ablated material between the target and substrate and they could also open a channel for deposition of the slower particles. There is thus a decrease in the amount of particles reaching the substrate at the end [4, 8].

Ablation in O<sub>2</sub> resulted in bigger agglomerated particles (small variation of about 10 nm compared to ablation in N<sub>2</sub>), see Fig. 9. This could be explained due to the small difference in the gas particle sizes between the O<sub>2</sub> and N<sub>2</sub> molecules [9]. O<sub>2</sub> molecules and bonding length between the atoms are a little bit bigger and thus creates a longer resident stay time for the particles in the plume so that they agglomerate into these bigger particles. Ar atom clusters are even bigger in size (about 20 nm) and they act as a plume buffer. The Ar atoms are almost static and the dense cloud of ablated material moves slowly through the diluted arrangements of Ar atoms. The ablated particles move *slower* through the Ar buffer but with lesser collisions which prevent the formation of bigger agglomerated particles (collisions are much more elastic) [8].



**Figure 9: Rough estimation of particle size distribution for 50 particles in a 500 x 500 nm area.**

### 5.3.3 Comparison: SET1 and 2

Comparisons were made in order to compare the particle diameter and particle density with the changes in the different process parameters, see Fig. 10 and 11.

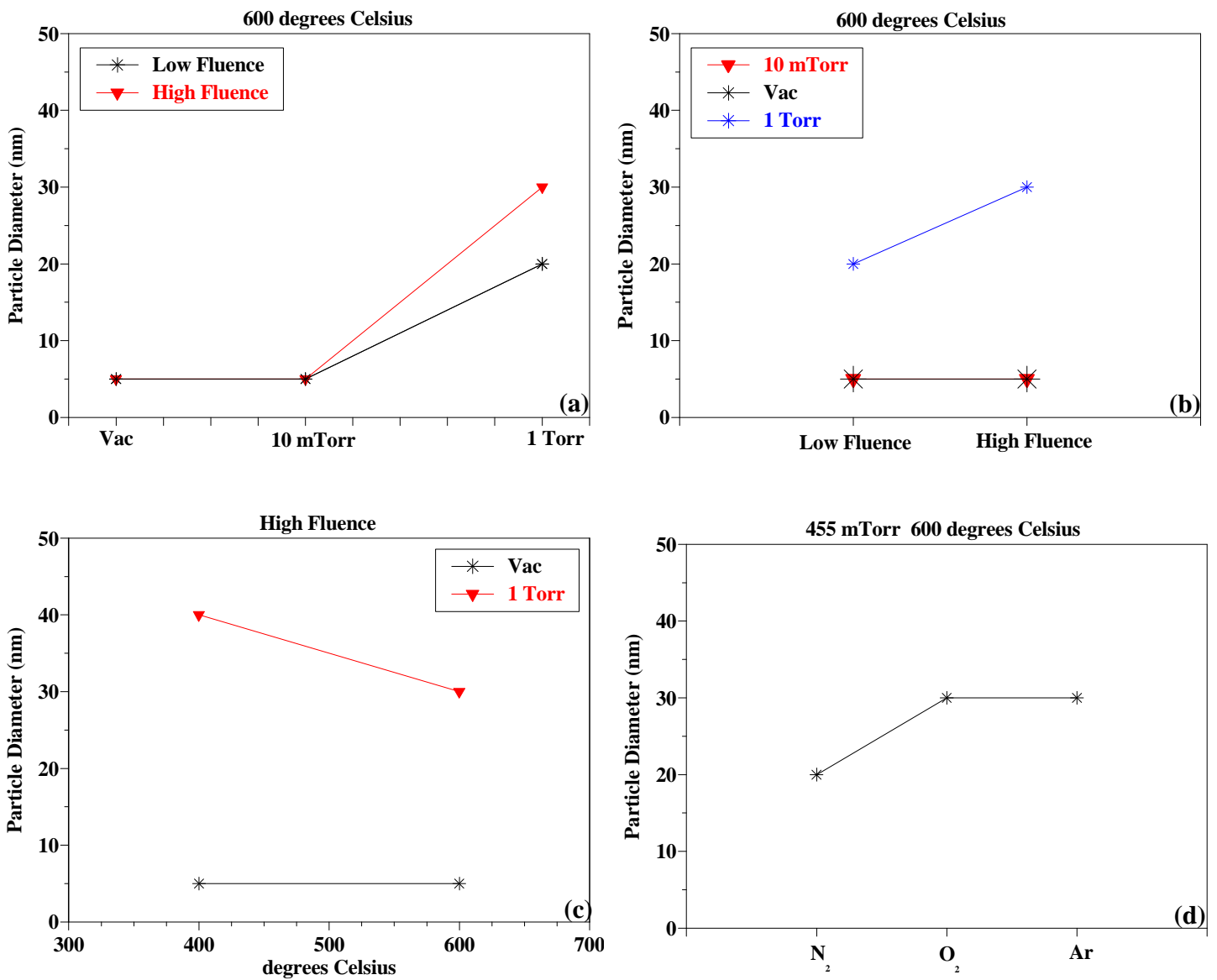


**Figure 10: Comparison of the particle diameter against the different process parameters, which is a) different O<sub>2</sub> gas pressures at 600 °C substrate temperature, b) low and high fluence at 600 °C substrate temperature (see table 1), c) different substrate temperatures at the high fluence of  $3 \pm 0.3 \text{ J/cm}^2$  and d) different gas species at 455 mTorr and 600 °C (Error of  $\pm 5 \text{ nm}$ ).**

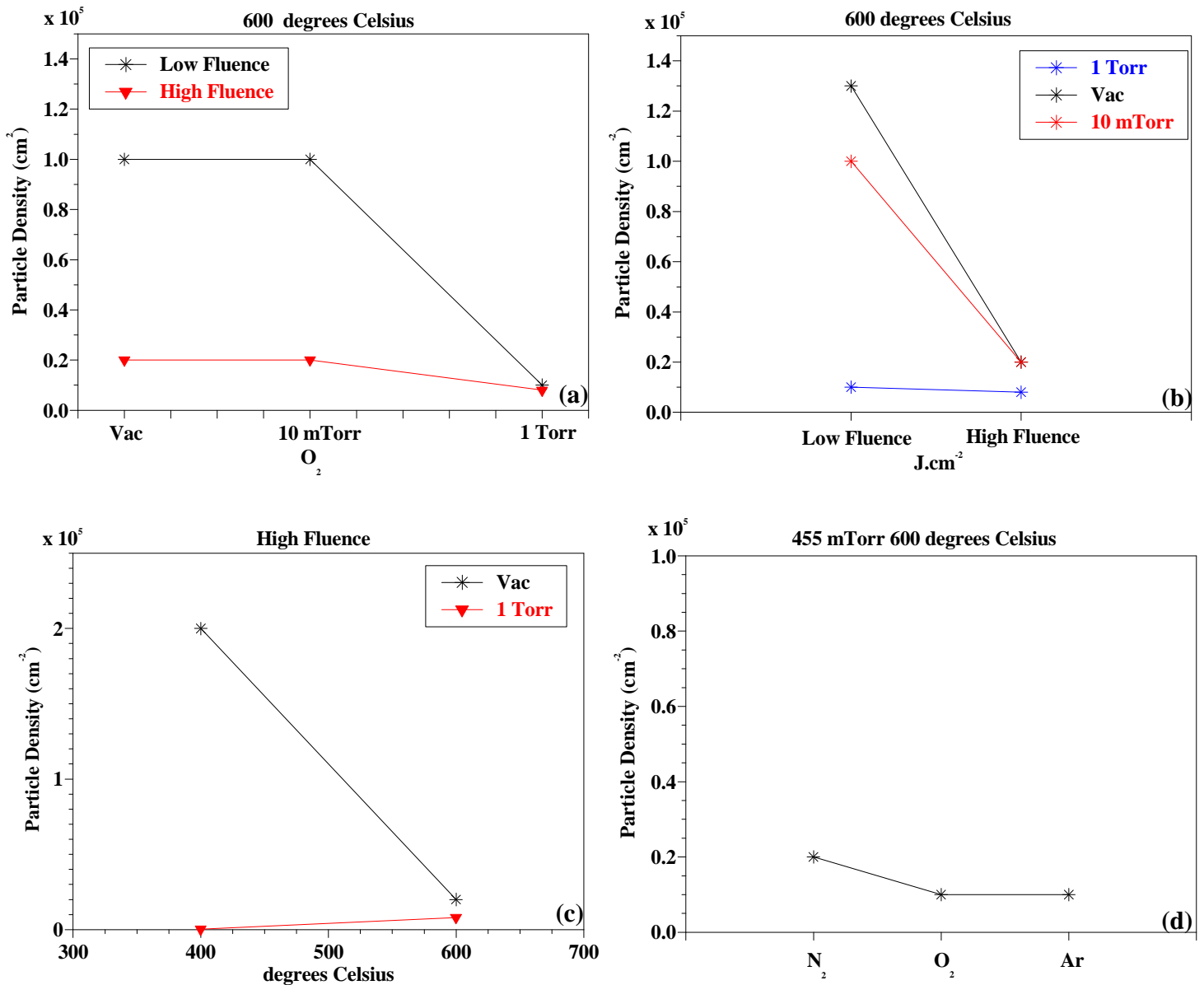


**Figure 11: Comparison of the particle density against the different process parameters, which is a) different O<sub>2</sub> gas pressures at 600 °C substrate temperature, b) low and high fluence at 600 °C substrate temperature (see table 1), c) different substrate temperatures at the high fluence of  $3 \pm 0.3$  J/cm<sup>2</sup> and d) different gas species at 455 mTorr and 600 °C (Error of  $\pm 0.06 \times 10^5$  particles per cm<sup>-2</sup>).**

In Fig. 10 50 particles were analysed in a 500 x 500 nm area. From Fig. 10a) and b) the bigger particles (diameter of 30 nm) appear with ablation at the higher fluence of  $3 \pm 0.3$

J/cm<sup>2</sup> in an O<sub>2</sub> ambient pressure of 1 Torr. The low fluence of  $1.6 \pm 0.1$  J/cm<sup>2</sup> result in particle diameter of mostly 20 nm in 1 Torr ambient while the vacuum and 10 mTorr ambient resulted in particle diameters of smaller than 10 nm (about 5 nm). Fig. 10c) shows that ablation in 1 Torr O<sub>2</sub> ambient at 400 °C substrate temperature resulted in particle diameters of about 40 nm and the increase to 600 °C lead to smaller particle diameters of 30 nm. Ablation in vacuum at both temperatures showed particle diameters of below 10 nm. Fig. 10d) showed that both the thin films that were ablated in O<sub>2</sub> and Ar ambient resulted in the bigger particle diameters of 30 nm.

From Fig. 11a) and b) it is clear that ablation with the higher fluence and in a ambient of 1 Torr show a lower particle density due to the bigger particles on the surface. The particle density was calculated in a 500 x 500 nm area. Fig. 11c) shows the lower particle density for the 1 Torr ambient at 400 °C also due to the bigger particles and in vacuum it shows a much higher density due to agglomerated particles on the surface. In Fig. 10d) the particle density of the thin films ablated in O<sub>2</sub> and Ar gas are both lower than the N<sub>2</sub> gas due to the bigger particles on the surface.

## 5.4 Conclusion

Y<sub>2</sub>SiO<sub>5</sub>:Ce thin films were successfully grown onto the Si (100) substrates and the effect of some of the process parameters indicated definite changes in particle sizes. Nano - particles appeared on the thin films when ablation was done with a ambient background. The size of the particles depended on the background pressure, the gas species and the substrate temperature as well as on the laser fluence. An increase in the ambient pressure to 1 Torr O<sub>2</sub> resulted in bigger particle sizes. Ablation with the higher fluence ( $3 \pm 0.3$  J.cm<sup>-2</sup>) also lead to bigger particle formation. The increase in the substrate temperature (from 400 to 600 °C) at high fluence showed big particles which are actually an agglomeration of smaller particles and therefore a rougher surface. Ablation in the Ar ambient showed 30 nm (bigger than the N<sub>2</sub>) particle sizes but lesser agglomeration than the O<sub>2</sub> ambient. The bigger particle sizes therefore result in lower particle densities.

## References

1. L. Chen, Particles generated by pulsed laser ablation, in D. B. Chrisey, G. K Hulber (Eds), Pulsed Laser Deposition of Thin Films, John Wiley & Sons, Inc, New York, (1994) 184.
2. E. Coetsee, H. C. Swart, J. J. Terblans, O. M. Ntwaeaborwa, K. T. Hillie, W. A. Jordaan, and U. Buttner, *Opt. Mater*, **29** (2007) 1338.
3. E. Coetsee, H. C. Swart, and J. J. Terblans, *J. Vac. Sci. Technol. A*, **25(4)** (2007) 1226.
4. T. Scharf and H. U. Krebs, *Appl. Phys. A, Mat. Sci. and Proc*, **75** (2002) 551.
5. X. L. Tong, D. S. Jiang, L. Liu, Z. M. Liu, M. Z. Luo, *Optics Communications*, **270** (2007) 356.
6. M. Liu, B. Y. Man, C. S. Xue, H. Z. Zhuang, H. C. Zhu, X. Q. Wei, C. S. Chen, *Appl. Phys. A*, **85** (2006) 83.
7. H. Krebs, M. Weisheit, J. Faupel, E. Suske, T. Scharf, C. Fuhse, M. Stormer, K. Sturm, M. Seibt, H. Kijewski, D. Nelke, E. Panchenko and M. Buback, Pulsed Laser Deposition (PLD) – a Versatile Thin Film Technique, B. Kramer, *Advances in Solid State Physics*, Springer Berlin/Heidelberg, **43** (2003) 101.
8. K. Sturm, S. Fahler and H. Krebs, *Appl. Surf. Sci*, **154-155** (2000) 462.
9. [http://www.webelements.com/oxygen/atom\\_sizes.html](http://www.webelements.com/oxygen/atom_sizes.html) [Accessed 20 January 2009].

## Chapter 6

### Crystal structure and luminescent properties of the $\text{Y}_2\text{SiO}_5\text{:Ce}$ thin films: Part two

The crystal structure of the thin films in SET1 and 2 were determined by XRD analysis. The results are presented in this chapter. The luminescent properties were investigated with CL scanning images obtained (SET3 thin films) and with CL and PL measurements for SET1 and 2 thin films.

#### 6.1 Introduction

As mentioned in section 2.4,  $\text{Y}_2\text{SiO}_5\text{:Ce}$  has a very complicated crystal structure and analysis done by Coetsee *et al.* [1] on the crystal structure of the phosphor thin films and powders showed that it has the monoclinic  $X_1$  phase structure. Together with research done on the crystal structure, luminescent properties were also analyzed. The main purpose of this study is to improve the luminescent efficiency of the phosphors used in field emission displays (FEDs) [2, 3]. The need for smooth and uniform thin films for possible application in high performance electronic and optical devices (e.g FEDs) leads to more advance investigation on the growth of thin films. Smooth uniform thin films result in low intensity luminescence whereas a rougher surface would result in a higher intensity [4, 5]. This was also proved by Coetsee *et al.* [6]. The following chapters involve the luminescent properties investigation that was done on the thin films prepared with different process parameters.

#### 6.2 Experimental Procedure

##### 6.2.1 Characterization of the $\text{Y}_2\text{SiO}_5\text{:Ce}$ thin films: SET 1 and 2

The crystal structure was analyzed by using a Siemens Diffractometer D5000 equipped with a Cu source with XRD.

### 6.2.2 Characterization of the Y<sub>2</sub>SiO<sub>5</sub>:Ce thin films: SET 3

CL scanning images were done during SEM measurements with a Mono-CL 3 system from Gatan to investigate the effect of the tin oxide (SnO<sub>2</sub>) coated layer on the light output.

### 6.2.3 CL and PL spectrometry for the thin films: SET 1 and 2

CL measurements were performed with an electron beam current density of 26.3 mA.cm<sup>-2</sup>, 2 keV energy electrons in a ultra high vacuum chamber with base pressure 6 x 10<sup>-9</sup> Torr. CL was done in the PHI Model 549 system and the CL data were collected with an Ocean Optics S2000 spectrometer. PL measurements were done with a HeCd laser ( $\lambda = 325$  nm) with a power of 3 mW.

## 6.3 Results and Discussion

### 6.3.1 XRD

Figs.1 and 2 show the XRD results for the thin films in SET1 and 2 compared to the X<sub>1</sub>-phase of monoclinic Y<sub>2</sub>SiO<sub>5</sub>. The powder used as a target has a monoclinic crystal structure of Y<sub>2</sub>SiO<sub>5</sub>:Ce X<sub>1</sub> - phase with space group P2<sub>1</sub>/c [1]. The XRD results for the thin films showed very low intensity peaks which is an indication that the layers are almost amorphous with only some indication of small peaks that belong to the monoclinic crystal structure. Sun *et al.* [2] studied silicate phosphor (Y<sub>2</sub>SiO<sub>5</sub>:Ce, Zn<sub>2</sub>SiO<sub>4</sub>:Mn and CaSiO<sub>3</sub>:MnPb) thin films prepared by PLD. The substrate temperature used was 300 °C (as grown) and the thin films were annealed for 5 hr in air, at 800 and then 1000 °C. The XRD results for the Y<sub>2</sub>SiO<sub>5</sub>:Ce thin films showed an increase in crystallinity with an increase in annealing temperature with the two main peaks for the X<sub>1</sub> - phase only visible after annealing at 1 000 °C, (-402) and (013). A PL intensity increase was clearly observed for the higher annealing temperature. The enhanced luminescence was attributed to the increased crystallinity as well as the rougher surface morphology [2].

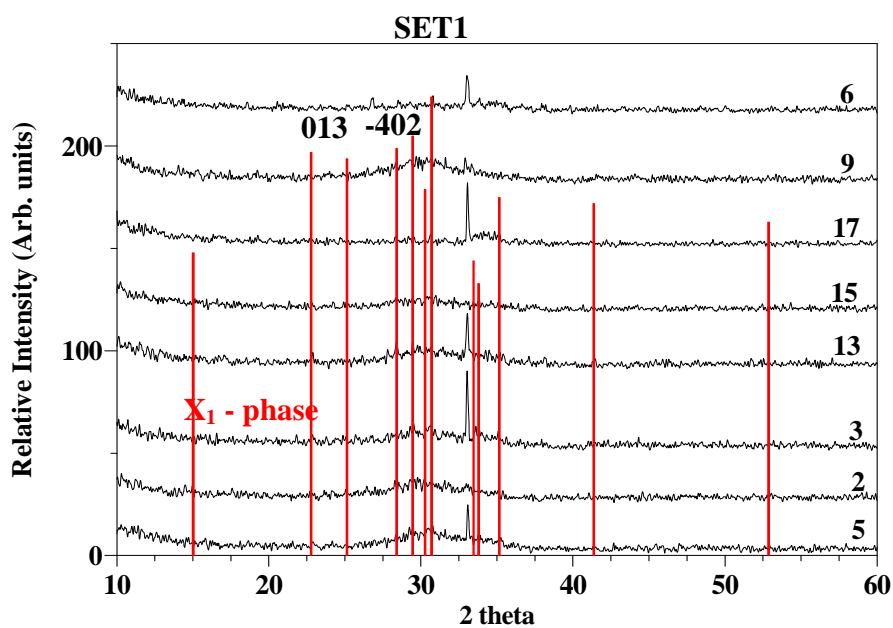


Figure 1: XRD results showing the amorphous crystal structure of the various thin films in SET1 compared to the X<sub>1</sub>- phase.

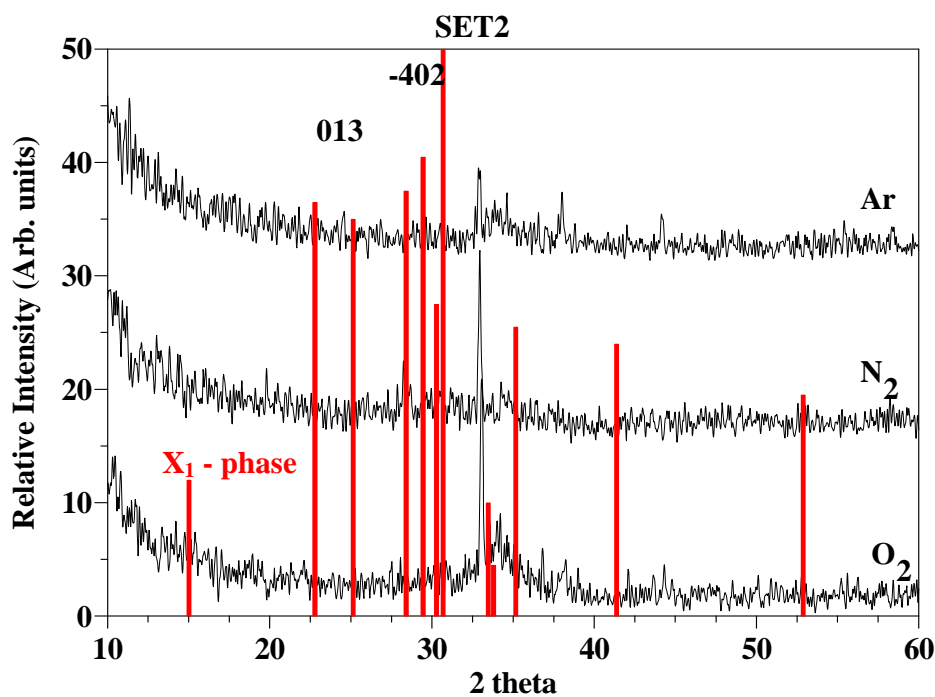


Figure 2: XRD results showing the amorphous crystal structure of the various thin films in SET2 compared to the X<sub>1</sub>- phase.

Fig. 2 shows only the Si (200) peak at about  $33^\circ$  (substrate surface) with the two low intensity main peaks of  $\text{Y}_2\text{SiO}_5\text{:Ce}$  which are not clearly resolved. The Si (200) peak can be detected due to the fact that the Si (100) substrate is doped with boron and the Si (400) would be detected at  $69^\circ$  [7, 8]. Su *et al.* [9] also found a small peak at  $33^\circ$  and labelled it to be the Si (200) peak during their investigation on (211)  $\text{BaTiO}_3$  thin films that were grown on Pt-coated Si (100) substrates by radio frequency magnetron sputtering. They have conclude that the Si (200) peak can only be detected due to a result from multiple scattering effects because Si has a diamond structure in which the (200) reflection is not allowed.

From these XRD results (Fig. 1 and 2) it is clear that amorphous thin films developed during the PLD process. XRD completed the characterization on these thin films. Although the effect of the different process parameters on the crystal structure could not clearly be detected with XRD, the surface morphology (particle shapes and sizes) was sufficiently described with SEM, EDS and AFM. In the next sections the luminescent properties will be discussed in order to investigate the effect of the different thin film surfaces.

### 6.3.2 CL Scanning

CL scanning images were obtained for some of the thin films during SEM measurements. CL images were obtained during the scanning process in order to see whether the larger micron size particles on the surface are luminescent and how the intensity compared with the surface layer. Such CL scanning images were done on one thin film in SET1 and on the two films in SET3.

Interesting to note was the CL scanning image of a larger particle on the surface of the thin film that was ablated with PLD in a 1 Torr  $\text{O}_2$  ambient ( $600^\circ\text{C}$ , low fluence,  $1.6 \pm 0.1 \text{ J.cm}^{-2}$ ). The thin film consists of nano-  $\text{Y}_2\text{SiO}_5\text{:Ce}$  particles with larger micron size particles on the substrate as can also be seen from Fig. 3a). The CL scanning images that were obtained, Fig. 3b), at a PMT voltage of 650 eV, indicated emission from 3 small light emitting centres inside the bigger micron particle. These centres are not clearly

defined in the SEM image, Fig. 3a). In Fig. 3c) the PMT voltage was increased to 850 V and the effect of a higher luminescence is clearly visible. Emission seems to occur from the whole micron particle as well as from the smaller particles around the particle. The smaller particles did not show effective emission with the lower PMT voltage, Fig. 3b). Fig. 4 shows the CL scan results of the uncoated a) and tin oxide coated b) thin films. There is a definite increase in luminescent intensity with the uncoated thin film which indicates the photon absorption effect of the extra tin oxide coated layer. CL intensity is mainly coming from the bigger spherical particles on the surface as seen from these images.

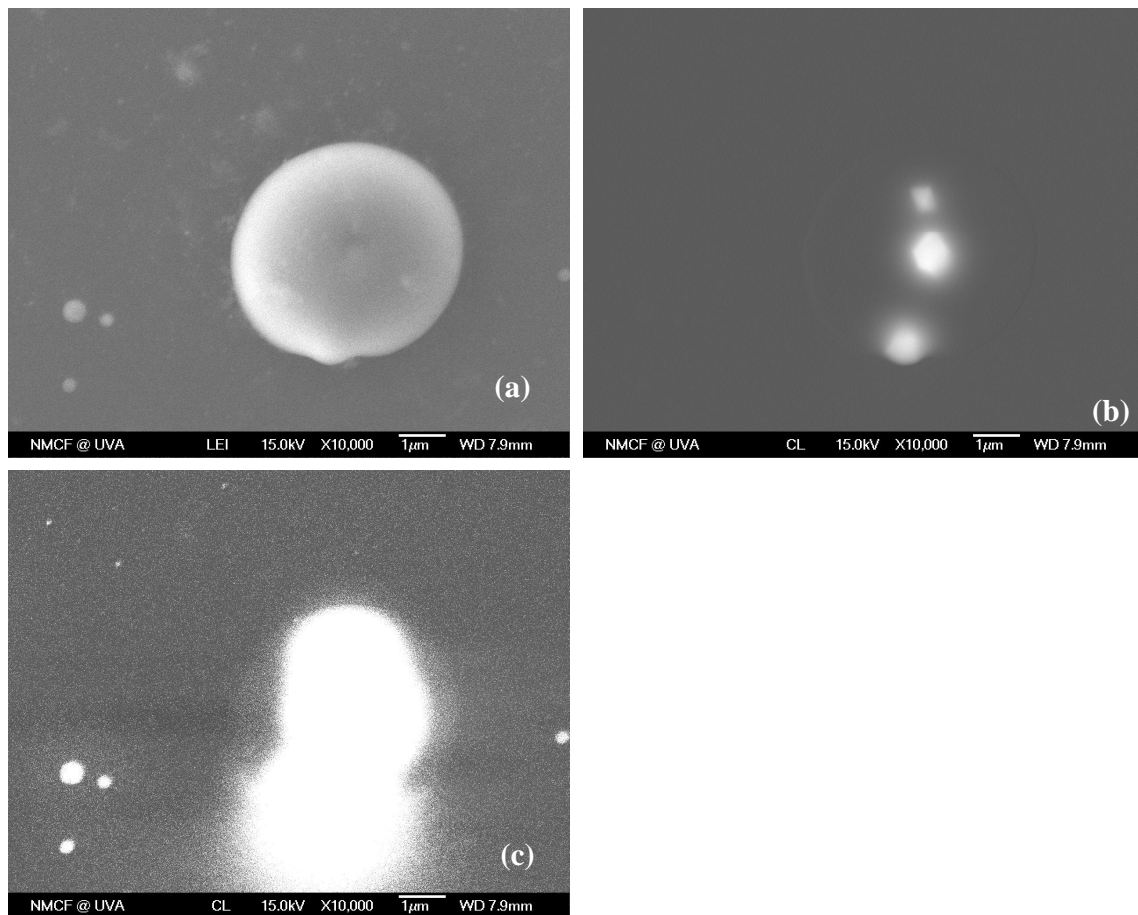


**Figure 3: a) SEM image and b, c) CL images of the  $Y_2SiO_5:Ce$  thin film (1 Torr, low fluence, 600 °C) performed at 15 kV electron beam energy, magnification of  $\times 10\,000$  and a scale of 1  $\mu m$  with a photomultiplier tube (PMT) voltages of 650 and 850 V, respectively.**

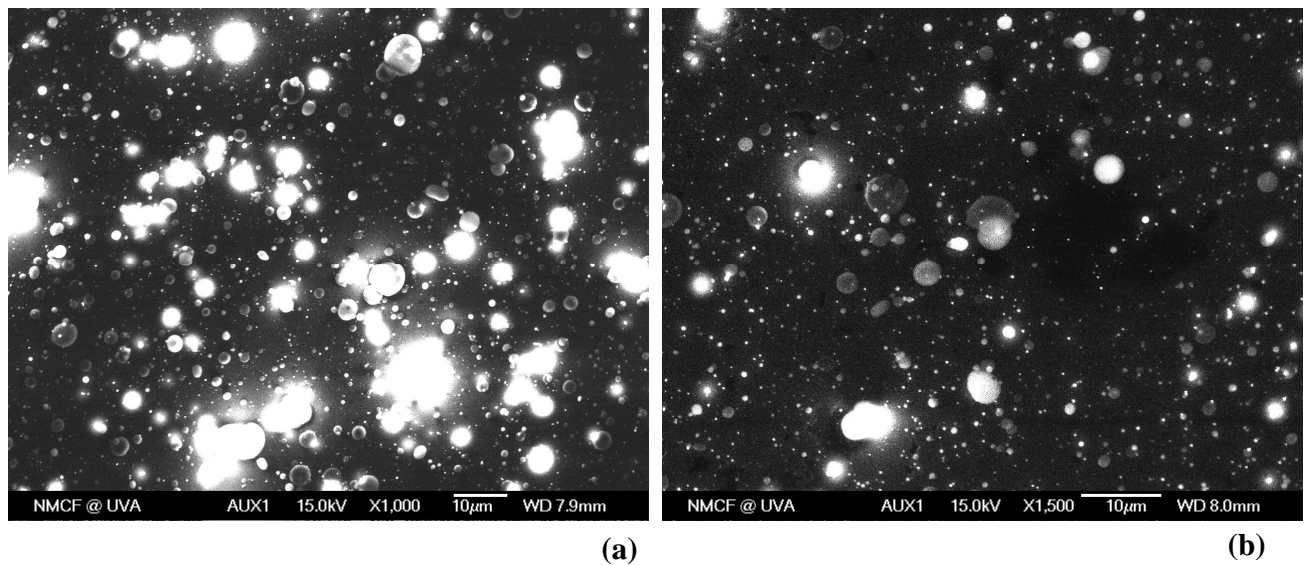


**Figure 4: CL images of a) the uncoated  $Y_2SiO_5:Ce$  and b) tin oxide coated thin films performed at 15 kV electron beam energy, magnification of  $\times 1\,000$  and  $\times 1\,500$  respectively, a scale of  $10\ \mu m$  with a photomultiplier tube (PMT) voltage of 650 V.**

The tin oxide coated thin film in Fig.4 was ablated for previous investigation on the degradation of the thin films. The tin oxide acts as a coated layer to prevent electron stimulated reactions with the phosphor surface and thus inhibits degradation [10]. However it was found that the degradation was prevented but the coated layer decreased the luminescent intensities. This was also showed by the CL scanning images from Fig. 4. CL and PL measurements were then performed on the thin films for further investigations.

### 6.3.3 CL measurements

As mentioned before, the growth process during PLD is not a uniform process (due to the fact that only the target is rotating) and it was observed during AFM height profile analysis that some areas on the film are thicker and have bigger particles compared to other areas. Luminescence from a thin film normally results in a lower intensity due to the internal reflection of the light exiting the layer. A rougher surface would therefore result in a better light output (compared to a uniform surface layer) and higher intensity [1].

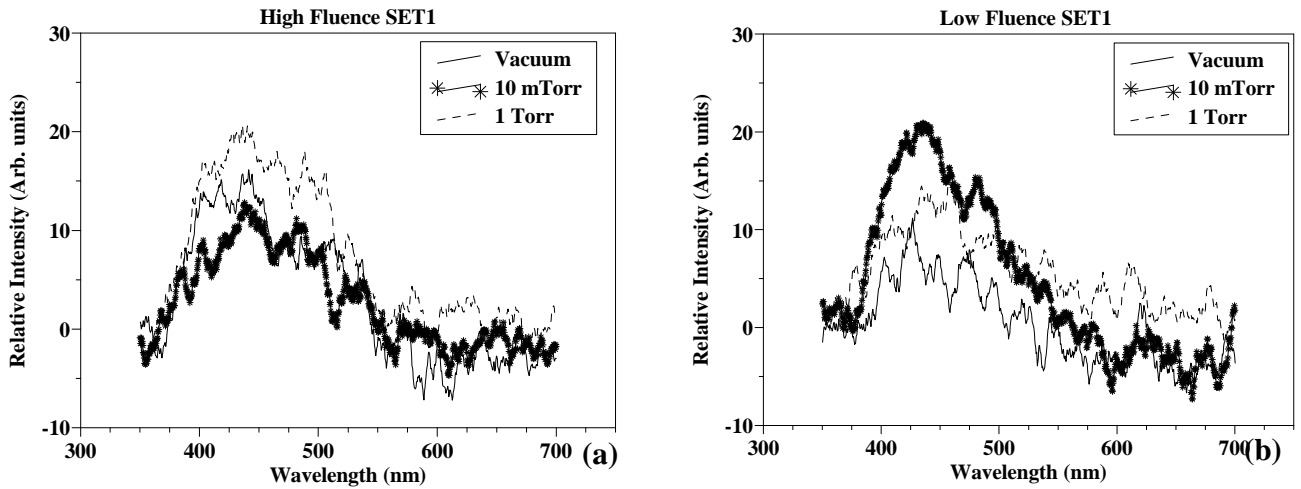


**Figure 5: CL spectra for the thin films in SET1 ablated with a) a high fluence of  $3 \pm 0.3 \text{ J.cm}^{-2}$  and b) low fluence of  $1.6 \pm 0.1 \text{ J.cm}^{-2}$ . ( $\text{O}_2$  ambient and  $600 \text{ }^\circ\text{C}$  substrate temperature).**

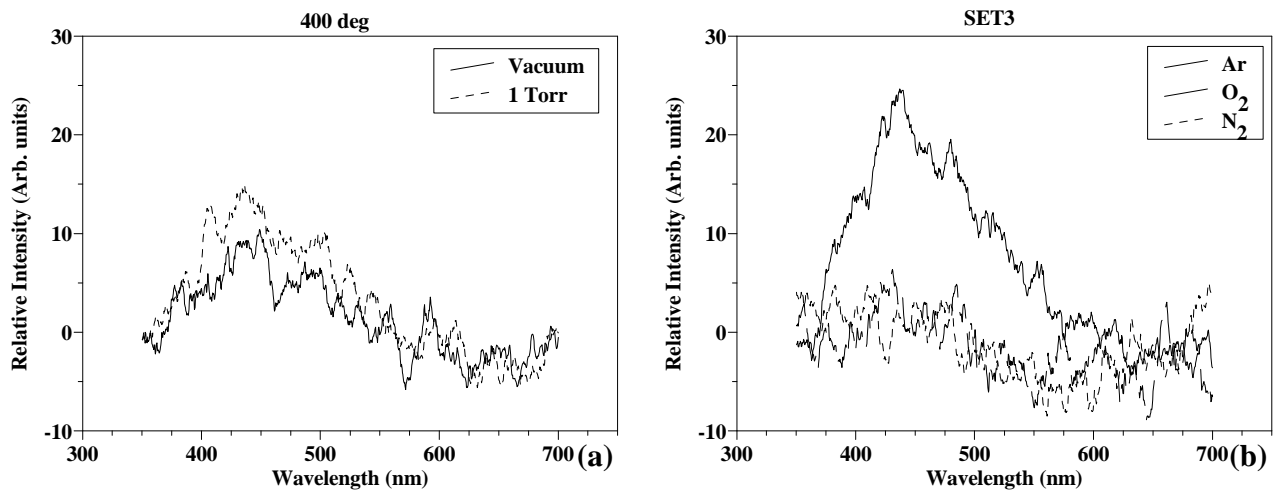


**Figure 6: CL spectra for the two thin films in SET1 ablated with a) a high fluence of  $3 \pm 0.3 \text{ J.cm}^{-2}$  and substrate temperature of  $400 \text{ }^\circ\text{C}$  ( $\text{O}_2$  ambient). b) CL spectra for the thin films in SET3 ablated with a low fluence of  $1.6 \pm 0.2 \text{ J.cm}^{-2}$  in three different ambients (Ar,  $\text{O}_2$  and  $\text{N}_2$ ) at a pressure of  $455 \text{ mTorr}$  and substrate temperature of  $600 \text{ }^\circ\text{C}$ .**

From Fig. 5a) and b) and 6a) it is clear that the increased  $\text{O}_2$  ambient (1 Torr) resulted in a higher CL intensity compared to the thin films ablated in vacuum. This is in agreement

with the PL results from section 6.3.4 where the nano - particles' shape ensure better light output due to lesser photons being totally reflected internally. The ablation in high fluence Fig. 5a) also showed a higher CL intensity with the vacuum and 1 Torr thin films compared to the low fluence in 5b).

The 10 mTorr thin film in 5b) showed a much higher CL intensity but this can be ascribed to the fact that the film was not evenly grown during the PLD process. Fig. 6a) shows the lower CL intensity compared to Fig. 5a) which is also in agreement with the PL results where the higher temperature resulted in better intensities.

The thin film ablated in 455 mTorr Ar gas Fig. 6b) showed a much higher CL intensity than the other two thin films. This is due to the more spherically shaped, and less agglomerated, particles on the surface of the substrate (section 5.2.2). The thin film ablated in O<sub>2</sub>, however, has a more agglomerated, particle layer on the surface. The particle sizes of the film ablated in N<sub>2</sub> is much smaller. The small particles (thin film ablated in N<sub>2</sub>) and the big agglomerated particles (thin film ablated in O<sub>2</sub>) resulted in very low CL intensities. The next section contains further investigations (PL) and explanations on the luminescent intensities.

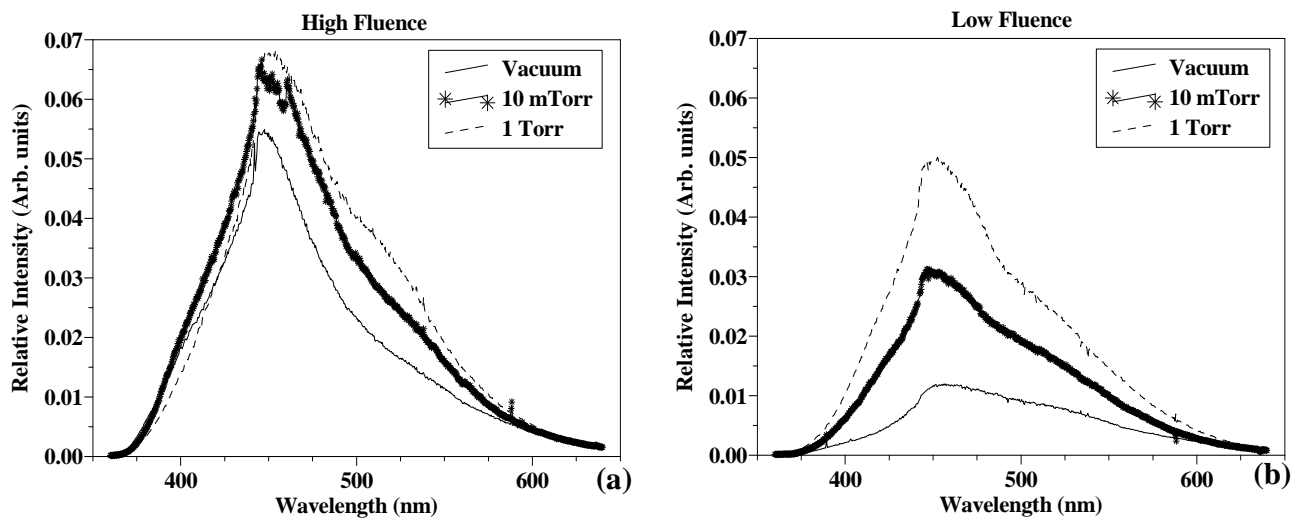
#### **6.3.4 PL measurements**

Fig. 7 shows the increased PL intensity for the increased O<sub>2</sub> (vacuum, 10 mTorr and 1 Torr) pressure for a) high fluence and b) low fluence at 600 °C. Fig. 8a) shows the two different temperatures (400 and 600 °C) at vacuum and 1 Torr O<sub>2</sub> at a high fluence and b) shows the difference in vacuum and 1 Torr O<sub>2</sub> at the high and low fluence ( $3 \pm 0.3$  and  $1.6 \pm 0.1$  J/cm<sup>2</sup>) at 600 °C. The increase in the ambient pressure leads to the formation of the nano - particles (see section 5.2) and thus an increase in the luminescent intensity. The increased intensity from the nano – particles is as a result of more photons exiting the spherically shaped nano - particles (rougher surface) in comparison with the thin layers were the nano - particles are not clearly defined and formed (acting as a uniform surface layer). As mentioned earlier, the photons get totally internally reflected in a uniform surface layer and therefore result in a lower intensity. This was also reported by Coetsee

*et al.* [1, 10] during the investigation of the CL intensity degradation of tin oxide coated  $\text{Y}_2\text{SiO}_5\text{:Ce}$  thin films grown by PLD.

If the laser power is kept constant and the laser spot size is focussed more tightly, the fluence will increase and this will also increase the particle number density [11]. The higher fluence would result in ablation of a thicker and denser thin layer with improved crystallinity, and this would result in an increased luminescent intensity (see also (section 5.2)). It is also known that higher substrate temperature result in better luminescent intensity due to the rougher surface formed, Fig. 8a) [2, 11].

During the PLD process the growth of the thin films resulted in  $\text{Ce}^{3+}$  occupying different lattice sites in the complex crystal structure of the  $\text{Y}_2\text{SiO}_5$  host. The broad band spectra, observed in Figs. 5, 6, 7 and 8 is a contribution of the two different sites of the  $\text{Ce}^{3+}$  ion in the host matrix and the difference in orientation of the neighbour ions in the crystal [12, 13, 14, 15] - see also chapter 4.



**Figure 7: PL results for the increased  $\text{O}_2$  (vacuum, 10 mTorr and 1 Torr) pressure for a) high fluence and b) low fluence at 600 °C.**

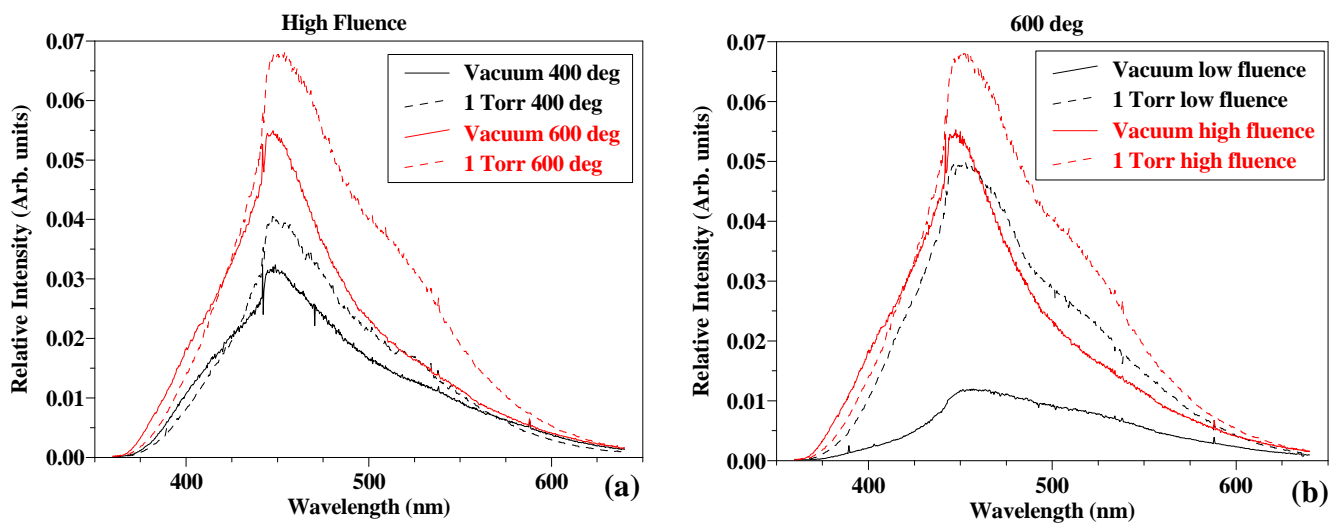


**Figure 8: PL intensities at a) two different temperatures (400 and 600 °C) at vacuum and 1 Torr O<sub>2</sub> at a high fluence and b) shows the difference in vacuum and 1 Torr O<sub>2</sub> at the high and low fluence ( $3 \pm 0.3$  and  $1.6 \pm 0.1$  J/cm<sup>2</sup>) at 600 °C.**

### 6.3.5 Comparison: SET1 and 2

Comparisons were made in order to compare the CL and PL intensities with the changes in the different process parameters respectively see Fig. 9 and 10.

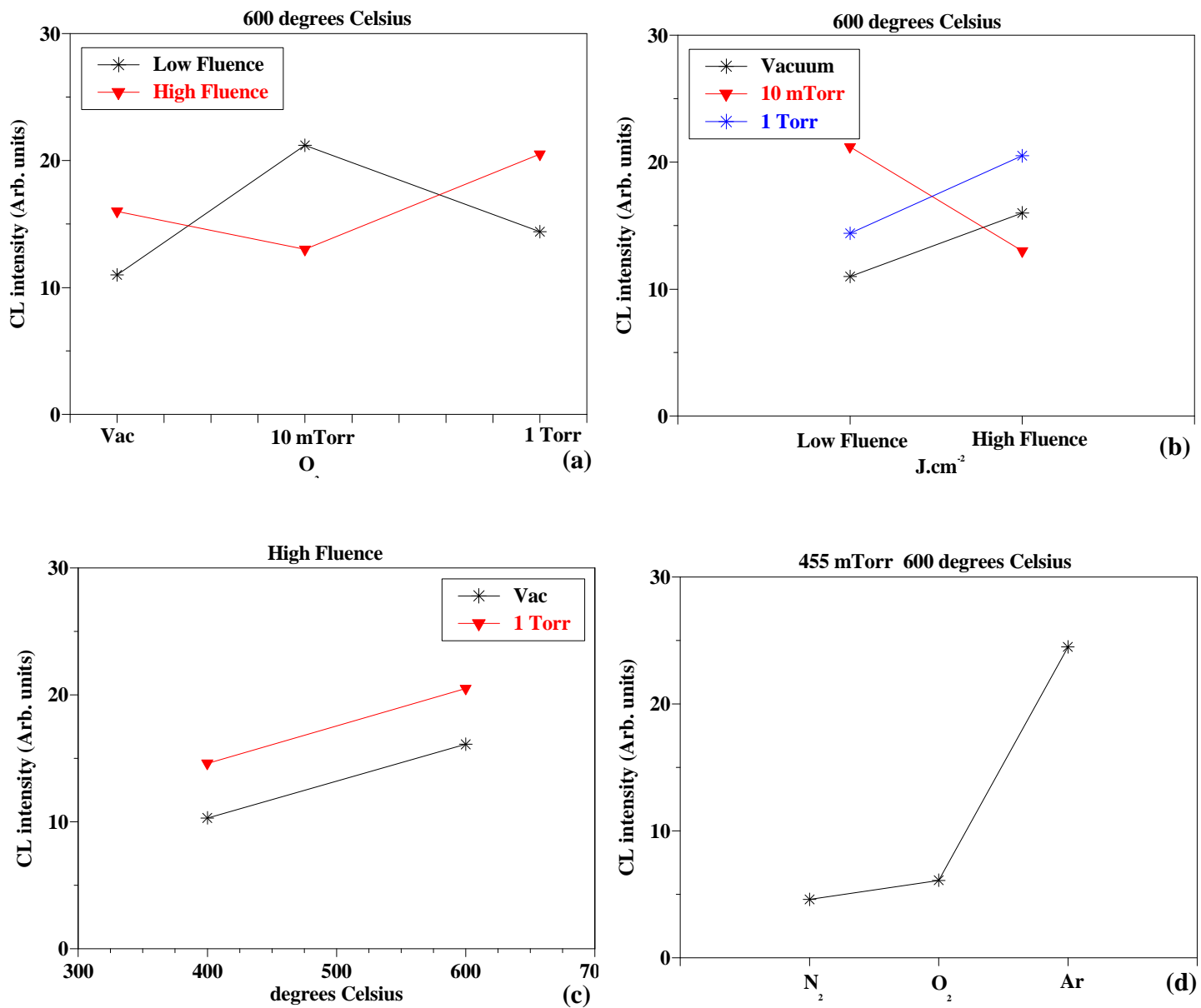


**Figure 9: Comparison of the CL intensities against the different process parameters, which is a) different  $O_2$  gas pressures at 600 °C substrate temperature, b) low and high fluence at 600 °C substrate temperature, c) different substrate temperatures at the high fluence of  $3 \pm 0.3 \text{ J/cm}^2$  and d) different gas species at 455 mTorr and 600 °C.**

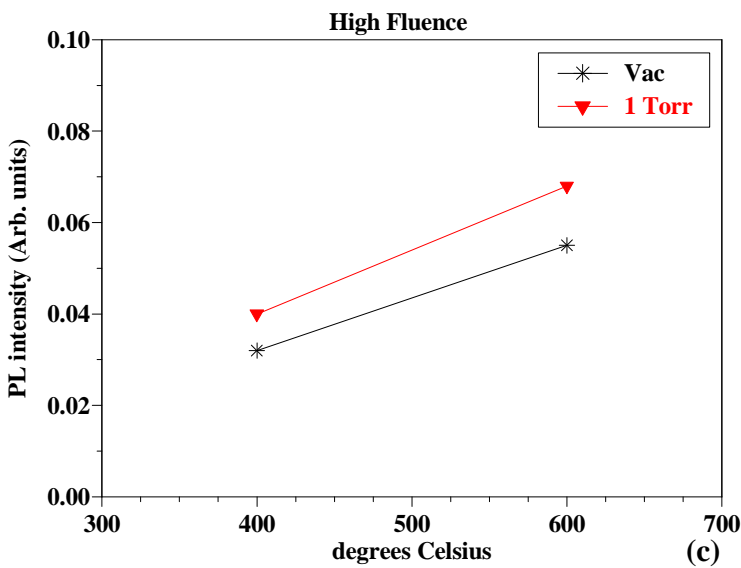
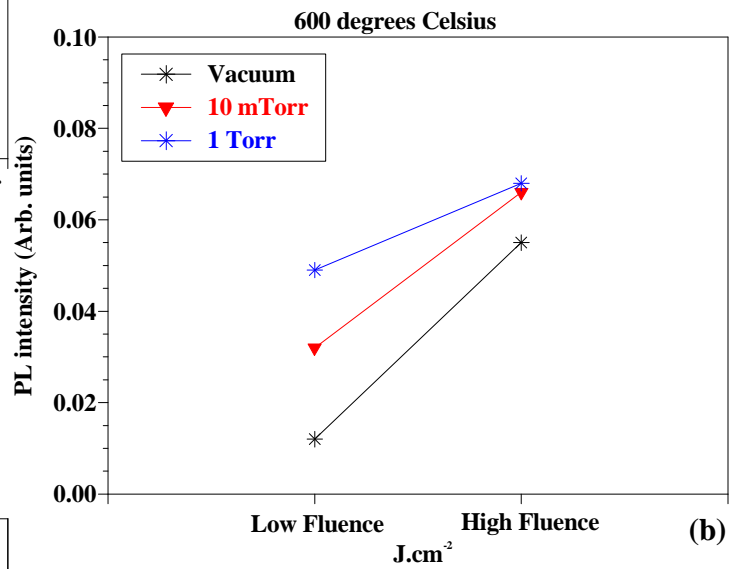
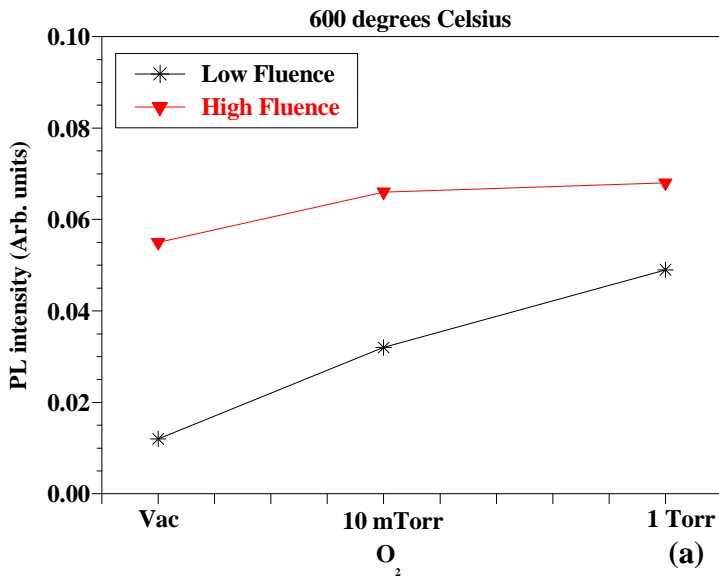


Figure 10: Comparison of the PL intensities against the different process parameters, which is a) different O<sub>2</sub> gas pressures at 600 °C substrate temperature, b) low and high fluence at 600 °C substrate temperature and c) different substrate temperatures at the high fluence of  $3 \pm 0.3 \text{ J/cm}^2$ .

These comparisons are a short summary of the CL and PL intensities obtained from the thin films that were analyzed. A detailed analysis would require much more data points consisting of more pressure values (for example 100, 200, 300, 400 mTorr etc.) and many different fluences or more variety in substrate temperatures. From both Fig. 9 and 10a), b) and c) it is however clear that the high fluence ablation in 1 Torr O<sub>2</sub> result in a higher CL and PL intensity. It is important to see that in all the figures the 1 Torr O<sub>2</sub> pressure films' intensities are higher than the vacuum layers' and that the higher fluence also results in higher CL and PL intensity than the lower fluence. The PL results clearly show the expectation of an increase in intensity as the ambient pressure increases to 1 Torr. This is however not the case in the CL results and the reason for the 10 mTorr intensities to be higher in Fig. 9a) and b) could be as mentioned in section 6.2.4; viz. uneven PLD growth process.

The increase in intensity for the films ablated at 600 °C, Fig. 9c) and 10c) is due to the rougher surface that formed but a further increase to 800 °C and a decrease to room temperature should also be investigated. Fig. 9d) shows a dramatic increase in CL intensity with the thin film ablated in an Ar ambient, as also can be seen from Fig. 6b). The results obtained for the CL and PL are therefore in agreement with what was obtained from literature, as was discussed in chapter 3. It therefore confirms the expectation of a higher ambient pressure, a higher fluence and a higher substrate temperature that should result in higher luminescent intensities. The higher ambient pressure resulted in nano-particles, the higher fluence should result in better crystallinity and thicker layers and the higher temperature to a rougher surface. Ar gas proved to be the ideal ambient during the growth process to achieve this.

## 6.4 Conclusion

XRD results for the thin films in SET1 and 2 were compared to the X<sub>1</sub>- phase of monoclinic Y<sub>2</sub>SiO<sub>5</sub>. The powder used as a target has a monoclinic crystal structure of Y<sub>2</sub>SiO<sub>5</sub>:Ce X<sub>1</sub> - phase with space group P2<sub>1</sub>/c. The XRD results for the thin films showed very low intensity peaks which are an indication that the layers are almost

amorphous with only some indication of small peaks that belong to the monoclinic crystal structure. During the CL scanning emission seems to occur from the whole micron particles on the surface as well as from the smaller particles around the bigger particles. The smaller particles did not show effective emission with low PMT voltage. There is a definite increase in luminescent intensity with the uncoated thin film which indicates the photon absorption effect of the extra tin oxide coated layer. CL intensity is coming mainly from the bigger spherical particles on the surface.

The nano - thin films lead to an increase in PL and CL intensity. The thin films grown with the increased O<sub>2</sub> pressure to 1 Torr and higher fluence ( $3 \pm 0.3 \text{ J.cm}^{-2}$ ) resulted in better luminescent intensities. The increase in substrate temperature from 400 to 600 °C also resulted in an increased luminescence due to a rougher surface that formed. For better luminescent intensity the thin films should have a rougher surface (spherically shaped particles achieved via increased substrate temperature and increased ambient pressure). A degradation study on the stability of the thin film ablated in Ar follows in the next chapter.

## References

1. E. Coetsee, H. C Swart, J. J. Terblans, O. M. Ntwaeaborwa, K. T. Hillie, W. A. Jordaan and U. Buttner, *Opt. Mat.*, **29** (2007) 1338.
2. X. W. Sun and H. S. Kwok, *Appl. Phys. A, Mat. Sci. and Proc.*, **69** (1999) 39.
3. P. H. Holloway, J. Sebastian, T. Trottier, S. Jones, H. C. Swart and R. O. Peterson, *Mat. Res. Soc. Symp. Proc.*, **424** (1997) 425.
4. K. T. Hillie and H. C. Swart, *Appl. Surf. Sci.*, **183** (2001) 304.
5. K. T. Hillie, C. Curren and H. C. Swart, *Appl. Surf. Sci.*, **177** (2001) 73.
6. H. C. Swart, E. Coetsee, J. J. Terblans, J. M. Fitz-Gerald and J. R. Botha, *Luminescence of Y<sub>2</sub>SiO<sub>5</sub>:Ce nanocrystalline thin films*, *EJSSNT*, **7** (2009) 369.

7. M. Fink, J. Laimer, H. Stori and C. Mitterer, *Surf. And Coatings Tech*, **200(1-4)** (2005) 360.
8. Z. Dai, H. Naramoto, K. Narumi and S. Yamaoto, *J. Phys: Condens. Matter*, **11** (1999) 8511.
9. Q. X. Su, T. A. Rabson, M. Robert, J. X. Z. Xiong and S. C. Moss, *Thin Solid Films*, **305** (1997) 227.
10. E. Coetsee, H. C. Swart and J. J. Terblans, *J. Vac. Sci. Technol. A*, **25(4)** (2007) 1226.
11. L. Chen, Particles generated by pulsed laser ablation, in D. B. Chrisey, G. K. Hulber (Eds), *Pulsed Laser Deposition of Thin Films*, John Wiley & Sons, Inc, New York, (1994) chap. no. 6, p. 167 and 184.
12. H. Jiao, F. Liao, S. Tian and X. Jing, *J. of the Electrochem. Soc*, **151 (7)** (2004) 39.
13. J. Wang, S. Tian, G. Li, F. Liao and X. Jing, *J. of Electrochem. Soc*, **148 (6)** (2001) 61.
14. E. J. Bosze, G. A. Hirata, L. E. Shea-Rohwer and J. McKittrick. *J. of Lumen*, **104 (1-2)** (2003) 47.
15. T. Aitasalo, J. Holsa, M. Lastusaari, J. Niittykoski, F. Pelle, *Opt. Mat*, **27** (2005) 1511.

## Chapter 7

### CL degradation and APPH depth profiles of PLD thin films: Part three

In this chapter a 144 hr CL degradation study was done on the thin film ablated in Ar gas in order to investigate the stability of the thin film. The expectation is that the phosphor thin films would have higher chemical stability compared to phosphor powders. Auger peak to peak heights (APPH) depth profiles were also obtained and investigated to monitor chemical changes.

#### 7.1 Introduction

Degradation studies are important to determine the stability and lifetime of phosphors. Previous CL degradation studies done by Coetsee *et al.* [1] on tin oxide coated  $\text{Y}_2\text{SiO}_5\text{:Ce}$  thin films, showed that the tin oxide prevented degradation, (fig 1a). The  $\text{SnO}_2$  layer acted as a protective coating layer that resulted in a constant but lower CL intensity in comparison with the uncoated thin film, (Fig. 1b), after 24 hr electron bombardment. It was however also mentioned that the layer unfortunately would be removed with continued electron bombardment.

Light emission from both the thin films in a  $1 \times 10^{-6}$  Torr oxygen environment was blue before and after 24 hr electron bombardment. The CL intensity of the uncoated thin film was about 60 % higher than that of the coated thin film (see Fig. 1b). The lower CL intensity of the coated thin film is thus due to the energy loss of primary electrons penetrating the  $\text{SnO}_2$  layer on the phosphor surface, as well as scattering effects of the photons exiting the phosphor surface and the  $\text{SnO}_2$  layer. A uniform layer covering the surface of the spherical particles results in a small critical angle for transmission and a large fraction of the light being totally internally reflected [2].

The importance of adventitious C on the surface was also described. The C layer on the surface creates an extra layer that also contributes to a loss in CL intensity. The C however was depleted from the surface of the tin oxide within the first 24 hr electron bombardment (within the first  $300 \text{ C.cm}^{-2}$  (about 3 hr)). The C gets depleted due to the electron stimulated reactions (ESSCR). These reactions occur because of i) increased  $\text{O}_2$  pressures that result in more reactive oxygen species which react with the C to create volatile species such as OH, CO and  $\text{CO}_2$ . ii) A decrease in the electron beam current (from 20 to  $10 \mu\text{A}$ ) that resulted in a lower temperature beneath the electron beam that result in longer mean stay time of the oxygen species on the surface area for depletion of the C [3]. As the C decreases the Sn and O APPHs increased and then stayed almost constant. A decrease in the C layer increases the CL intensity, which then stayed almost constant.

From these results the expectation of a thin film being much more stable was created. Would thin films, even though they result in lower luminescent intensities than powders, be chemically much more stable? In the sections to follow a detailed degradation study was done on the thin film ablated in Ar gas as this film proved to be the ideal luminescent candidate for this investigation, as was seen from chapter 6. A profile was also obtained to monitor the changes in the APPH's of C, O, Y and Si with time.

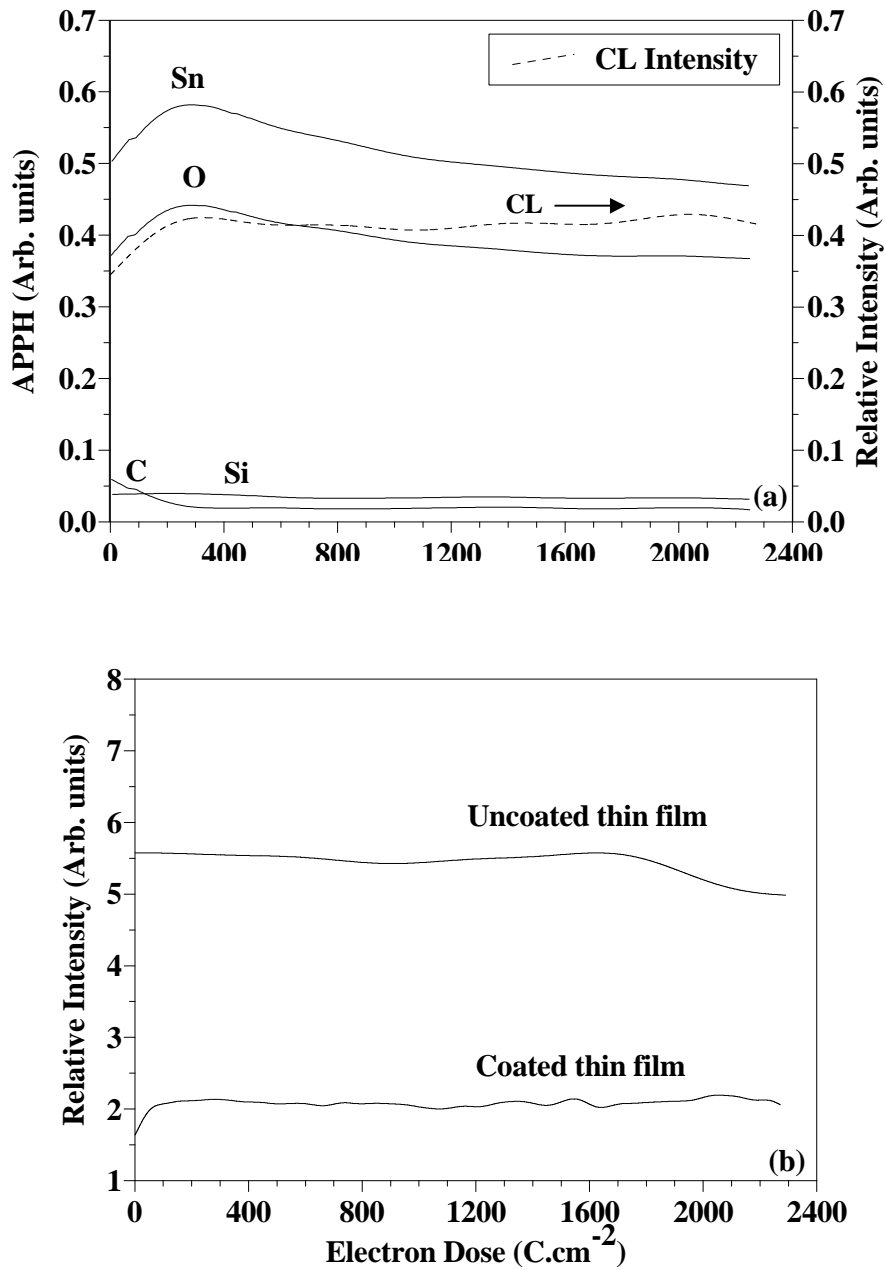


Figure 1: a) Auger peak to peak heights as function of electron dose at an oxygen pressure of  $1 \times 10^{-6}$  Torr and b) CL intensity as function of electron dose ( $\text{C}\cdot\text{cm}^{-2}$ ) for the coated and uncoated thin films in  $1 \times 10^{-6}$  Torr oxygen pressure with a beam current density of  $26 \text{ mA}\cdot\text{cm}^{-2}$  [1].

## **7.2 Experimental Procedure**

### **7.2.1 Rutherford Backscattering (RBS)**

RBS was done on TF17 (the thin film ablated at a low fluence in 1 Torr O<sub>2</sub> at 600 °C substrate temperature) and TF5 (thin film ablated at a high fluence in vacuum at 600 °C substrate temperature) in order to investigate the composition of the thin films. The results were then also used to calculate the sputtering rate during APPH profile in order to obtain the thin film thicknesses. RBS was done by using a 2000 MeV <sup>4</sup>He<sup>+</sup> beam.

### **7.2.2 Auger peak to peak height (APPH) depth profiles**

APPH depth profiles were done to determine the thin film thickness and to monitor the changes in APPHs with time. The APPH changes were monitored with an electron beam current of 15 μA, 2kV energy electrons. The ion gun used for sputtering was an Ar ion gun, 2 kV energy ions, 0.1 μA beam current and raster area of 2 x 2 mm.

### **7.2.3 Degradation**

The thin film obtained during deposition in the Ar atmosphere was degraded under electron bombardment for 144 hr (coulomb dose of  $1.4 \times 10^4$  C.cm<sup>-2</sup>) at an O<sub>2</sub> pressure of  $1 \times 10^{-6}$  Torr, 2 keV electron energy and 10 μA electron beam current. The CL, AES and degradation measurements were done in an UHV chamber with a PHI model 549 system to monitor changes in the surface chemical composition and luminous efficiency. Residual gas mass (RGA) analysis was done with a Anavac-2 mass analyzer to determine the different kind of gas species present in the environment during AES and CL spectroscopy.

## **7.3 Results and discussions**

### **7.3.1 RBS**

RBS results, (not shown here), showed that TF5 was 165 nm thick while TF17 was 40 nm. TF5 is a thin film ablated in vacuum (high fluence). The thick layer can therefore be explained as a consequence of no obstruction from gas particles deliberately pumped into

the chamber, see section 3.2.2. TF17 is a much thinner and non uniform layer, which is due to the nano-particles that formed during PLD. This is indeed in agreement with the expectations and results obtained in chapter 6. High fluence results in thicker layers and an ambient (deliberately added) during PLD leads to nano-particle layers.

### 7.3.2 APPH depth profiles

APPH depth profiles were done on TF17 and A3 (thin film ablated in Ar gas) in order to monitor the changes in the elemental composition with time. Except for the difference in the thickness of the two layers, the same results were obtained. Fig. 2 shows the APPH depth profile for TF17 and Fig. 3 for A3. The Si peak position (AES results not shown here) changed from 82 to 93 eV which indicates the Si binding state in  $Y_2SiO_5:Ce$  before sputtering and afterwards the Si state of the substrate. The main Y peak position before sputtering is at 124 eV which is in agreement with previous degradation studies done by Coetsee *et al.* on the powders [4] and the thin films [1].

In Fig. 2 the interface of the Si substrate was reached after 400 sec of sputtering and in Fig. 3 at 1300 sec. This indicates again that a thicker phosphor layer (A3) was ablated in 455 mTorr Ar gas compared to the thinner layer ablated in 1 Torr  $O_2$  (TF17) gas (both layers were ablated with a low fluence). TF17 was calculated to be about 40 nm thick from RBS measurements. The thickness of thin film A3 was therefore calculated to be about  $133 \pm 10$  nm thick. This concludes the comparison from section 5.2.3 stating that ablation in Ar gas results in bigger nano-particles and therefore the thicker layer. Both layers show broad interfaces, indicating atomic diffusion between the substrate and ablated layers occurred. This is due to the heating of the substrate at 600 °C during PLD.

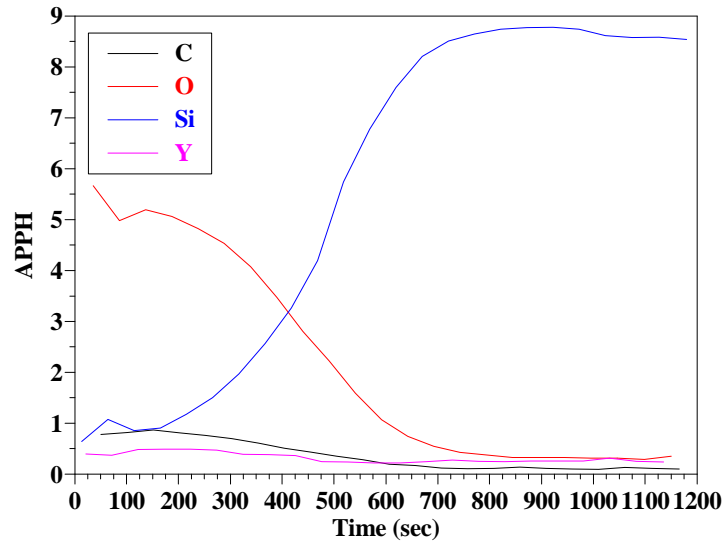


Figure 2: Depth profile of APPH vs time for TF17.

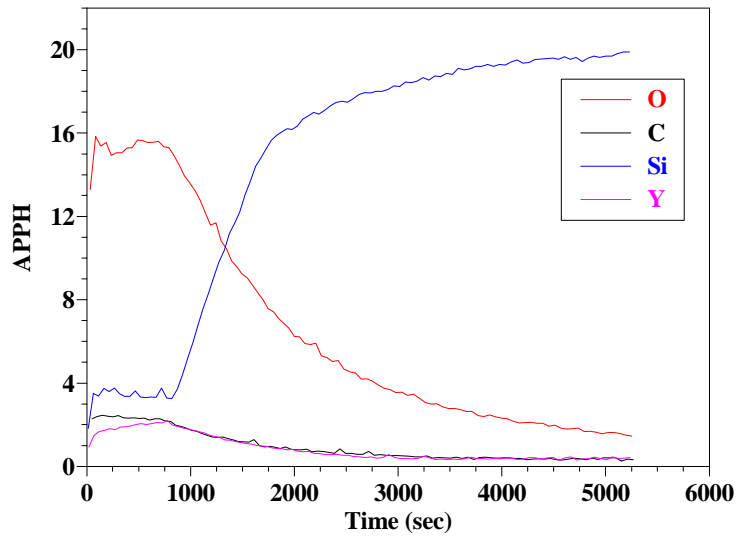


Figure 3: Depth profile of APPH vs time for A3.

### 7.3.3 CL degradation: Area 1

The thin film ablated in Ar gas was bombarded with 2 keV electrons (beam current density of  $26 \text{ mA}\cdot\text{cm}^{-2}$ ) on two different areas. Fig. 4 shows the APPH ratios and CL intensity versus the electron dose for the first area. This area was bombarded with electrons for 24 hr under an  $\text{O}_2$  pressure of  $1 \times 10^{-6}$  Torr. The adventitious C depleted

from the surface within the first 50 C.cm<sup>-2</sup> and this resulted in the increase in the O/C and Si/C ratios. The increase in CL intensity is also due to the depletion of the C.

Fig. 5a) shows the AES spectra before and after 24 hr. The energy peaks of Y and Si in the silicate composition for this thin film were measured at 124 and 82 eV before and after 24 hr. This is in agreement with previous AES measurements done by Coetsee *et al.* [4] during a CL degradation study that was done on the yttrium silicate powders. The adventitious N also gets depleted from the surface during the electron bombardment. Fig. 5b) shows the residual gas mass analyses performed with the electron beam on and off during the CL degradation. It is clear from Fig. 5b) that with the electron beam on there is a definite increase in the volatile species such as CO and CO<sub>2</sub>. This is due to the electron stimulate reactions and the depletion of the C. Fig. 6 shows the increased CL spectra after 24 hr electron bombardment. The low CL intensity is due to the C layer and the broad band is characteristic for Y<sub>2</sub>SiO<sub>5</sub>:Ce emission as can be seen from chap. 4.

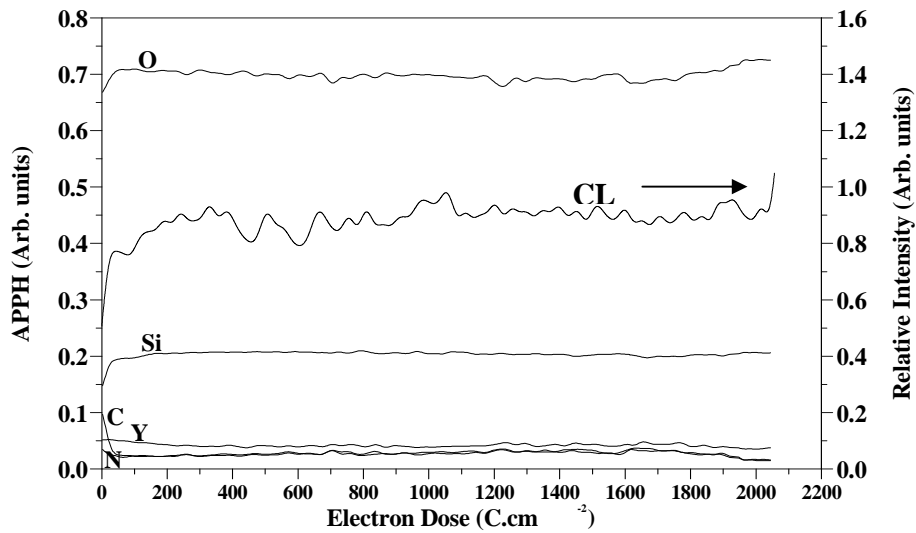


**Figure 4: APPH ratios and CL intensity (emission peak at 440 nm) against electron dose (C.cm<sup>-2</sup>) in O<sub>2</sub> pressure of 1 x 10<sup>-6</sup> Torr with a beam current density of 26 mA.cm<sup>-2</sup> on the first degradation area for 24 hr.**

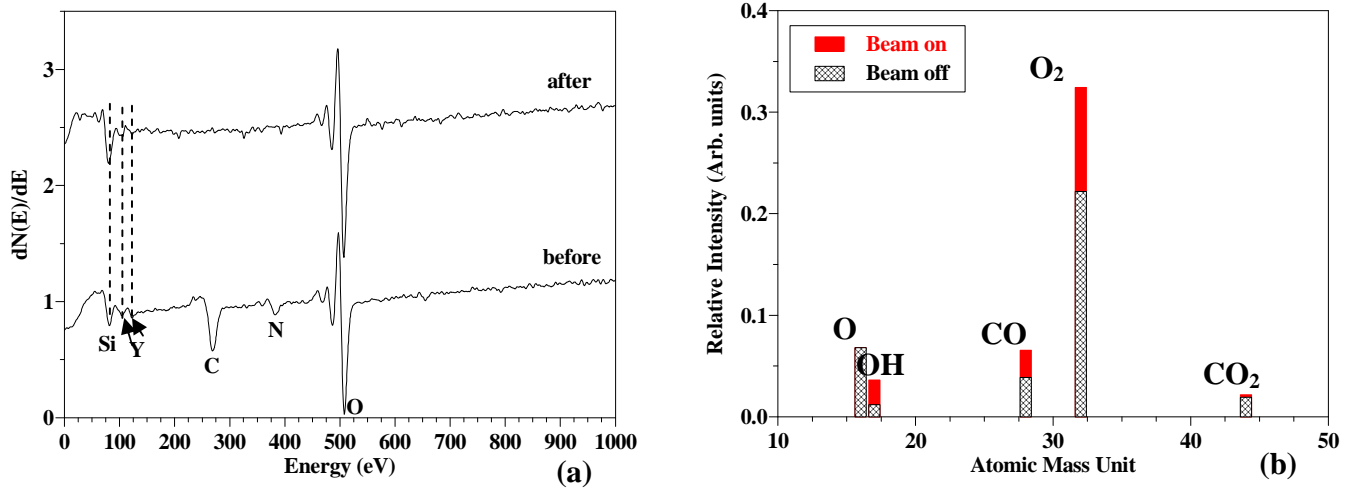


**Figure 5: a) AES spectra before and after 24 hr electron bombardment on the first area on the thin film ablated in Ar gas. b) RGA with the electron beam on and off in an O<sub>2</sub> pressure of  $1 \times 10^{-6}$  Torr.**

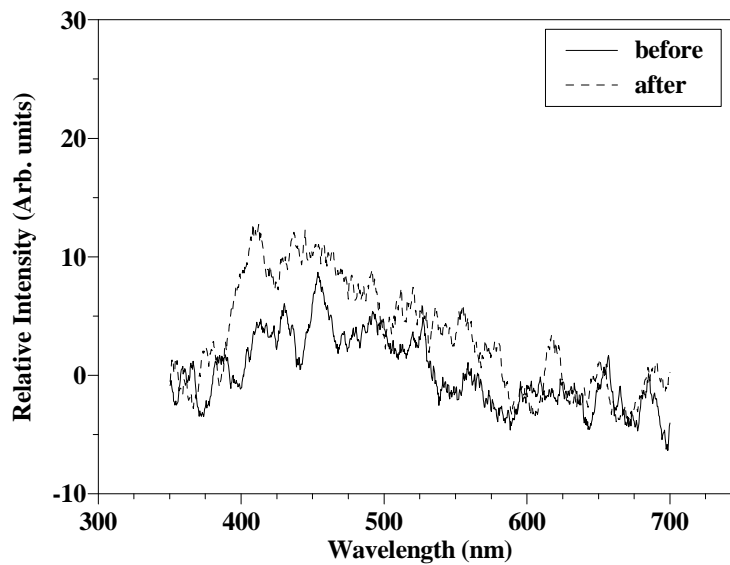


**Figure 6: CL intensity against wavelength for the first degradation area on the thin film ablated in Ar gas, before and after 24 hr electron bombardment.**

These results show a chemically stable thin film under 24 hr electron bombardment. Further investigations were done to monitor the stability of the thin film for more than 24 hr. The next section shows the results for 144 hr electron bombardment on a different area.

### 7.3.4 CL Degradation Area 2

Another area on the same thin film was bombarded with the same electron current density of  $26 \text{ mA.cm}^{-2}$  but this time for 144 hr (electron dose of  $1.4 \times 10^4 \text{ C.cm}^{-2}$ ). Fig. 7 shows the APPH ratios for the first 24 hr with the AES spectra in Fig. 8. The results monitored after 24 hr did not show severe changes and Y and Si peaks were again measured at 124 and 82 eV before and after 24 hr. Detailed chemical analysis with XPS will be reported in more detail in chapter 8 before and after 144 hr degradation. Fig. 9 shows the CL spectra before, after 24, 96 and 144 hr CL degradation with the inset of digital images of the colour of the light before and after 144 hr.

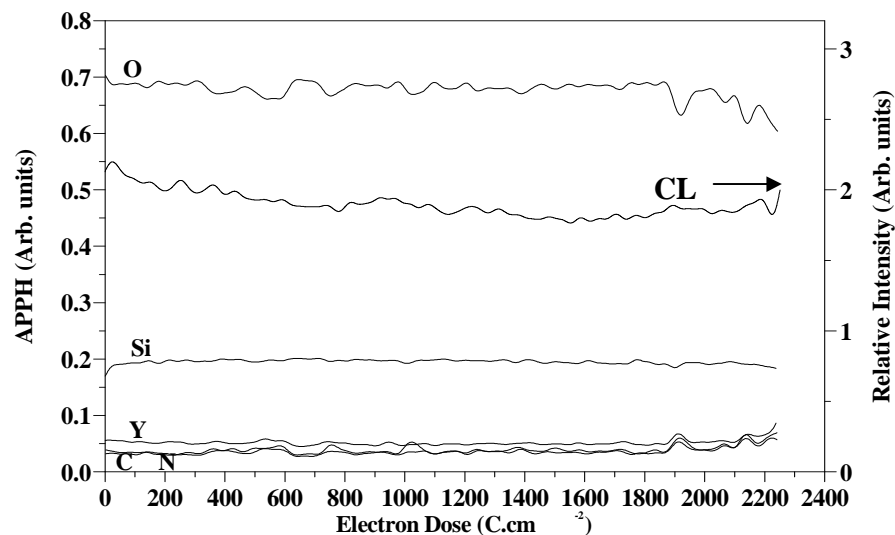


**Figure 7: APPH ratios and CL intensity (emission peak at 440 nm) against electron dose ( $\text{C.cm}^{-2}$ ) in  $\text{O}_2$  pressure of  $1 \times 10^{-6}$  Torr with a beam current density of  $26 \text{ mA.cm}^{-2}$  on the second degradation area for 24 hr.**

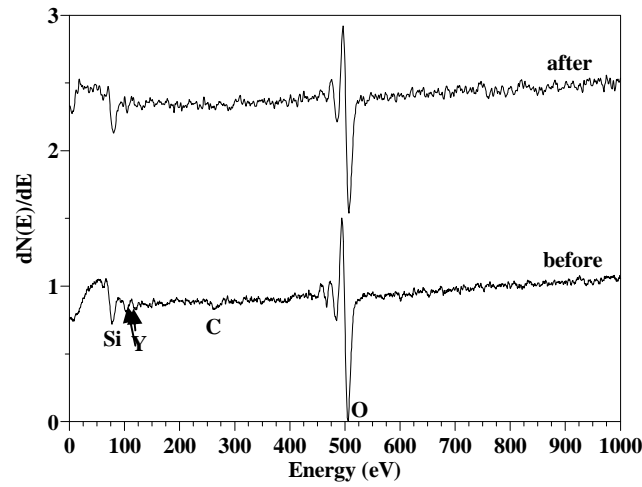


Figure 8: AES spectra before and after 24 hr electron bombardment on the second area on the thin film ablated in Ar gas.

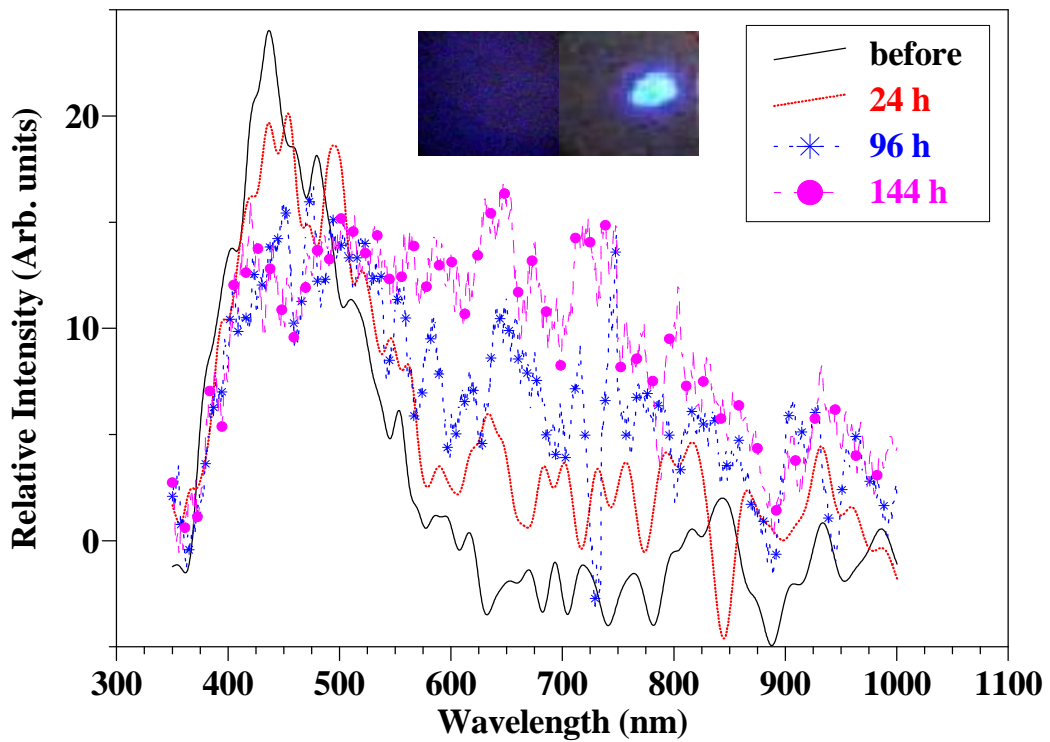


Figure 9: CL spectra for the thin film ablated in an Ar ambient before, after 24, 96 and 144 hr, in an  $O_2$  environment with a pressure of  $1 \times 10^{-6}$  Torr. The inset is a picture of the blue colour before and the whitish colour after electron bombardment.

There was a decrease in CL intensity from the main 440 nm emission peak after 144 hr and the decrease for the first 24 hr can also be seen from Fig. 9. A second broad band peak emerged at 650 nm which increased with an increase in the degradation time leading to a broad spectrum ranging from 400 to 850 nm after 144 hr. This is ascribed to a defect level in SiO<sub>2</sub> (1.9 eV/ 650 nm) that formed on the surface due to electron stimulated surface chemical reactions (ESSCR). The proof for this is provided in chapter 8. From the inset images it is clear that the blue colour again changed (the same as with the powders [4 below]) to a whitish colour with the bright area the spot of maximum degradation due to the shape of the electron beam which is more intensified in the centre of the beam.

Skuja *et al.* [5] reported two peak intensities for SiO<sub>2</sub> at 1.9 eV (650 nm) and 2.7 eV (459 nm) with a proposal that the two peaks are related to intrinsic defects involving breaking of the Si–O bonds. A definite contribution from the SiO<sub>2</sub> 1.9 eV defect to the transition from the higher 5d levels to the 4f<sub>7/2</sub> levels leads to the increase in the CL intensity and peak emission between 600 and 700 nm, (this can also be seen after 96 hr in Fig. 9) thus also resulting in the change in colour. There could be a very low intensity contribution from the 2.7 eV defect to the peak emission between 400 and 500 nm, which results in the increase in the intensity in that region (after 96 hr).

Similar defect states were created during the implantation of Si<sup>2+</sup> in a SiO<sub>2</sub> matrix by Dhara *et al.* [6]. PL spectra showed a broad emission peak ranging from ~1.5 to 1.9 eV and a bright red emission (1.7 eV) was observed during the investigation of room temperature PL properties of nano - crystalline (nc-) Si grown by Si ion implantation in both amorphous and crystalline SiO<sub>2</sub> matrices and the subsequent annealing process. The luminescent process was ascribed to the defects that are created during the growth of the nano - crystalline Si at the interface between the nc- Si and the SiO<sub>2</sub> matrix. The presence of these defect states were supported by absorption bands identified at ~1.74 to 1.8 eV. Linnros *et al.* [7] presented time-resolved PL decay measurements of high-dose Si nano - crystallites embedded in SiO<sub>2</sub>, annealed at 1100 °C (thin films of various thicknesses were used). Optimum PL efficiency was found to be in the range of 700 –

850 nm. A spectral redshift was also observed for thinner oxide films and higher implantation doses and this was explained as being due to excess Si concentration along the implantation profile. The PL emission was ascribed to excitonic recombination in the Si nano - crystals.

From these degradation results it is clear that this yttrium silicate phosphor thin film did not show the same severe chemical changes within 24 hr as the phosphor powder. The thin film therefore proved to be chemically more stable. The only major disadvantage is the lower luminescent intensities which unfortunately is a necessity for ideal FED and plasma operations.

#### **7.4 Conclusion**

RBS revealed that the higher fluence ablation in vacuum (TF5) leads to a thicker layer than the low fluence ablation that was done in 1 Torr O<sub>2</sub> (TF17). These RBS results were used to determine the thickness of the thin film ablated with a low fluence in 455 mTorr Ar gas to be  $133 \pm 10$  nm. APPH depth profiles done on TF17 and A3 showed broad interfaces which indicate atom diffusion between the substrate and ablated layers. This is due to the heating of the substrate at 600 °C during PLD. Adventitious C depleted from the surface of the thin film ablated in Ar gas for the first 24 hr degraded area, within the first  $50 \text{ C.cm}^{-2}$ , and this resulted in the increase in the O/C and Si/C APPH ratios. The increase in CL intensity is therefore due to the depletion of the C from the surface. The CL degradation study of 144 hr on the same thin film but a different area showed a decrease in the main emission peak (440 nm) and an increase of a second emission peak emerging (after 24 hr) between 600 and 700 nm (with a change in the colour of the light from blue to whitish after 144 hr). This is in agreement with previous research studies done on the phosphor powders. Detailed XPS chemical analyses are needed to prove the formation of the SiO<sub>2</sub> layer on the surface with the defect levels that might also emit light. These results proved that the thin films are chemically more stable than the phosphor powders.

## Reference

1. E. Coetsee, H. C. Swart and J. J. Terblans, *J. Vac. Sci. Technol, A*, **25(4)** (2007) 1226.
2. H. C. Swart and K. T. Hillie, *Surf. Interface Anal*, **30** (2000) 383.
3. J. Sebastian, S. Jones, T. Trottier, H. C. Swart and P. Holloway, *J. Soc. Inf. Disp*, **3/4** (1995) 147.
4. E. Coetsee, J. J. Terblans and H. C. Swart, *J. of Lumin*, **126** (2007) 37.
5. L. N. Skuja, W. Entzian, *Phys. Stat. Sol. (a)*, **96** (1986) 191.
6. S. Dhara, C-Y. Lu, K. G. M. Nair, K-H. Chen, C-P. Chen, Y-F. Huang, C. David, L-C. Chen and B. Raj, *Nanotechnology*, **19** (2008) 395.
7. L. Linnros, A. Galeckas, N. Lalic and V. Grivickas, *Thin Solid Films*, **297** (1997) 167.

## Chapter 8

### XPS before and after electron degradation: Part four

This chapter contains XPS results and Gaussian-Lorentz peak fits for the Si 2p, O 1s, Y 3d and Ce 3d peaks before and after degradation, in order to investigate the chemical species that formed during the electron degradation process. Results for the standard phosphor powders and for the thin film ablated in Ar gas are shown (undegraded, 24 hr and 6 days degraded areas).

#### 8.1 Introduction

As mentioned in section 4.3, the degradation of the  $Y_2SiO_5:Ce$  phosphor powders investigated with AES and CL spectroscopy first resulted in a decrease in CL intensity measured at 440 nm and then to an increase after about  $300 \text{ C.cm}^{-2}$  due to the chemical change in surface concentration in the phosphor surface. XPS and CL indicated that the change in peak shape is due to the formation of a luminescent  $SiO_2$  layer on the surface which is formed according to the ESSCR mechanism [1, 2]. The emission of light from the  $SiO_2$  defect levels contributed to the CL intensity in the 600 to 700 nm wavelength range. The colour changed from blue to orange-reddish during the degradation process.  $CeO_2$  and  $CeH_3$  were also formed on the phosphor surface during the degradation process [1].

A similar second CL peak emerged when the degradation was done under the same conditions on the thin film ablated in Ar gas, for 144 hr, see section 7.2.2. The following sections contain the XPS results and peak fits in order to investigate any chemical composition changes on the surface of the thin film.

## **8.2 Experimental Procedure**

### **8.2.1 Characterization**

Secondary X-ray Imaging (SXI) and X-ray Photoelectron Spectroscopy (XPS) were done with a PHI 5000 Versaprobe system. SXI was done with a 10  $\mu\text{m}$ , 1.25 W and a 15 kV x-ray beam and the XPS was done with a 50  $\mu\text{m}$ , 12.5 W and 15 kV x-ray beam, monochromatic  $\text{AlK}_\alpha$  lines. XPS analysis was also done on the standard  $\text{Y}_2\text{SiO}_5\text{:Ce}$  phosphor powders. The Ce 3d peak for the thin film were analysed with a 100  $\mu\text{m}$ , 25 W and 15 kV x-ray beam (for higher counts).

### **8.2.2 Peak fits**

Gaussian-Lorentz peak fits were done on the Si 2p, O 1s, Y 3d and Ce 3d peaks and the possible chemical states identified with the Multipak version 8.2c computer software [3].

## **8.3 Results and Discussions**

### **8.3.1 SXI**

Fig. 1a) shows the SXI image of the undegraded powder while Fig. 1b), c) and d) show the undegraded, the 24 hr and 6 days degraded areas of the thin film, respectively.

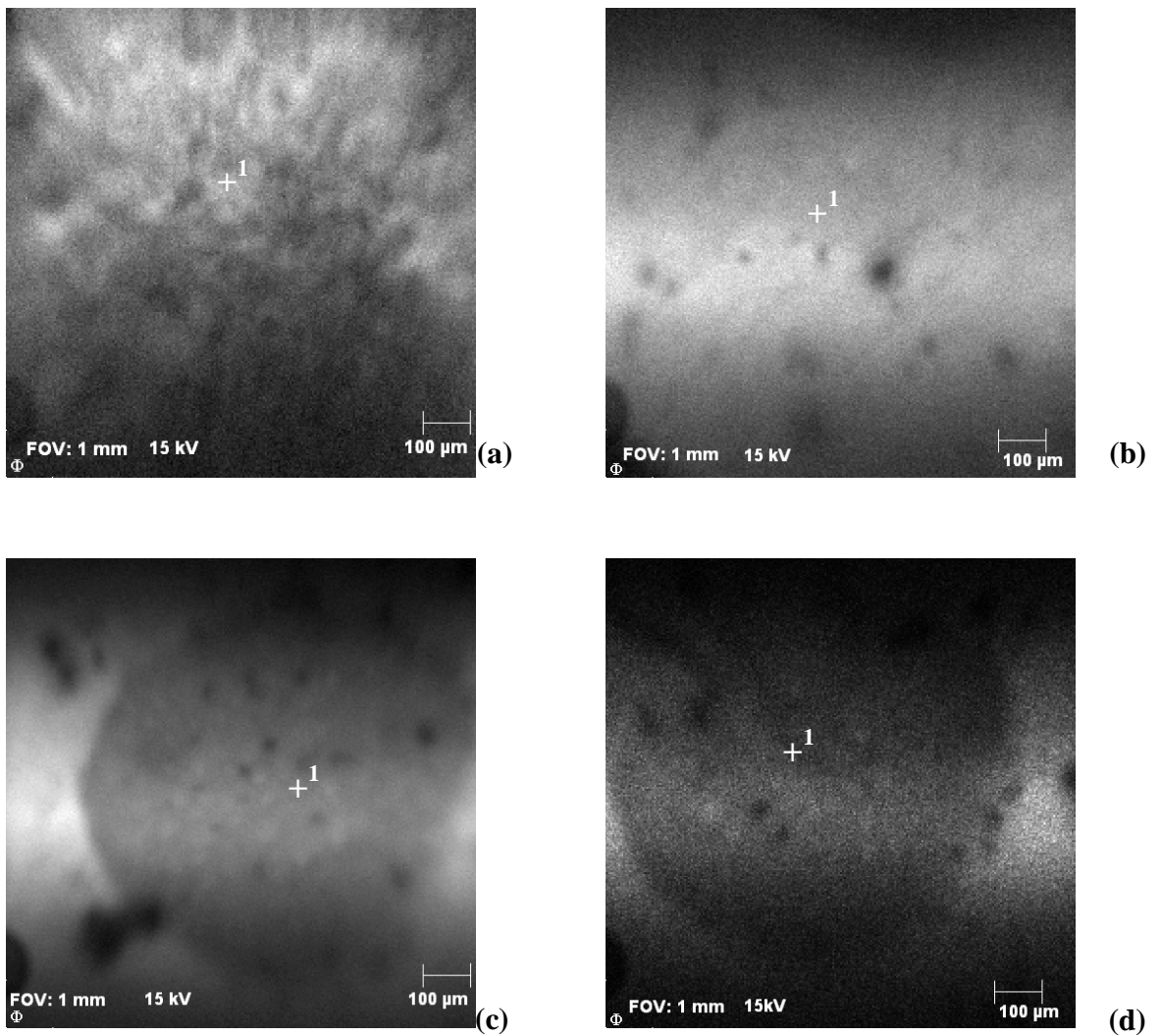


**Figure 1: SXI images of the a) standard powder b) undegraded, c) 24 hr degraded and d) 6 days degraded areas, (FOV: 1mm, scale of 100 μm)**

### 8.3.2 XPS

Fig. 2 shows stackplots of the four different analysis regions for a) the C 1s, b) O 1s, c) Y 3d and d) Si 2p peak positions for the samples as indicated on the plots.

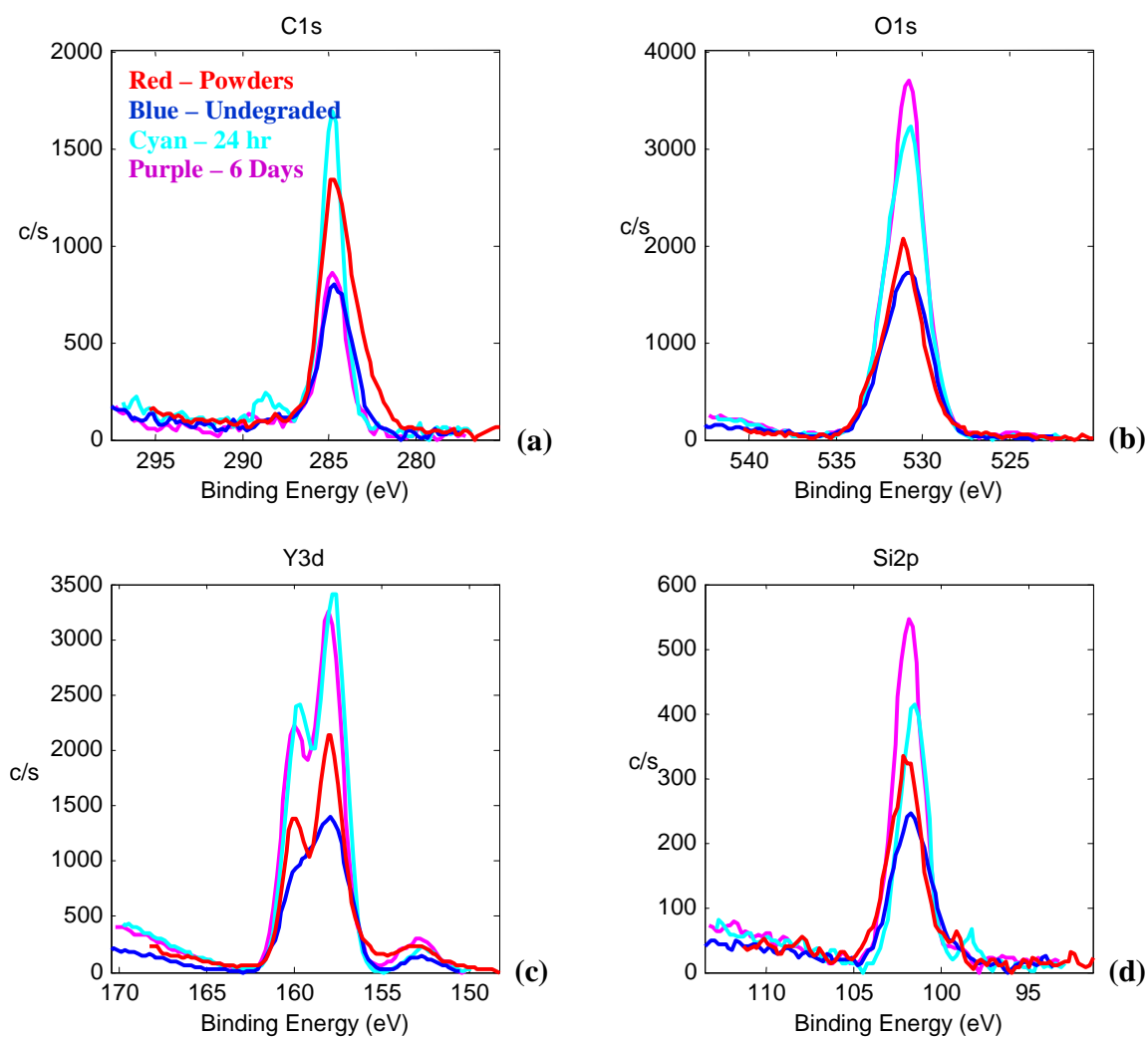


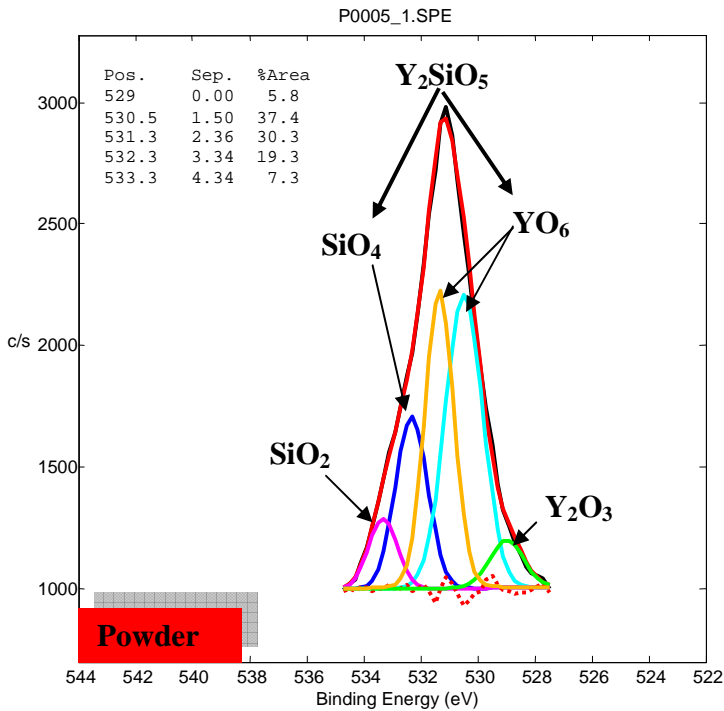
**Figure 2: Stackplot spectra for the four different analysis areas for the a) C 1s, b) O 1s, c) Y 3d and d) Si 2p binding energy peak positions.**

From Fig. 2 it seems that all peaks are situated on the same energy positions with only differences in the intensities. The peaks' shapes look almost the same with only the Y 3d undegraded peak not clearly indicating the difference between the two Y 3d peaks ( $3d_{5/2}$  and  $3d_{3/2}$ ). This could be due to the coverage of the adventitious C on the surface or due to a different chemical composition. Gaussian-Lorentz peak fits were performed in order to get detailed peak identities and to investigate any chemical changes that occurred during degradation. The C on the surface is due to handling contamination.

**Gaussian-Lorentz peak fits:**

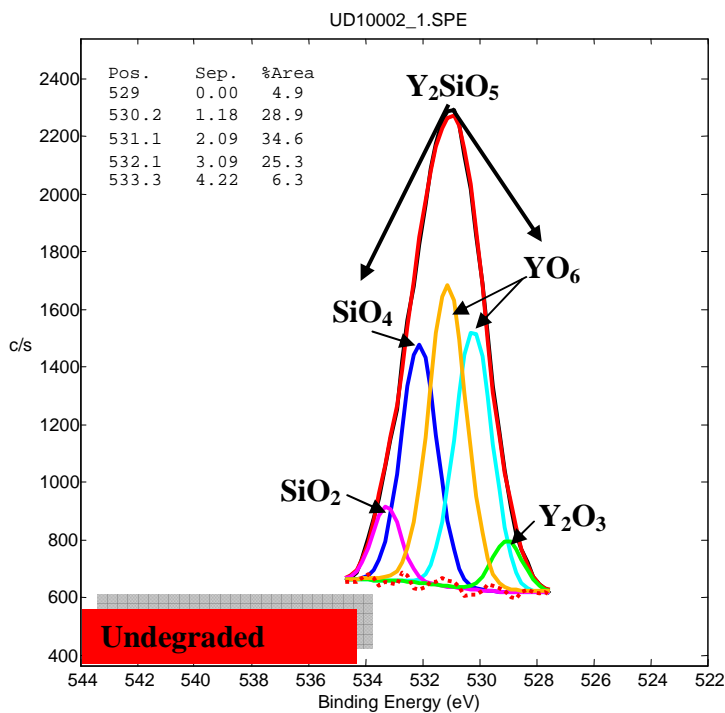
**O 1s:**

Fig. 3 shows the peak fits that were done on a) the standard phosphor powder, b) the undegraded, c) the 24 hr degraded and d) the 6 days degraded area with a table of possible chemical states for each binding energy position.

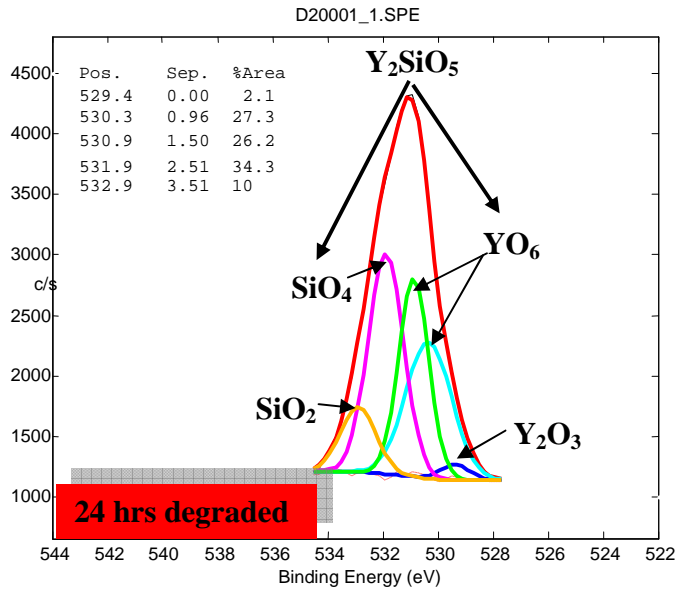


O1s	E <sub>b</sub>	Possible chemical state
	529	Y <sub>2</sub> O <sub>3</sub>
	530.5	Y <sub>2</sub> SiO <sub>5</sub>
	531.3	Y <sub>2</sub> SiO <sub>5</sub>
	532.3	Y <sub>2</sub> SiO <sub>5</sub>
	533.3	SiO <sub>2</sub>

(a)

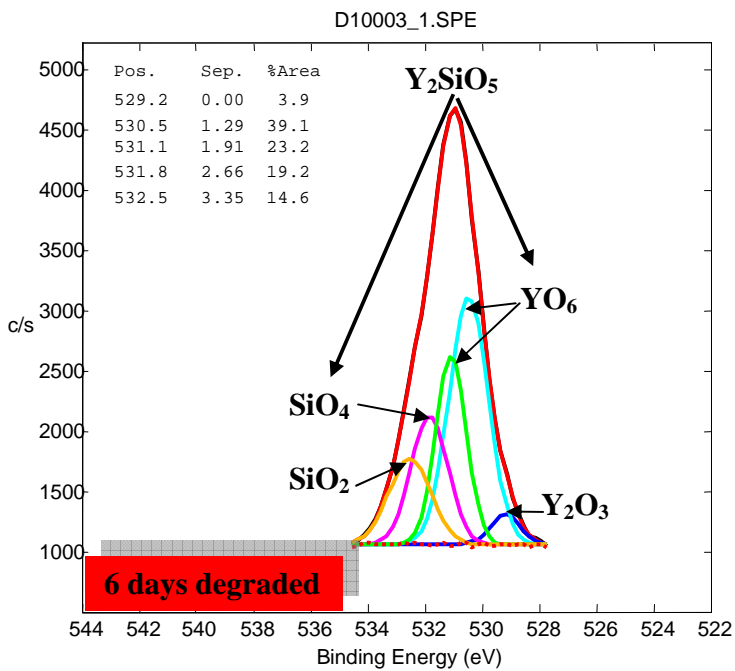


O1s	E <sub>b</sub>	Possible chemical state
	529	Y <sub>2</sub> O <sub>3</sub>
	530.2	Y <sub>2</sub> SiO <sub>5</sub>
	531.1	Y <sub>2</sub> SiO <sub>5</sub>
	532.1	Y <sub>2</sub> SiO <sub>5</sub>
	533.3	SiO <sub>2</sub>



(b)

O1s	E <sub>b</sub>	Possible chemical state
	529.4	Y <sub>2</sub> O <sub>3</sub>
	530.3	Y <sub>2</sub> SiO <sub>5</sub>
	530.9	Y <sub>2</sub> SiO <sub>5</sub>
	531.9	Y <sub>2</sub> SiO <sub>5</sub>
	532.9	SiO <sub>2</sub>



(d)

O1s	E <sub>b</sub>	Possible chemical state
	529.2	Y <sub>2</sub> O <sub>3</sub>
	530.5	Y <sub>2</sub> SiO <sub>5</sub>
	531.1	Y <sub>2</sub> SiO <sub>5</sub>
	531.8	Y <sub>2</sub> SiO <sub>5</sub>
	532.5	SiO <sub>2</sub>

Figure 3: Gaussian-Lorentz peak fits for O 1s in the a) standard powder, b) undegraded, c) 24 hr degraded and d) 6 days degraded areas.

From Fig. 3a), b), c) and d) the first O 1s peak situated at 529 eV provides a possibility that there is a small amount of  $Y_2O_3$  [4, 5] present. A possible explanation could be that if  $Y_2O_3$  is present in the standard powder and also shows in the undegraded and degraded areas, then it must have formed during the synthesizing process of  $Y_2SiO_5:Ce$ . Chambers *et al.* [4] studied the effects of surface pretreatments on interface structure during formation of ultra-thin yttrium silicate dielectric films on silicon. In their study yttrium was deposited on a thin ( $\sim 10 \text{ \AA}$ )  $SiO_2$  film and oxidized. An yttrium silicate film formed with bonding and composition similar to films formed on bare silicon. However when the interface was changed to a thin nitride, the silicon consumption rate was significantly reduced and the resulting film composition was closer to  $Y_2O_3$ .

Coetsee *et al.* [6] measured the O 1s peak of  $Y_2SiO_5:Ce$  standard phosphor powders in a CL degradation study. The peak position before degradation was 530.4 eV and after degradation there were four fitted peaks situated at 529, 530.4, 532.1 and 533.6 eV. The peak before degradation was attributed to the measured O 1s peak in the  $Y_2SiO_5:Ce$  binding position and after degradation the 529 eV peak to  $CeO_2$  [7], 530.4 and 532.1 eV to  $Y_2SiO_5:Ce$  and the 533.6 eV peak to  $SiO_2$  [8, 9]. The measured O 1s peaks at 530, 531 and 532 eV ( $< 532.5 \text{ eV}$ ) in Fig. 3 are attributed to  $Y_2SiO_5:Ce$  with the peaks at 530 and 532 eV that correlate well with the measured O 1s peaks done by Coetsee *et al.* [6].

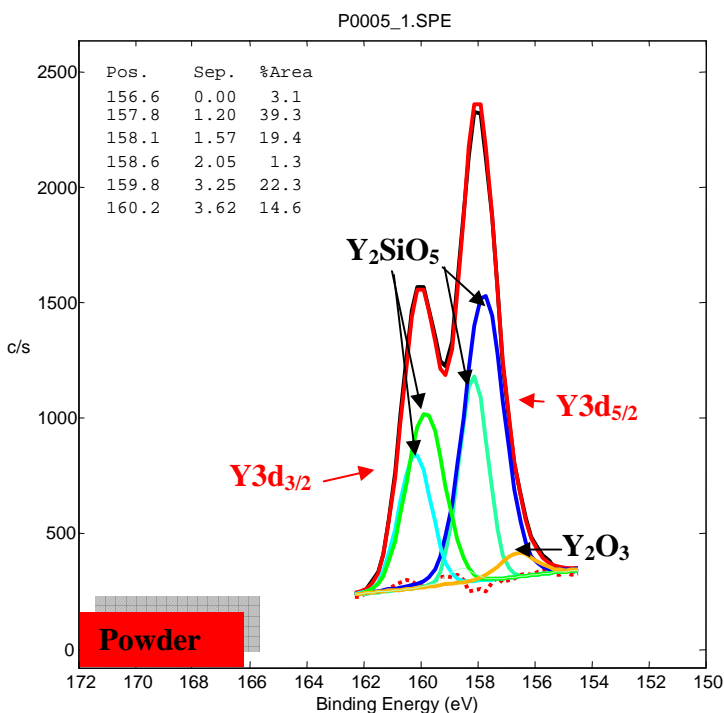
There is also a peak situated at 533 eV, see Fig. 3, which can be attributed to the O 1s oxidation state in  $SiO_2$  (silica) ( $533 \pm 0.5 \text{ eV}$ ) [10]. In both the powders and the undegraded areas there is also a small silica peak, which might have formed during the synthesis of the standard powders, as is the case with  $Y_2O_3$ . In the 24 hr degradation area, Fig. 3c), the silica peak at 532.9 eV shows an increase in the percentage area and a further increase in the 6 days degradation area at 532.5 eV. The increase in the silica peak provides proof for the formation of  $SiO_2$  on the surface during degradation, which correlates with the CL degradation study done on the standard phosphor powders by Coetsee *et al.* [6]. The electron stimulated reactions therefore cause breaking of the Y-Si-O bonds and results in new chemical compositions [3, 6]. Chambers *et al.* [4, 11] also reported on the O 1s peak measured at 532.8 eV in the yttrium silicate dielectric films on

silicon. This peak was reported as being very wide (FWHM = 3 eV) and the broadness was contributed to peaks for O 1s at energies between 533 eV for silica and 529.5 eV for  $Y_2O_3$ .

The 3 peaks attributed to  $Y_2SiO_5:Ce$  situated at 530, 531 and 532 eV correlate well with the chemistry for the bonding structure of the  $SiO_4$  and  $YO_6$  tetra- and octahedron structures as described in chapter 2, section 2.4. For each  $YO_6$  octahedron structure there are two possible sites for each Y bonding structure due to the two different co-ordination numbers (CN of 9 and 7, see section 2.4) for Y in this complicated monoclinic crystal structure. This means two of the three peaks are representing the two Y sites and the third peak (532 eV) is representing the bonding structure for  $SiO_4$ . The peak with CN of 9 (low oxidation state O 1s peak) is situated at 530 eV and the higher oxidation state peak at 531 eV is the peak for the CN of 7.

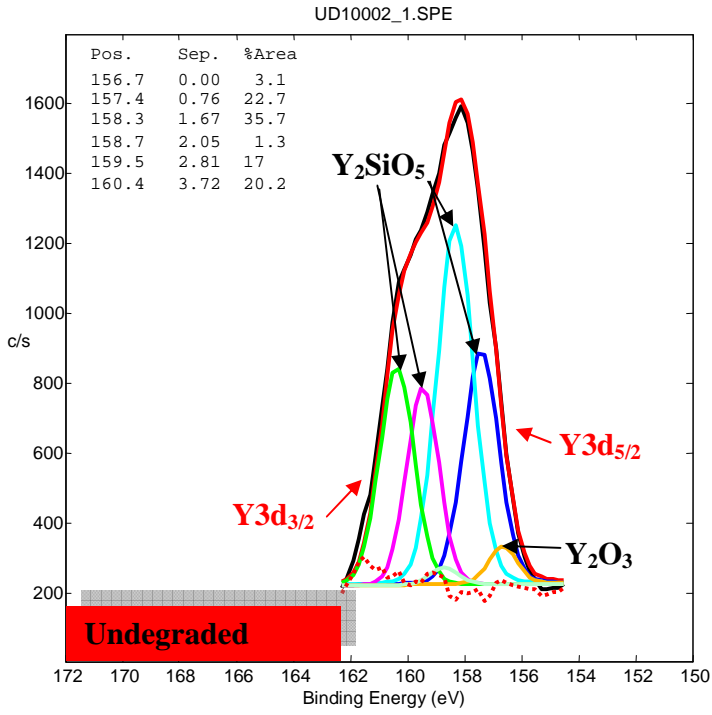
### Y 3d:

Fig. 4 shows the Gaussian peak fittings that were done on a) the standard powder, b) the undegraded, c) the 24 hr degraded and d) the 6 days degraded area with a table of possible chemical states for each binding energy position.



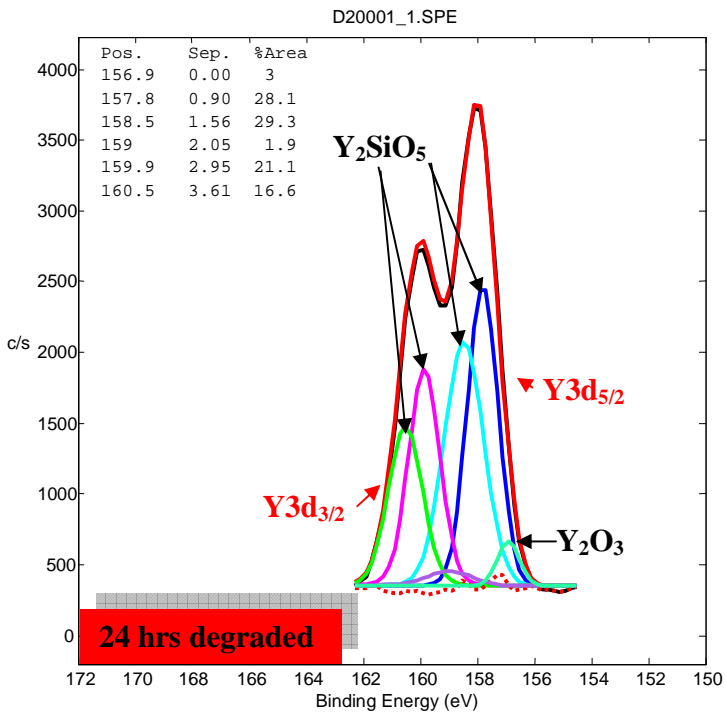
Y3d	$E_b$	Possible chemical state
$3d_{5/2}$	156.6	$Y_2O_3$
$3d_{5/2}$	157.8	$Y_2SiO_5$
$3d_{5/2}$	158.1	$Y_2SiO_5$
$3d_{3/2}$	158.6	$Y_2O_3$
$3d_{3/2}$	159.8	$Y_2SiO_5$
$3d_{3/2}$	160.2	$Y_2SiO_5$

(a)



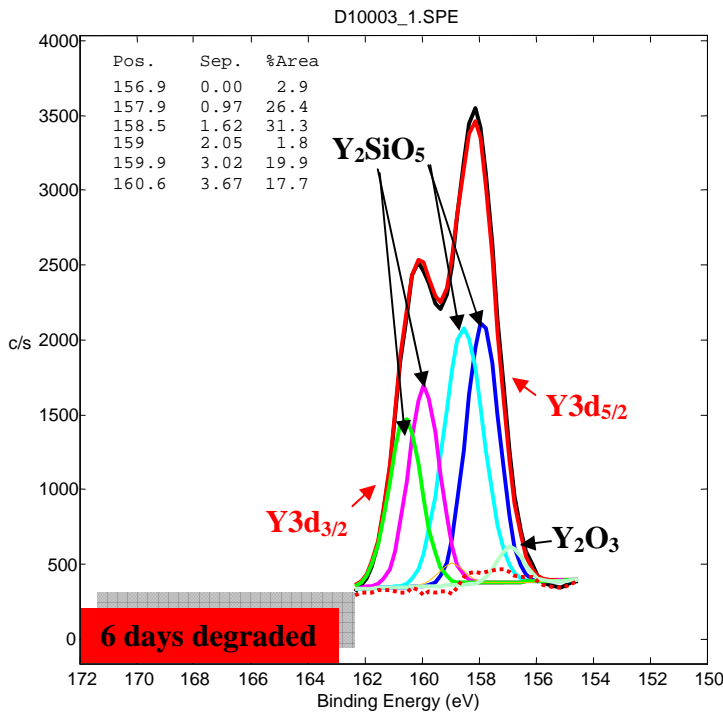
Y3d	E <sub>b</sub>	Possible chemical state
3d <sub>5/2</sub>	156.7	Y <sub>2</sub> O <sub>3</sub>
3d <sub>5/2</sub>	157.4	Y <sub>2</sub> SiO <sub>5</sub>
3d <sub>5/2</sub>	158.3	Y <sub>2</sub> SiO <sub>5</sub>
3d <sub>3/2</sub>	158.7	Y <sub>2</sub> O <sub>3</sub>
3d <sub>3/2</sub>	159.5	Y <sub>2</sub> SiO <sub>5</sub>
3d <sub>3/2</sub>	160.4	Y <sub>2</sub> SiO <sub>5</sub>

(b)



Y3d	E <sub>b</sub>	Possible chemical state
3d <sub>5/2</sub>	156.9	Y <sub>2</sub> O <sub>3</sub>
3d <sub>5/2</sub>	157.8	Y <sub>2</sub> SiO <sub>5</sub>
3d <sub>5/2</sub>	158.5	Y <sub>2</sub> SiO <sub>5</sub>
3d <sub>3/2</sub>	159	Y <sub>2</sub> O <sub>3</sub>
3d <sub>3/2</sub>	159.9	Y <sub>2</sub> SiO <sub>5</sub>
3d <sub>3/2</sub>	160.5	Y <sub>2</sub> SiO <sub>5</sub>

(c)



Y3d	E <sub>b</sub>	Possible chemical state
3d <sub>5/2</sub>	156.9	Y <sub>2</sub> O <sub>3</sub>
3d <sub>5/2</sub>	157.9	Y <sub>2</sub> SiO <sub>5</sub>
3d <sub>5/2</sub>	158.5	Y <sub>2</sub> SiO <sub>5</sub>
3d <sub>3/2</sub>	159	Y <sub>2</sub> O <sub>3</sub>
3d <sub>3/2</sub>	159.9	Y <sub>2</sub> SiO <sub>5</sub>
3d <sub>3/2</sub>	160.6	Y <sub>2</sub> SiO <sub>5</sub>

(d)

**Figure 4: Gaussian-Lorentz peak fits for Y 3d in the a) standard powder, b) undegraded, c) 24 hr degraded and d) 6 days degraded areas.**

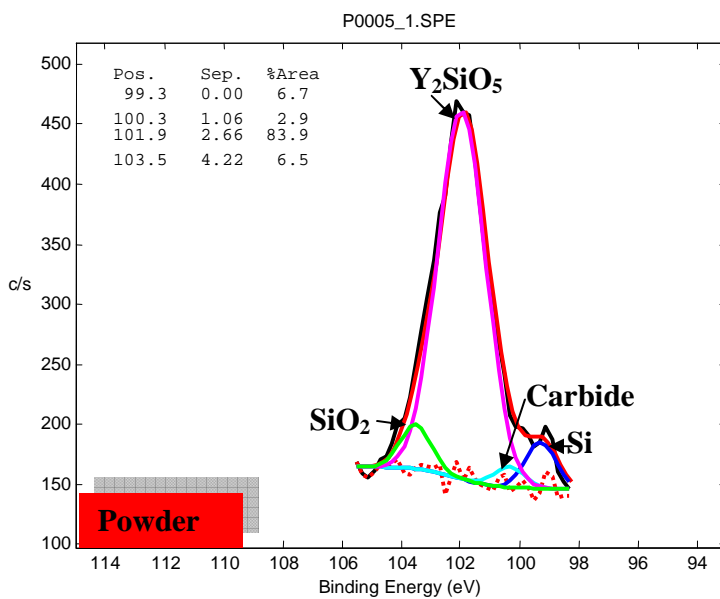
The small amount of Y<sub>2</sub>O<sub>3</sub>, mentioned in the O 1s section, also reflects in the Y 3d peaks in all four areas. The Y 3d peak at 156 eV in Fig. 4 correspond well with the reference Y 3d peak position in Y<sub>2</sub>O<sub>3</sub> [4]. In CL degradation studies done by Coetsee *et al.* [6] the Y 3d peak showed a slight shift from 157.6 to 157.1 eV before and after degradation and this could be due to the formation of a Y<sub>2</sub>O<sub>3</sub> layer on the surface during the degradation process. Parsons [5] indicated a Y 3d peak in Y<sub>2</sub>O<sub>3</sub> at 157 eV and in silicate a peak at 158 eV during investigation on the mechanisms for interface layer formation (silicon oxidation forming SiO<sub>2</sub> and/or metal silicate) during post-deposition processing of high-ε insulators on silicon.

The two doublet Y 3d peaks (Y 3d<sub>5/2</sub> and Y 3d<sub>3/2</sub>) in Y<sub>2</sub>SiO<sub>5</sub>:Ce were measured in the standard phosphor powders at 157 and 158 eV (3d<sub>5/2</sub>), Fig. 4a) and are present throughout the rest of the areas. The two measured peaks for Y 3d at 157 and 158 eV in Fig. 4 were also measured by Parsons (158 eV in silicate) [5] and Chambers *et al.* (in Y-

Si-O bonds) [4, 11]. The two Y sites for  $Y_2SiO_5$  (two CN numbers) are therefore the reason for the two Y 3d peaks. The small peak situated at 153 – 154 eV in Fig. 2c) is due to Si 2s [4].

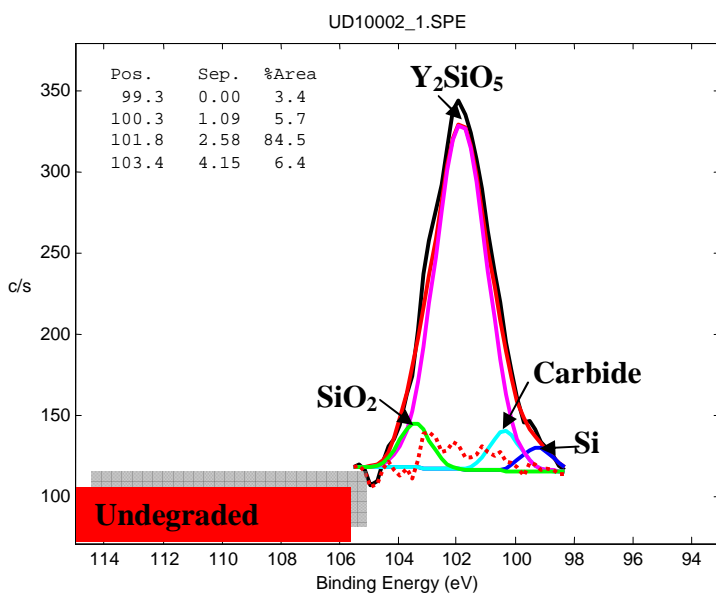
**Si 2p:**

Fig. 5 shows the Gaussian peak fits that were done on a) the standard powder, b) the undegraded, c) the 24 hr degraded and d) the 6 days degraded area with a table of possible chemical states for each binding energy position.



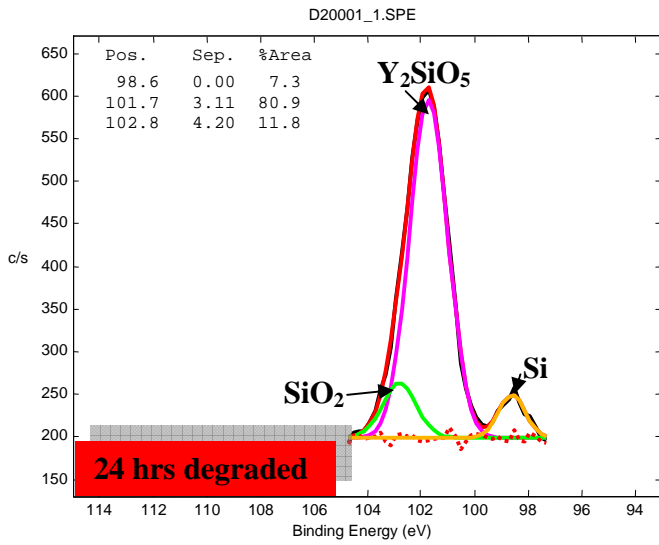
Si2p	$E_b$	Possible chemical state
	99.3	Si
	100.3	Carbide
	101.9	$Y_2SiO_5$
	103.5	$SiO_2$

(a)



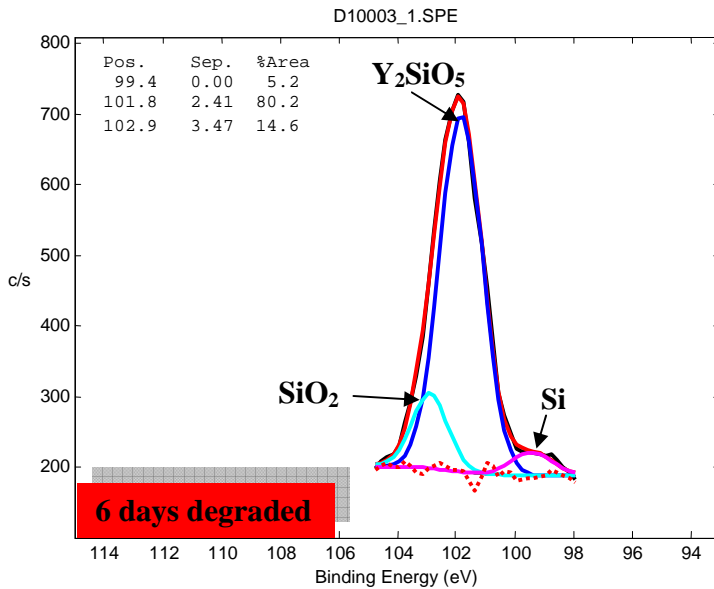
Si2p	$E_b$	Possible chemical state
	99.3	Si
	100.3	Carbide
	101.8	$Y_2SiO_5$
	103.4	$SiO_2$

(b)



Si2p	E <sub>b</sub>	Possible chemical state
	98.6	Si
	101.7	Y <sub>2</sub> SiO <sub>5</sub>
	102.8	SiO <sub>2</sub>

(c)



Si2p	E <sub>b</sub>	Possible chemical state
	99.4	Si
	101.8	Y <sub>2</sub> SiO <sub>5</sub>
	102.9	SiO <sub>2</sub>

(d)

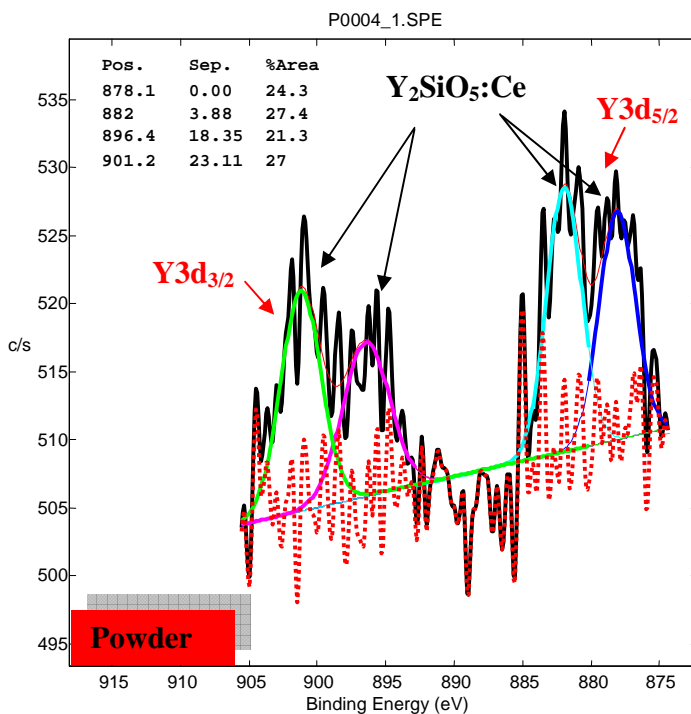
**Figure 5: Gaussian-Lorentz peak fits for Si 2p in the a) standard powder, b) undegraded, c) 24 hr degraded and d) 6 days degraded areas.**

The existence of silica in the standard phosphor powders is again proved by the Si 2p peak fits done in Fig. 5a) and b). There is a small amount of silica present as is also showed by the O 1s peak fits section above. The Si 2p peak in silica measured at 103 eV [12] also shows an increase in area percentage to the 24 hr and 6 days degraded areas. This is then proof for the formation of a SiO<sub>2</sub> layer on the surface as expected and mentioned in the O 1s section above. The electron bombardment during the degradation process in the presence of O<sub>2</sub> gas causes the Y-Si-O bonds to break and form new

chemical compounds. Chambers *et al.* [4, 11] measured a Si 2p peak at 101 eV and at 102.9 eV which is in the expected range of 102 – 103 eV for Si-O bonds in metal silicates. They also measured a peak at 99.3 eV which is assigned to the silicon substrate. In Fig. 5 the low intensity Si 2p peak at 98/99 eV can therefore be assigned to silicon which could be a result of broken bonds during the degradation process or during the manufacturing process of the standard phosphor powders. The peak situated at 100 eV in a) and b) could be a carbide [12] contribution due to the adventitious C on the surface. According to the chemistry mentioned in section 2.4, the Si 2p peak measured in Fig. 5 at 101 eV is the corresponding Si peak for the SiO<sub>4</sub> tetrahedron structure in Y<sub>2</sub>SiO<sub>5</sub>.

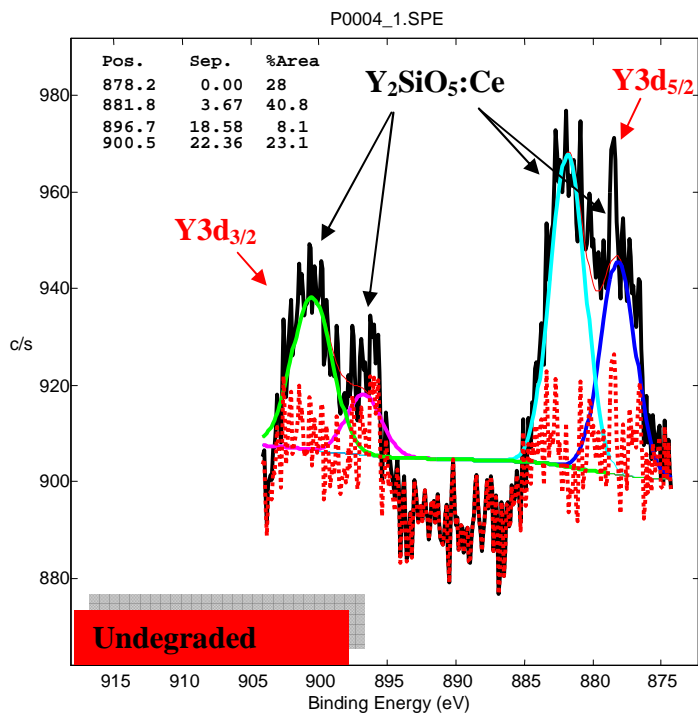
### Ce 3d:

Fig. 6 shows the Gaussian peak fits that were done on a) the standard powder, b) the undegraded, c) the 24 hr degraded and d) the 6 days degraded area with a table of possible chemical states for each binding energy position.



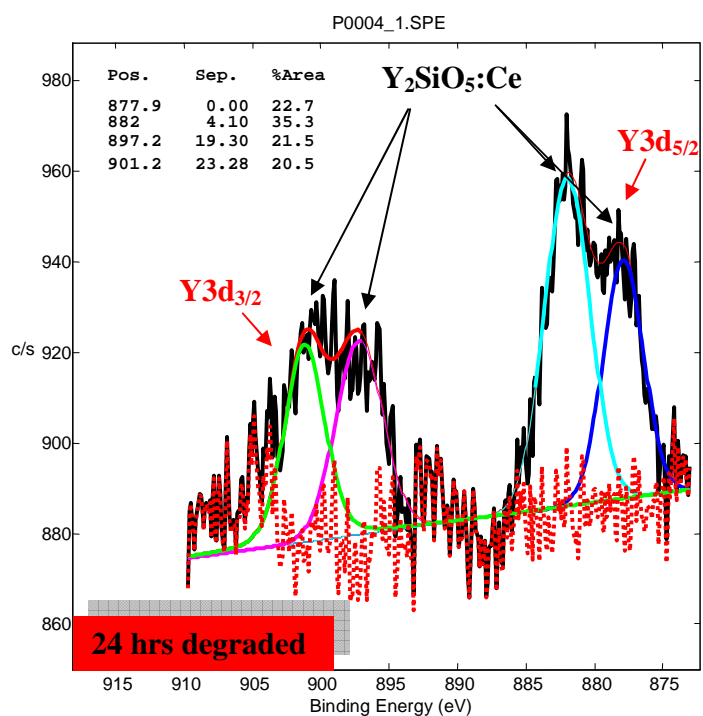
Ce3d	E <sub>b</sub>	Possible chemical state
3d <sub>5/2</sub>	878.1	Y <sub>2</sub> SiO <sub>5</sub> :Ce
3d <sub>5/2</sub>	882	Y <sub>2</sub> SiO <sub>5</sub> :Ce
3d <sub>3/2</sub>	896.4	Y <sub>2</sub> SiO <sub>5</sub> :Ce
3d <sub>3/2</sub>	901.2	Y <sub>2</sub> SiO <sub>5</sub> :Ce

(a)



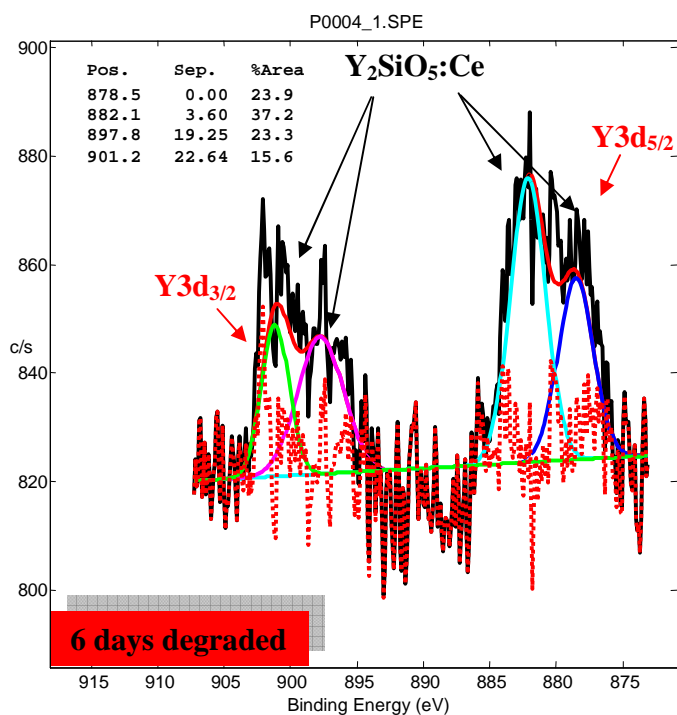
Ce3d	E <sub>b</sub>	Possible chemical state
3d <sub>5/2</sub>	878.2	Y <sub>2</sub> SiO <sub>5</sub> :Ce
3d <sub>5/2</sub>	881.8	Y <sub>2</sub> SiO <sub>5</sub> :Ce
3d <sub>3/2</sub>	896.7	Y <sub>2</sub> SiO <sub>5</sub> :Ce
3d <sub>3/2</sub>	900.5	Y <sub>2</sub> SiO <sub>5</sub> :Ce

(b)



Ce3d	E <sub>b</sub>	Possible chemical state
3d <sub>5/2</sub>	877.9	Y <sub>2</sub> SiO <sub>5</sub> :Ce
3d <sub>5/2</sub>	882	Y <sub>2</sub> SiO <sub>5</sub> :Ce
3d <sub>3/2</sub>	897.2	Y <sub>2</sub> SiO <sub>5</sub> :Ce
3d <sub>3/2</sub>	901.2	Y <sub>2</sub> SiO <sub>5</sub> :Ce

(c)



Ce3d	E <sub>b</sub>	Possible chemical state
3d <sub>5/2</sub>	878.5	Y <sub>2</sub> SiO <sub>5</sub> :Ce
3d <sub>5/2</sub>	882.1	Y <sub>2</sub> SiO <sub>5</sub> :Ce
3d <sub>3/2</sub>	897.8	Y <sub>2</sub> SiO <sub>5</sub> :Ce
3d <sub>3/2</sub>	901.2	Y <sub>2</sub> SiO <sub>5</sub> :Ce

(d)

**Figure 6: Gaussian-Lorentz peak fits for Ce 3d in the a) standard powder (100 μm 25 W 15 kV X-ray beam), b) undegraded, c) 24 hr degraded and d) 6 days degraded areas. (100 cycles were done)**

Coetsee *et al.* [6] measured the Ce 3d peak before degradation at 881.7 and 885.4 eV and after degradation at 882.7 and 886.5 eV. The Ce 3d peak before degradation must therefore be the Ce peak in the Y<sub>2</sub>SiO<sub>5</sub>:Ce host matrix. The peak positions after degradation were assigned to CeO<sub>2</sub> and CeH<sub>3</sub> which might have formed during the degradation process. In Fig. 6 two Ce 3d peaks were measured in the standard powders and in the undegraded areas at 878 and 881 eV which can be assigned to the two Ce peak positions in the host matrix [13]. In the 24 hr and 6 days degraded areas, Fig. 7c) and d), the two Ce peaks are situated at 877, 882 eV and 878 and 882 eV.

As mentioned in section 2.4, Ce<sup>3+</sup> can easily substitute for Y<sup>3+</sup> in the Y<sub>2</sub>SiO<sub>5</sub>:Ce host matrix. This implies that if there are two sites for Y in the host matrix then there should be two sites for Ce having the same CN of 9 and 7. The two peaks measured in this Ce 3d spectra therefore correlates well with the two different sites. These two sites are also explained as a situation for mixed final states [14]. If shifts of surface atom core level

binding energies are observed then it is often viewed as evidence for changing oxidation states. A brief overview for the phenomenon of mixed valence and final states are given by Lindquist *et al.* [15]. They have mentioned that these mixed final states occur for systems in which two atomic electronic configurations are close in energy. The result is a net ground-state configuration which is a strong mixture of the two nearly iso-energetic states.

In the case of cerium mixed-valent compounds, the two electronic configurations  $[\text{Xe}](5d6s)^34f^1$  and  $[\text{Xe}](5d6s)^44f^0$  can be very close in energy. The photoionized atom, however, is not a mixture of states because the two once iso-energetic initial-state configurations have very different final-state relaxation effects which depend on the extent of interaction between the nucleus and remaining electrons in each configuration. In the ion, states with high f density are of lower energy than those with low f density as a result of the small radius of the f orbital relative to the 5d and 6s orbitals. The f electrons experience the increased effective nuclear charge of the photo-ion more than do the 5d and 6s electrons. Thus, the configuration  $(5d6s)^34f^1$  will be of lower energy in the final state than  $(5d6s)^44f^0$ . In the model proposed by Schonhammer and Gunnarsson [16] hybridization of the f orbitals with the 5d6s band allows for a high probability of electron transfer from the 5d6s band into an f orbital as a result of the lower energy of the f orbital accompanying photoionization. This process of final-state electronic rearrangement, called "shakedown", produces a third possible final state with electronic configuration  $[\text{Xe}^+](5d6s)^24f^2$  (where  $[\text{Xe}^+]$  represents the photoionized xenon core). Such a process could lead to a third Ce peak situated at 896 eV [15].

Bêche *et al.* [14] collected Ce 3d features for  $\text{CeO}_2$  and  $\text{CePO}_4$  reference powders in order to determine the positions of the various components. This data was collected during their Ce 3d investigation of cerium oxides and mixed cerium oxides ( $\text{Ce}_x\text{Ti}_y\text{O}_z$ ). Six peaks corresponding to the pairs of spin-orbit doublets were identified in their Ce 3d spectrum measured in  $\text{CeO}_2$ . There were two high binding energy state peaks located at 916.9 ( $3d_{3/2}$ ) and 898.3 eV ( $3d_{5/2}$ ), which were assigned to the  $\text{Ce } 3d^9 4f^0 \text{ O } 2p^6$  final

state. The low binding energy state peaks were located at 901.3, 882.7 ( $3d_{5/2}$ ), 907.3 and 888.5 eV ( $3d_{5/2}$ ) which are the result of Ce  $3d^9 4f^2 O 2p^4$  and Ce  $3d^9 4f^1 O 2p^5$  final states.

To conclude this mixed final states for Ce 3d, the two main luminescent peaks in section 4.2.2, chapter 4 can therefore be attributed to these two different Ce 3d sites (A1 and A2) measured with XPS. The high binding energy peak situated at 881/882 eV would be the site with CN of 7.

## 8.4 Conclusion

The degradation of the  $Y_2SiO_5:Ce$  phosphor thin film ablated in Ar gas, investigated with XPS and peak fits resulted in small changes in peak intensities. This is mainly due to the formation of a luminescent  $SiO_2$  layer on the surface which is formed according to the ESSCR mechanism. The O 1s peak situated at 529 eV in all four areas point to the possibility that there is a small amount of  $Y_2O_3$  present. The measured O 1s peaks at 530 eV, 531 and 532 eV ( $< 532.5$  eV) (in all four areas) can be associated with  $Y_2SiO_5:Ce$  with a peak situated around 533 eV, which can be contributed to  $SiO_2$  (silica) ( $533 \pm 0.5$  eV). In the 24 hrs degradation area the silica peak at 532.9 eV shows an increase in the percentage area and a further increase in the 6 days degradation area, 532.5 eV. This proves the formation of an extra  $SiO_2$  layer on the surface as expected and discussed in chapter 7.

The small amount of  $Y_2O_3$  also appears in all four Y 3d areas. The two measured peaks for Y 3d at 157 and 158 eV can be attributed to Y 3d in the  $Y_2SiO_5:Ce$  oxidation state. The Si 2p peak in silica measured at 103 eV also shows an increase in area percentage to the 24 hr and 6 days degraded areas. This together with the O 1s fits also proves the formation of a  $SiO_2$  layer on the surface as expected. The electron bombardment during the degradation process in the presence of  $O_2$  gas causes the Y-Si-O bonds to break and form new chemical compounds. A small silicon peak at 99 eV was also measured. The peak situated at 100 eV could be a carbide contribution due to the adventitious C on the

surface. The two Ce peaks in all four areas measured at 877/878 and 881/882 eV can be assigned to the two sites for the Ce peak positions in the host matrix substituting for Y.

These XPS analyses showed that a SiO<sub>2</sub> layer formed on the surface under electron bombardment. The thin films are therefore also degrading but are chemically more stable than the phosphor powders. The light intensity however is lower and this aspect requires further investigation.

## References

1. E. Coetsee, H. C. Swart and J. J. Terblans, *J. Vac. Sci. Technol. A*, **25(4)** (2007) 1226.
2. J. Sebastian, S. Jones, T. Trottier, H. C. Swart and P. Holloway, *J. Soc. Inf. Disp*, **3/4** (1995) 147.
3. F. Moulder, W. F. Stickle, P. E. Sobol and K. D. Bomben, *Handbook of X-ray Photoelectron Spectroscopy*, ULVAC-PHI, Inc. 370 Enzo, Chigasaki 253-8522 Japan, (1995).
4. J. J. Chambers, B. W. Busch, W. H. Schulte, T. Gustafsson, E. Garfunkel, S. Wang, D. M. Maher, T. M. Klein and G. N. Parsons, *Appl. Surf. Sci*, **181(1-2)** (2001) 78.
5. G. N. Parsons, *High Dielectric Constant Materials*, Springer Berlin Heidelberg, ISSN 1437-0387, **16** (2006) 287.
6. E. Coetsee, J. J. Terblans and H. C. Swart, *J. Lumin*, **126** (2007) 37.
7. E. Paparazzo, *Surface Sci*. **234** (1990) L253.
8. D. Sprenger, H. Bach, W. Meisel and P. Gulich, *J. Non-crystal. Solids*, **126** (1990) 111.
9. T. A. Clarke and E. N. Rizkalla, *Chem. Phys. Lett*, **37** (1976) 523.

10. F. Moulder, W. F. Stickle, P. E. Sobol and K. D. Bomben, Handbook of X-ray Photoelectron Spectroscopy, ULVAC-PHI, Inc. 370 Enzo, Chigasaki 253-8522 Japan, (1995) 45.
11. J. J. Chambers and G. N. Parsons, J. Appl. Phys, **90(2)** (2001) 918.
12. F. Moulder, W. F. Stickle, P. E. Sobol and K. D. Bomben, Handbook of X-ray Photoelectron Spectroscopy, ULVAC-PHI, Inc. 370 Enzo, Chigasaki 253-8522 Japan, (1995) 57.
13. F. Moulder, W. F. Stickle, P. E. Sobol and K. D. Bomben, Handbook of X-ray Photoelectron Spectroscopy, ULVAC-PHI, Inc. 370 Enzo, Chigasaki 253-8522 Japan, (1995) 143.
14. E. Bêche, P. Charvin, D. Perarnau, S. Abanades and G. Flament, Surf. Interface Anal, **40** (2008) 264.
15. J. M. Lindquist and J. C. Hemminger, J. Phys. Chem, **91** (1987) 5535.
16. K. Schonhammer and O. Gunnarsson, Solid State Commun, **23** (1977) 691.

## Chapter 9

### Conclusion and future work

This chapter contains the overall conclusions of the results obtained for the luminescent mechanism and the luminescent properties of the  $\text{Y}_2\text{SiO}_5\text{:Ce}$  thin films that were grown with PLD.

#### 9.1 Conclusion

##### 9.1.1 Luminescent mechanism

CL and PL results were investigated and the best profiles for the Gaussian peak fits showed four peaks that fit the broad band spectrum. The origin of these four peaks is due to the two different  $\text{Ce}^{3+}$  sites in the host matrix (A1 and A2) and the crystal field split of the 4f levels. Defect levels also play an important role in the excitation process. A better understanding of the luminescent mechanism creates opportunities for enhancement in the  $\text{Y}_2\text{SiO}_5\text{:Ce}$  phosphor application field. The degradation of the  $\text{Y}_2\text{SiO}_5\text{:Ce}$  phosphor powders investigated with AES and CL spectroscopy resulted in an initial decrease in CL intensity measured at 450 nm and then to an increase after about  $300 \text{ C.cm}^{-2}$  due to the chemical change in the phosphor surface. XPS and CL indicated that the change in peak shape is due to the formation of a luminescent  $\text{SiO}_2$  layer on the surface which is formed according to the ESSCR mechanism. The emission of light from the  $\text{SiO}_2$  defect levels contributed to the CL intensity in the 600 to 700 nm wavelength range. The colour changed from blue to orange-reddish during the degradation process.

##### 9.1.2 Thin films: Part one

$\text{Y}_2\text{SiO}_5\text{:Ce}$  thin films were successfully grown on the Si (100) substrates and the effect of some of the process parameters indicated definite changes in particle sizes. Nano - particles appeared on the thin films when ablation was done with an ambient background.

The size of the particles depended on the background pressure, the gas specie and the substrate temperature as well as on the laser fluence. An increase in the ambient pressure to 1 Torr O<sub>2</sub> resulted in bigger particle sizes. Ablation with the higher fluence ( $3 \pm 0.3 \text{ J.cm}^{-2}$ ) also lead to bigger particle formation. The increase in the substrate temperature (from 400 to 600 °C) at high fluence yielded big particles which are actually an agglomeration of smaller particles and therefore a rougher surface. Ablation in the Ar ambient yielded 30 nm (bigger than the N<sub>2</sub>) particle sizes but less agglomeration than the O<sub>2</sub> ambient. The bigger particle sizes therefore result in lower particle densities.

### **9.1.3 Thin films: Part two**

The powder used as a target has a monoclinic crystal structure of Y<sub>2</sub>SiO<sub>5</sub>:Ce X<sub>1</sub> - phase with space group P2<sub>1</sub>/c. The XRD results for the thin films showed very low intensity peaks which are an indication that the layers are almost amorphous with only some indication of small peaks that belong to the monoclinic crystal structure. During the CL scanning emission seems to occur from the whole micron particles on the surface as well as from the smaller particles around the bigger particles. The smaller particles did not show effective emission with low PMT voltage. There is a definite increase in luminescent intensity with the uncoated thin film which indicates the photon absorption effect of the extra tin oxide coated layer. CL intensity is mainly coming from the bigger spherical particles on the surface.

The nano - thin films lead to an increase in PL and CL intensity. The thin films grown with the increased O<sub>2</sub> pressure to 1 Torr and higher fluence ( $3 \pm 0.3 \text{ J.cm}^{-2}$ ) resulted in better luminescent intensities. The increase in substrate temperature from 400 to 600 °C also resulted in an increased luminescence due to a rougher surface that formed. For better luminescent intensity the thin films should have a rougher surface (spherically shaped particles achieved via increased substrate temperature and increased ambient pressure).

#### **9.1.4 Thin films: Part three**

RBS showed that the higher fluence ablation in vacuum (TF5) led to a thicker layer than the low fluence ablation that was done in 1 Torr O<sub>2</sub> (TF17). These RBS results were used to determine the thickness of the thin film ablated with a low fluence in 455 mTorr Ar gas to be 133 nm. APPH depth profiles done on TF17 and A3 showed broad interfaces which indicate atom diffusion between the substrate and ablated layers. This is due to the heating of the substrate at 600 °C during PLD. Adventitious C depleted from the surface of the thin film ablated in Ar gas on the first 24 hr degraded area, within the first 50 C.cm<sup>-2</sup> and this resulted in the increase in the O/C and Si/C APPH ratios. The increase in CL intensity is therefore due to the depletion of the C from the surface. The CL degradation study of 144 hr on the same thin film but a different area showed a decrease in the main emission peak (440 nm) and an increase of a second emission peak emerging (after 24 hr) between 600 and 700 nm (with a change in the colour of the light from blue to whitish after 144 hr). This is in agreement with previous research studies done on the phosphor powders and XPS detailed chemical analyses are needed to prove the formation of the SiO<sub>2</sub> layer on the surface with the defect levels that might also emit light. These results proved that the thin films are chemically more stable than the phosphor powders.

#### **9.1.5 Thin films: Part four**

The degradation of the Y<sub>2</sub>SiO<sub>5</sub>:Ce phosphor thin film ablated in Ar gas, investigated with XPS and peak fits, resulted in small changes in peak intensities. This is mainly due to the formation of a luminescent SiO<sub>2</sub> layer on the surface which is formed according to the ESSCR mechanism. The O 1s peak situated at 529 eV in all four areas (powders, undegraded, 24 hr and 6 days degraded areas) point to the possibility that there is a small amount of Y<sub>2</sub>O<sub>3</sub> present. The measured O 1s peaks at 530 eV, 531 and 532 eV (< 532.5 eV) (in all four areas) can be associated with Y<sub>2</sub>SiO<sub>5</sub>:Ce with a peak situated around 533 eV, which can be contributed to SiO<sub>2</sub> (silica) (533 ± 0.5 eV). In the 24 hr degradation area the silica peak at 532.9 eV shows an increase in the percentage area and a further increase in the 6 days degradation area, 532.5 eV. This proves the formation of an extra SiO<sub>2</sub> layer on the surface as expected.

A small amount of  $Y_2O_3$  was also detected in all four Y 3d areas. The two measured peaks for Y 3d at 157 and 158 eV can be attributed to Y 3d in the  $Y_2SiO_5:Ce$  oxidation state. The Si 2p peak in silica measured at 103 eV also shows an increase in area percentage to the 24 hr and 6 days degraded areas. This together with the O 1s fits also proves the formation of a  $SiO_2$  layer on the surface as expected. The electron bombardment during the degradation process in the presence of  $O_2$  gas causes the Y-Si-O bonds to break and form new chemical compounds. A small silicon peak at 99 eV was also measured. The peak situated at 100 eV could be a carbide contribution due to the adventitious C on the surface. The two Ce peaks in all four areas measured at 877/878 and 881/882 eV can be assigned to the two sites for the Ce peak positions in the host matrix substituting for Y.

These XPS analyses showed that a  $SiO_2$  layer formed on the surface under electron bombardment. The thin films are therefore also degraded but are chemically more stable than the phosphor powders. The light intensity however is lower and this should be investigated further.

## **9.2 Future work**

### **Direct continuation of nano-thin films:**

#### **9.2.1 More PLD process parameters**

Future work would include a greater variety of process parameters such as ablation at room temperature, substrate temperature and at 200, 400 °C and higher with the three different gas species ( $O_2$ ,  $N_2$  and Ar). Ablation in each of the three different gas species at 1 and 3 Torr pressures and investigating the effect on the plume. The effect of the laser frequency, amount of pulses and target to substrate distance can also be investigated. Characterization and luminescent properties will then be investigated.

#### **9.2.2 Off axis geometry**

Applying the off axis PLD technique is an option of also trying to minimize the formation of the bigger unwanted micron particles on the surface. This is a technique where the substrate is mounted either upside down in the chamber or at an angle where

the plume is not directly focussed onto the substrate. Rotating the substrate would also aid in uniform thickness growth of the thin films.

### **9.2.3 Heating and cooling luminescent properties**

The luminescent properties of the commercial powder and also the thin films could also be investigated by heating the samples to about 1200 °C and cooling it with liquid N<sub>2</sub> to about -160 °C. Then to monitor the luminescent intensity in temperature steps with time.

### **9.2.4 Characterization**

Detailed Depth profiling and XPS analysis would then follow.

### **Future Phosphor Research:**

#### **9.2.5 Nano-technology**

Nano-technology is currently one of the fastest growing technologies in material science research areas. Nano-materials include any form of material with the nano-scale dimension. The beauty in nano-technology reflects in the fact that the physics of a material's properties in the nano-scale sometimes differs from the physics of the same material in the micro-scale. One well known example is that a semiconductor's band gap can be varied by changing the materials' dimension. There may be many more physical properties that changes that is not yet known to us. These new properties would then lead to further advancement in technology. Contributing to the nano-technology research would include new and improved methods that would allow control of the size of the nano-scale materials. Also, new and improved characterization tools and instruments are needed to study materials at the nano-scale.

There is a very broad range of nano-technology applications that include nano-scale electronics and optics to nano-biological systems and nano-medicine. All this research applications require a combination from multidisciplinary teams of physicist, chemists, material scientists, engineers, molecular biologists and pharmacologists that work together. The most important aspect is synthesis and processing of nano-materials and nano-structures. Nano-properties cannot be studied if the material is not in the nano-

dimension. Nano-dimension could then therefore result in miniaturization of current and new machines, instruments and sensors for example. Possible miniaturization are computers with great power that compute algorithms that mimic the human brain, biosensors that warn us at the early stage of a disease infecting on the molecular level and nano-robots that can repair internal damage and remove chemical toxins in human bodies.

### **9.2.6 Luminescence**

Living standards have been improved by illumination in the dark and communication skill by means of recording and reading information on various media. Luminescence evolved from wood fires, to torch flames, the burning of oil, candles, gas flames, incandescent lamps, fluorescent lamps, light emitting diodes and photoluminescence from phosphor particles. Luminescent improvement (especially from PL from phosphor screens) prolonged life's activities into the night hours. Life's activities are accompanied by communication with others. Communication of information has evolved from the faces of rock cliffs, to the walls of caves, clay tablets, wood and bamboo plates, sheets of paper, magnetic tapes to electronic chips. Electronic device increased the speed of communication of information. Information stored on chips in electronic devices are invisible to the human eye so the development of display screens aided as an interface between human and electronic devices for the visualization of invisible information. The images on display devices are illustrated on screens by CL or PL from phosphor screens. Optimization of CL and PL generation in the tiny phosphor particles in the display screen involves a very broad research field. Some of this research includes theoretical understanding of absorption, excitation, radiative and non-radiative relaxation, energy transfer and migration as well as the practical part of phosphor synthesis, nano-dimensions, morphology, characterizing, lifetimes and degradation.

### **9.2.7 Modern luminescence spectroscopy:**

What about laser excitation studies? Could laser excitation lead to time –resolved detection of resulting emission and scattering? Could the time-resolved technique improve spectroscopic sensitivity and selectivity? A time-resolved technique is the

signal detection only during a certain time gate after a certain delay following the end of a laser pulse. It would definitely result in new data which would contribute to the fundamental knowledge of phosphor materials. The experimental setup would require a laser source (Ar, excimer, Nd-YAG, nitrogen or dye), an imaging monochromator, gated detector (Intensified Charged Couple Device) and a computer with corresponding software. Detail investigation would be needed on the materials' crystal structure, ligand field theory, molecular orbitals theory, band scheme approximation and optically active luminescence centres.

Research will never end.

## Appendix A

### Publications

1. E. Coetsee, H. C. Swart and J. J. Terblans, Degradation of  $Y_2SiO_5:Ce$  phosphor powders, *J. Lumin*, **126(1)** (2007) 37. (Best M.Sc publication in the CMPMS division at SAIP 2007).
2. E. Coetsee, H. C. Swart, J. J. Terblans, O. M. Ntwaeaborwa, K. T. Hillie, W. A. Jordaan and U. Buttner, Characterization of  $Y_2SiO_5:Ce$  thin films, *Opt. Mat*, **29(11)** (2007) 1338.
3. E. Coetsee, H. C. Swart and J. J. Terblans, Cathodoluminescence degradation of  $Y_2SiO_5:Ce$  thin films, *JVST A*, **25(4)** (2007) 1226.
4. H. C. Swart, J. J. Terblans, E. Coetsee, O. M. Ntwaeaborwa, M. S. Dhlamini, S. Nieuwoudt and P. H. Holloway, Review on electron stimulated surface chemical reaction mechanism for phosphor degradation, *JVST A*, **25(4)** (2007) 917.
5. E. Coetsee, J. J. Terblans, H. C. Swart, Degradering van  $Y_2SiO_5:Ce$  fosforpoelier, *Die Suid-Afrikaanse Tydskrif vir Natuurwetenskap en Tegnologie (SAAWK)*, **26(2)** (2007) 151.
6. J. J. Dolo, J. J. Terblans, B. F. Dejene, O. M. Ntwaeaborwa, E. Coetsee and H. C. Swart, Degradation of commercially  $Gd_2O_2S:Tb$  phosphor, *Phys.Stat.Sol. (c)*, **5(2)** (2008) 594.
7. E. Coetsee, J. J. Terblans and H. C. Swart,  $Y_2SiO_5:Ce$  thin films grown by PLD, *Phys.Stat.Sol. (c)*, **5(2)** (2008) 634.
8. S. B Mishra, A. K. Mishra, A. S. Luyt, N. Revaprasadu, K. T. Hillie, W. J. v. d. M. Steyn, E. Coetsee and H. C. Swart, Ethyl vinyl acetate copolymer -  $SrAl_2O_4:Eu,Dy$  and  $Sr_4Al_{14}O_{25}:Eu,Dy$  phosphors based composites: Preparation and Material properties, *Polymer Composites, J. Appl. Polymer. Sci*, **115** (2010) 579.
9. H. C. Swart, E. Coetsee, J. J. Terblans, J. M. Fitz-Gerald and J. R. Botha, Luminescence of  $Y_2SiO_5:Ce$  nanocrystalline thin films, *EJSSNT*, **7** (2009) 369.

10. S. B. Mishra, A. K. Mishra, N. Revaprasadu, K. T. Hillie, W. J. v. d. M. Steyn, E. Coetsee and H. C. Swart, Strontium Aluminate/Polymer Composites: Morphology, Luminescent Properties, and Durability, *J. Appl. Polymer. Sci*, **112(6)** (2009) 3347.
11. H. C. Swart, J. J. Terblans, O. M. Ntwaeaborwa, E. Coetsee, B. M. Mothudi and M. S. Dhlamini, Photon emission mechanisms of different phosphors, *Nucl. Instr. and Meth. B*, **267 (16)** (2009) 2630.
12. E. Coetsee, J. R. Botha, J. J. Terblans en H. C. Swart, Luminesserende eienskappe van  $Y_2SiO_5:Ce$  nano-dunlagies, *Die Suid-Afrikaanse Tydskrif vir Natuurwetenskap en Tegnologie (SAAWK)*, **27(2)** (2008) 146.
13. S. Nieuwoudt, J. J. Terblans, J. Ngaruiya, O. M. Ntwaeaborwa, E. Coetsee, K. T. Hillie en H. C. Swart, Luminessensie-eienskappe van  $SrAl_2O_4:Eu^{2+}$ ,  $Dy^{3+}$  fosfor, *Die Suid-Afrikaanse Tydskrif vir Natuurwetenskap en Tegnologie (SAAWK)*, **27(2)** (2008) 154.
14. D. B. Bem, H. C. Swart, A. S. Luyt, E. Coetsee, F. B. Dejene, Properties of Green  $SrAl_2O_4$  Phosphor in LDPE and PMMA Polymers, *J. Appl. Polymer. Sci*, accepted March 2009. APP-2009-02-0338.
15. E. Coetsee, J. J. Terblans and H. C. Swart, Characteristic properties of  $Y_2SiO_5:Ce$  thin films grown with PLD, *Physica B*, **404** (2009) 4431.
16. H. C. Swart, E. Coetsee, J. J. Terblans and O. M. Ntwaeaborwa, Luminescent mechanism of  $Y_2SiO_5:Ce$  phosphor powder, *Physica B*, **404** (2009) 4426.
17. P. D. Nsimama, O. M. Ntwaeaborwa, E. Coetsee and H. C Swart, The influence of the number of pulses on morphological and photoluminescence properties of  $SrAl_2O_4:Eu^{2+}$ ,  $Dy^{3+}$  thin films prepared by pulsed laser deposition, *Physica B*, **404** (2009) 4489.
18. O. M. Ntwaeaborwa, P. D. Nsimama, J. T. Abiade, E. Coetsee and H. C Swart, The effect of substrate temperature and oxygen pressure on the structure and photoluminescence properties of pulsed laser deposited  $SrAl_2O_4:Eu^{2+}, Dy^{3+}$  thin films, *Physica B*, **404** (2009) 4436.

19. L. F. Koao, H. C. Swart, E. Coetsee, M. M. Biggs and F. B. Dejene, The effect of  $Mg^{2+}$  ions co-doping on the structural and optical properties  $Ce^{3+}$  doped Silica glasses, *Physica B*, **404** (2009) 4499.
20. E. Coetsee, J. J. Terblans and H. C. Swart, The growth of  $Y_2SiO_5:Ce$  thin films with pulsed laser deposition, 10<sup>th</sup> International Conference on Laser Ablation (COLA 2009), accepted January 2010.
21. H. C. Swart, E. Coetsee, J. J. Terblans, O. M. Ntwaeaborwa, P. D. Nsimama and J. J. Dolo, Cathodoluminescence degradation of PLD thin films, 10<sup>th</sup> International Conference on Laser Ablation (COLA 2009), submitted November 2009.
22. H. C. Swart, J. J. Terblans, E. Coetsee, V. Kumar, O. M. Ntwaeaborwa and M. M. Biggs, Auger Electron Spectroscopy and X-ray Photoelectron Spectroscopy study of the electron stimulated surface chemical reaction mechanism for phosphor degradation, submitted August 2009.
23. J. J. Dolo, O. M. Ntwaeaborwa, J. J. Terblans, E. Coetsee, B. F. Dejene, M-M Biggs and H.C. Swart, The effect of oxygen pressure on the structure, morphology and photoluminescence intensity of pulsed laser deposited  $Gd_2O_2S:Tb^{3+}$  thin film phosphor, 10<sup>th</sup> International Conference on Laser Ablation (COLA 2009), accepted January 2010.

## Proceedings

1. E. Coetsee, H. C. Swart, J. J. Terblans, O. M. Ntwaeaborwa, K. T. Hillie, W. A. Jordaan and U. Buttner, Characterization (EDS, SEM AND AFM) of  $Y_2SiO_5:Ce$  thin films grown with PLD, Proceedings of the 45<sup>th</sup> Annual Conference of the Microscopy Society of Southern Africa, **36** (2006) 31.
2. H. C. Swart, B. M. Mothudi, S. Nieuwoudt, J. J. Terblans, E. Coetsee, O. M. Ntwaeaborwa, Luminescent properties and degradation of  $SrAl_xO_y:Eu^{2+}, Dy^{3+}$  phosphors, Proceedings - 14<sup>th</sup> International Workshop on Inorganic and Organic Electroluminescence & 2008 International Conference on the Science and Technology of Emissive Displays and Lighting, 367.

## Conference participation

### South African Institute of Physics

1. E. Coetsee, J. J. Terblans, O. M. Ntwaeaborwa, U. Buttner and H. C. Swart, Characterization of Pulsed Laser Ablated Cerium doped Yttrium Silicate ( $Y_2SiO_5:Ce$ ) thin films on Si (100), SAIP Pretoria 2005.
2. E. Coetsee, H. C. Swart, J. J. Terblans, O. M. Ntwaeaborwa, K. T. Hillie, W. A. Jordaan and U. Buttner, Cathodoluminescence of  $Y_2SiO_5:Ce$  thin films, SAIP UWC 2006. (Best M.Sc poster in the CMPMS division).
3. E. Coetsee, H. C. Swart and J. J. Terblans, Degradation of  $Y_2SiO_5:Ce$  phosphor powders, SAIP UWC 2006.
4. E. Coetsee, J. J. Terblans and H. C. Swart, Luminescent properties of  $Y_2SiO_5:Ce$  thin films, SAIP Wits 2007.
5. S. Nieuwoudt, J. J. Terblans, O. M. Ntwaeaborwa, E. Coetsee, K. T. Hillie and H. C. Swart, Luminescent properties of nanoparticle  $SrAl_2O_4:Eu^{2+}, Dy^{3+}$  phosphor, SAIP Wits 2007.
6. J. J. Dolo, J. J. Terblans, E. Coetsee, B. F. Dejene and H. C. Swart, Degradation of  $Gd_2O_2S:Tb$  phosphor, SAIP Wits 2007.
7. P. D. Nsimama, O. M. Ntwaeaborwa, E. Coetsee and H. C Swart, The changes on properties of pulsed laser ablated  $SrAl_2O_4:Eu^{2+}, Dy^{3+}$  thin films with the deposition parameters; a case of working atmosphere, SAIP UKN Durban, July 2009.
8. L. F. Koao, H. C. Swart, E. Coetsee, M. M. Biggs and F. B. Dejene, The effect of temperature on the photoluminescence characteristics of Ce;Al or Ce;Mg doped  $SiO_2$ . Durban, July (2009).

### International conferences and other

1. E. Coetsee, H. C. Swart, J. J. Terblans O. M. Ntwaeaborwa, K. T. Hillie and U. Buttner, Energy Dispersive Spectroscopy (EDS), Scanning Electron (SEM) and Atomic Force Microscopy (AFM) of  $Y_2SiO_5:Ce$  thin films, MSSA at NMMU December 2006.

2. H. C. Swart, J. J. Terblans, E. Coetsee, O. M. Ntwaeaborwa, M. S. Dhlamini and P. H. Holloway, A short review on the ESSCR mechanism for phosphor degradation, AVS 53<sup>rd</sup> International Symposium & Exhibition, San Francisco, CA, USA, 12- 17 November 2006.
3. E. Coetsee, J. J. Terblans and H. C. Swart, Cathodoluminescence Degradation of Y<sub>2</sub>SiO<sub>5</sub>:Ce Thin Films, AVS 53<sup>rd</sup> International Symposium & Exhibition, San Francisco, CA, USA, 12 - 17 November 2006.
4. E. Coetsee, H. C. Swart en J. J. Terblans, Degradering van Y<sub>2</sub>SiO<sub>5</sub>:Ce fosfor poeiers, Afrikaanse studente symposium, SAAWK by Noordwes Universiteit, 2 November 2006. (Mathematica prize.)
5. E. Coetsee, H. C. Swart and J. J. Terblans, Y<sub>2</sub>SiO<sub>5</sub>:Ce thin films grown by PLD Kariega 2007, Conference on Photonic Materials, Kariega Game Reserve, South Africa, 2 - 6 May 2007.
6. J. J. Dolo, J. J. Terblans, B. F. Dejene, E. Coetsee and H. C. Swart, Degradation of commercially Gd<sub>2</sub>O<sub>2</sub>S:Tb phosphor. Kariega 2007, Conference on Photonic Materials, Kariega Game Reserve, South Africa, 2 - 6 May.
7. O. M. Ntwaeaborwa, J. M. Ngaruiya, E. Coetsee, H. C. Swart, Enhanced luminescence of SiO<sub>2</sub>:Tb<sup>3+</sup> induced by an energy transfer from encapsulated ZnO nanoparticles, International Center for Materials Research (ICMR), Zululand, 29th July-1st August 2007.
8. E. Coetsee, J. R. Botha, J. J. Terblans en H.C. Swart, Luminesserende eienskappe van Y<sub>2</sub>SiO<sub>5</sub>:Ce nano dun films, Afrikaanse studente symposium, SAAWK TUT Pretoria, 2 November 2007. (Mathematica prize.)
9. S. Nieuwoudt, J. J. Terblans, J. Ngaruiya, O. M. Ntwaeaborwa, E. Coetsee, K. T. Hillie en H. C. Swart, Luminessensie-eienskappe van SrAl<sub>2</sub>O<sub>4</sub>:Eu<sup>2+</sup>, Dy<sup>3+</sup> fosfor, Afrikaanse studente symposium, SAAWK TUT Pretoria, 2 November 2007.
10. J. M. Ngaruiya, O. M. Ntwaeaborwa, E. Coetsee and H. C. Swart, African Material Research Society conference, Dar es Salaam Tanzania, December 2007.
11. H. C. Swart, E. Coetsee, J. J. Terblans, J. M. Fitz-Gerald and J. R. Botha, Luminescence of Y<sub>2</sub>SiO<sub>5</sub>:Ce nanocrystalline thin films, 14<sup>th</sup> International

- Conference on Solid Films and Surfaces, Trinity College, Dublin, Ireland, 29<sup>th</sup> June - 4<sup>th</sup> of July 2008.
12. H. C. Swart, B. M. Mothudi, S. Nieuwoudt, J. J. Terblans, E. Coetsee, O. M. Ntwaeaborwa, Luminescent properties and degradation of  $\text{SrAl}_x\text{O}_y:\text{Eu}^{2+},\text{Dy}^{3+}$  phosphors, 14<sup>th</sup> International Workshop on Inorganic and Organic Electroluminescence & 2008 International Conference on the Science and Technology of Emissive Displays and Lighting, Bagni di Tivoli, Rome, Italy, 9-12 September 2008.
  13. H. C. Swart, J. J. Terblans, O. M. Ntwaeaborwa, E. Coetsee and M. S. Dhlamini, Photon emission mechanisms of different phosphors, 23<sup>th</sup> ICACS (International Conference on Atomic Collisions in Solids), Phalaborwa, Limpopo province of South Africa, 17 - 22 August 2008.
  14. E. Coetsee, J. J. Terblans en H. C. Swart, Luminesserende meganisme van yttriumsilikaat gedoteer met serium ( $\text{Y}_2\text{SiO}_5:\text{Ce}$ ) fosfor poeier, Afrikaanse studente simposium, SAAWK UJ, 31 Oktober 2008. (Mathematica prize.)
  15. E. Coetsee, J. J. Terblans and H. C. Swart, Characteristic properties of  $\text{Y}_2\text{SiO}_5:\text{Ce}$  thin films grown with PLD, 3<sup>rd</sup> South African Conference on Photonic Materials (SACPM 2009) Mabula March 2009.
  16. H. C. Swart, E. Coetsee, J. J. Terblans and O. M. Ntwaeaborwa, Luminescent mechanism of  $\text{Y}_2\text{SiO}_5:\text{Ce}$  phosphor powder, 3<sup>rd</sup> South African Conference on Photonic Materials (SACPM 2009), Mabula, March 2009.
  17. O. M. Ntwaeaborwa, P. D. Nsimama, E. Coetsee and H. C Swart, The effect of substrate temperature and oxygen pressure on the structure and photoluminescence properties of pulsed laser deposited  $\text{SrAl}_2\text{O}_4:\text{Eu}^{2+},\text{Dy}^{3+}$  thin films, 3<sup>rd</sup> South African Conference on Photonic Materials (SACPM 2009) Mabula, March 2009.
  18. P. D. Nsimama, O. M. Ntwaeaborwa, E. Coetsee and H. C Swart, The influence of the number of pulses on morphological and photoluminescence properties of  $\text{SrAl}_2\text{O}_4:\text{Eu}^{2+}, \text{Dy}^{3+}$  thin films prepared by pulsed laser deposition, 3<sup>rd</sup> South African Conference on Photonic Materials (SACPM 2009) Mabula, March 2009.

19. L. F. Koao, H. C. Swart, E. Coetsee, M. M. Biggs and F. B. Dejene, The effect of  $Mg^{2+}$  ions co-doping on the structural and optical properties  $Ce^{3+}$  doped Silica glasses, 3<sup>rd</sup> South African Conference on Photonic Materials (SACPM 2009) Mabula, March 2009.
20. E. Coetsee, J. J. Terblans and H. C. Swart, The growth of  $Y_2SiO_5:Ce$  thin films with pulsed laser deposition, 10<sup>th</sup> International Conference on Laser Ablation (COLA 2009) Singapore, November 22-27.
21. H. C. Swart, E. Coetzee, J. J. Terblans, O. M. Ntwaeaborwa, P. D. Nsimama and J. J. Dolo, Cathodoluminescence degradation of PLD thin films, 10<sup>th</sup> International Conference on Laser Ablation (COLA 2009) Singapore, November 22-27.
22. J. J. Dolo, H. C. Swart, J. J. Terblans, E. Coetsee, O. M. Ntwaeaborwa and B. F. Dejene, Effect of oxygen pressure on structural properties of pulsed laser deposition  $Gd_2O_3:Sr^{2+}$  thin films, International Conference on Nanotechnology and Advanced Materials 2009. (ICNAM 2009), University of Bahrain, 4 to 7 May 2009.
23. A. G. Ali, H. C. Swart, J. R. Botha, E. Coetsee, M. M. Biggs and F. B. Dejene, Structural and optical properties of  $ZnO$ ,  $SiO_2:Ce^{3+}$  and  $ZnO:SiO_2:Ce^{3+}$  nanoparticles prepared by a Sol-Gel process, International Conference on Nanotechnology and Advanced Materials 2009. (ICNAM 2009), University of Bahrain, 4 to 7 May 2009.
24. H. C. Swart, J. J. Terblans, E. Coetsee, V. Kumar, O. M. Ntwaeaborwa and M. M. Biggs, Auger Electron Spectroscopy and X-ray Photoelectron Spectroscopy study of the electron stimulated surface chemical reaction mechanism for phosphor degradation. Ecasia09, 13<sup>th</sup> European Conference on Applications of Surface and Interface Analysis, Antalya, Turkey, October 18-23, 2009.
25. J. J. Dolo, O. M. Ntwaeaborwa, J. J. Terblans, E. Coetsee, B. F. Dejene, M-M Biggs and H.C. Swart, The effect of oxygen pressure on the structure, morphology and photoluminescence intensity of pulsed laser deposited  $Gd_2O_3:Sr^{2+}$  thin film phosphor, 10<sup>th</sup> International Conference on Laser Ablation (COLA 2009) Singapore, November 22-27.